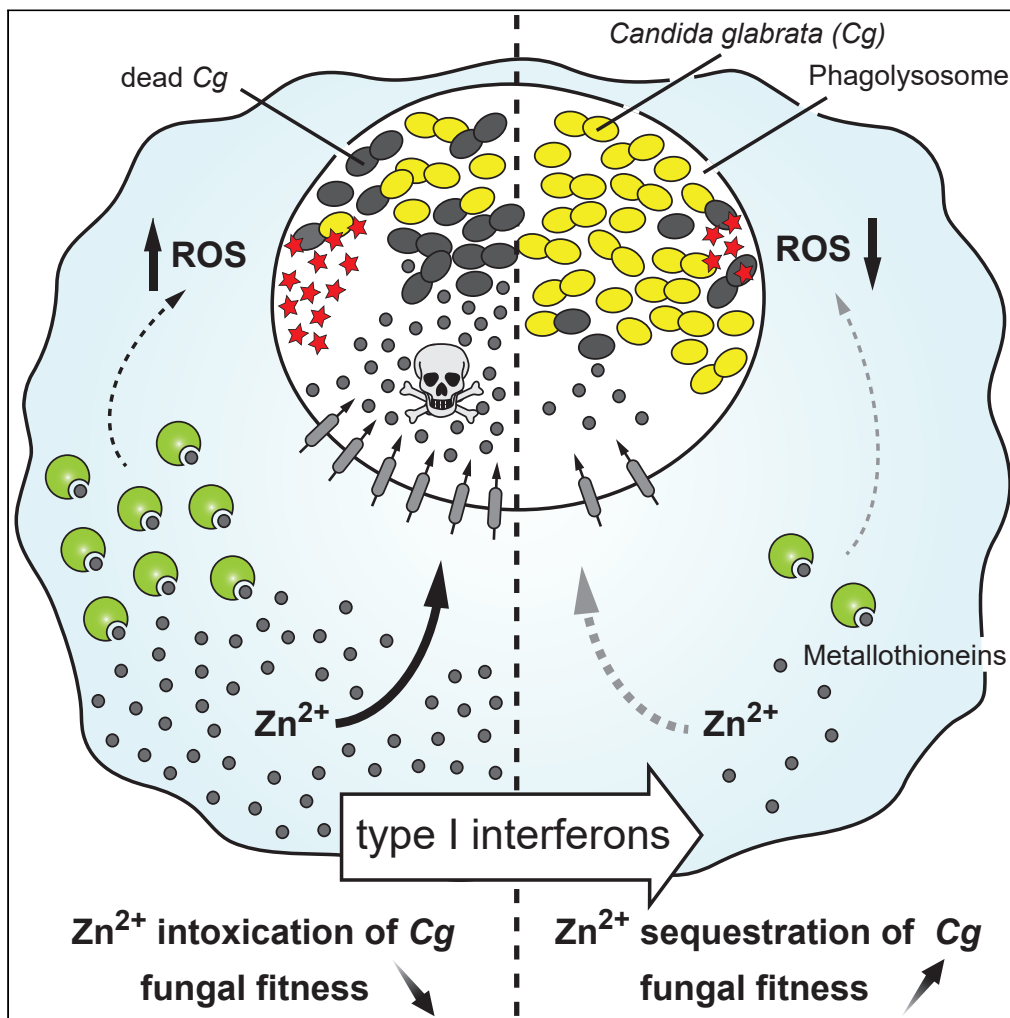# iScience

Article

Type I Interferons Ameliorate Zinc Intoxication of *Candida glabrata* by Macrophages and Promote Fungal Immune Evasion

Michael
Riedelberger,
Philipp Penninger,
Michael
Tscherner, ...,
Gernot
Schabbauer,
Guenter Weiss,
Karl Kuchler

karl.kuchler@meduniwien.ac.
at

HIGHLIGHTS
Metallothioneins shuttle
zinc into macrophage
phagosomes to elicit
pathogen killing

Zinc sequestration by
metallothioneins drives
potent fungicidal ROS
responses

IFN-I signaling
dysregulates host zinc
homeostasis during
invasive candidiasis

IFNs-I suppress zinc
intoxication and promote
pathogen fitness and
immune evasion

iScience

Article

Type I Interferons Ameliorate Zinc Intoxication of *Candida glabrata* by Macrophages and Promote Fungal Immune Evasion

Michael Riedelberger,[1] Philipp Penninger,[1] Michael Tscherner,[1] Bernhard Hadriga,[1] Carina Brunnhofer,[2] Sabrina Jenull,[1] Anton Stoiber,[1] Christelle Bourgeois,[1] Andriy Petryshyn,[1] Walter Glaser,[1] Andreas Limbeck,[2] Michael A. Lynes,[3] Gernot Schabbauer,[4,6] Guenter Weiss,[5] and Karl Kuchler[1,7,*]

SUMMARY

Host and fungal pathogens compete for metal ion acquisition during infectious processes, but molecular mechanisms remain largely unknown. Here, we show that type I interferons (IFNs-I) dysregulate zinc homeostasis in macrophages, which employ metallothionein-mediated zinc intoxication of pathogens as fungicidal response. However, *Candida glabrata* can escape immune surveillance by sequestering zinc into vacuoles. Interestingly, zinc-loading is inhibited by IFNs-I, because a Janus kinase 1 (JAK1)-dependent suppression of zinc homeostasis affects zinc distribution in macrophages as well as generation of reactive oxygen species (ROS). In addition, systemic fungal infections elicit IFN-I responses that suppress splenic zinc homeostasis, thereby altering macrophage zinc pools that otherwise exert fungicidal actions. Thus, IFN-I signaling inadvertently increases fungal fitness both *in vitro* and *in vivo* during fungal infections. Our data reveal an as yet unrecognized role for zinc intoxication in antifungal immunity and suggest that interfering with host zinc homeostasis may offer therapeutic options to treat invasive fungal infections.

INTRODUCTION

Candida glabrata represents an opportunistic intracellular human fungal pathogen, causing life-threatening infections in immunocompromised patients (Pappas et al., 2018). Of note, *C. glabrata* (*Cg*) infections have been sharply increasing over the past two decades, yet classical therapeutic options are limited owing to the inherent resistance against echinocandins and azoles (Fisher et al., 2018; Perlin et al., 2017; Taff et al., 2013; Vale-Silva and Sanglard, 2015). In addition, adaptive evolution equipped this fungal pathogen with a vast repertoire of defense mechanisms that facilitate immune evasion (Kasper et al., 2015; Kumar et al., 2019). For example, after phagocytosis by myeloid immune cells, *Cg* establishes an environmental niche in the host enabling growth and proliferation inside innate immune cells by suppressing the generation of reactive oxygen species (ROS), inhibiting phagolysosomal maturation, and nutrient acquisition through several pathways (Kumar et al., 2019; Seider et al., 2011). The immune defense in turn mounts local and systemic pro-inflammatory responses to boost clearing of *Cg* by macrophages and neutrophils (Netea et al., 2015).

The well-known type I interferon (IFN-I) cytokine family has been implicated in most if not all microbial and viral infections (McNab et al., 2015; Stifter and Feng, 2015). Remarkably, IFNs-I set pro-inflammatory stimuli aimed at supporting immune surveillance and defense. However, pro-inflammatory IFN-I actions can be both beneficial and detrimental in infectious settings, particularly in cases where excessive immunopathology drives self-imposed "collateral" oxidative damage to host tissues (Majer et al., 2012; McNab et al., 2015). Indeed, we have previously reported that IFNs-I drive the persistence of *Cg* in brain, liver, and spleen of *Ifnar1⁻/⁻* mice, thereby dysregulating the cellular iron homeostasis in macrophage subsets, which inadvertently facilitates fungal iron acquisition that enhances fungal fitness (Bourgeois et al., 2011; Riedelberger et al., 2020).

Among many pathways, iron homeostasis regulation appears as a major target of IFN-I and -II signaling (Nairz et al., 2008, 2018; Riedelberger et al., 2020). In addition, interferons share a common role in the

[1]Medical University of Vienna, Center for Medical Biochemistry, Max Perutz Labs Vienna, Campus Vienna Biocenter, Vienna, Austria

[2]Institute of Chemical Technologies and Analytics, TU Wien, Vienna, Austria

[3]Department of Molecular and Cell Biology, University of Connecticut, CT, USA

[4]Institute for Vascular Biology and Thrombosis Research, Center for Physiology and Pharmacology, Medical University of Vienna, Vienna, Austria

[5]Department of Internal Medicine II, Infectious Diseases, Immunology, Rheumatology, and Pneumology, Medical University of Innsbruck, Innsbruck, Austria

[6]Christian Doppler Laboratory for Arginine Metabolism in Rheumatoid Arthritis and Multiple Sclerosis, Vienna, Austria

[7]Lead Contact

*Correspondence: karl.kuchler@meduniwien.ac.at

https://doi.org/10.1016/j.isci.2020.101121

regulation of zinc (Zn) homeostasis. For example, IFN-I responses reduce plasma Zn concentrations by inducing hepatic metallothionein expression in various model organisms (Guevara-Ortiz et al., 2005; Van Miert et al., 1990; Morris and Huang, 1987; Sato et al., 1996), as well as in human cells (Friedman and Stark, 1985; Nagamine et al., 2005; Read et al., 2017). IFN-γ regulates plasma Zn concentrations (Morimoto et al., 1987), Zn transporter expression in intestinal epithelial cells and pancreatic β-cells (Egefjord et al., 2009; Melia et al., 2019), as well as Zn levels in mycobacteria-containing vacuoles (Wagner et al., 2005a). In contrast, IFN-λ3 increases intracellular Zn levels (Read et al., 2017). Although accumulating evidence suggests an interferon/Zn axis, the molecular players controlling the dynamic response have remained enigmatic. Interestingly, the interferon/Zn axis is under reciprocal control, because interferons regulate both cellular and systemic zinc levels. Labile Zn is required for optimal STAT1-dependent IFN signaling (Reiber et al., 2017) and modulates TLR signaling as well (Brieger et al., 2013; Maares and Haase, 2016; Wessels et al., 2017).

Proper innate and adaptive immune responses require tightly regulated intracellular Zn levels (Weiss and Carver, 2018). Indeed, Zn deficiency arising from malnutrition or mutations increases the susceptibility for infections and various other diseases (Ferreira and Gah, 2017; Lopez and Skaar, 2018; Vaeth and Feske, 2018). Of note, invading microbial pathogens inevitably rely on Zn for successful host infection and propagation within the host owing to metabolic restrictions within a given host. For example, neutrophils use calprotectin secretion to sequester Zn, thus creating a Zn-limited environment for pathogens (Zackular et al., 2015). By contrast, macrophages exert at least two context-dependent Zn defense strategies for several microbes (Subramanian Vignesh and Deepe, 2016). After phagocytosis of *Histoplasma capsulatum*, macrophages shuttle Zn from the phagolysosome into the cytoplasm to elicit fungal Zn starvation and elevated ROS production (Subramanian Vignesh et al., 2013a, 2016). In contrast, during infections with *Mycobacterium tuberculosis*, *Escherichia coli*, and *Salmonella enterica serovar Typhimurium* (*S. Typhimurium*), macrophages actually trigger phagolysosomal Zn accumulation to drive Zn intoxication and killing of the invading bacterial pathogens (Botella et al., 2011; Kapetanovic et al., 2016; Stocks et al., 2019). Thereby, macrophages exploit Zn-binding metallothioneins to control intracellular Zn sequestration and spatiotemporal Zn distribution during antimicrobial responses (Subramanian Vignesh and Deepe, 2017).

Here, we show that IFN-I responses dysregulate the Zn homeostasis in macrophages *in vitro* and *in vivo* during systemic *Cg* infections. We provide an in-depth mechanistic view of how macrophages employ Zn intoxication of fungal pathogens as a fungicidal defense. However, IFN-I signaling attenuates this defense by transcriptional suppression of host Zn transport systems. This response inadvertently leads to altered spatiotemporal Zn distribution that impairs otherwise fungicidal ROS production in macrophages. Invasive fungal infections by *Cg* elicit strong IFN-I responses, which in turn dysregulate splenic Zn homeostasis and the antifungal response of splenic macrophages. Thus, targeting the IFN-I-driven host immune surveillance or targeting fungal Zn homeostasis might provide therapeutic concepts to treat disseminated fungal infections or other microbial pathogens in general. Such therapeutic concepts targeting nutritional immunity would be highly advantageous, because they may help combating *Cg* or *C. auris*, as these fungal pathogens display pronounced inherent antifungal drug resistance rendering them refractory to conventional treatment.

RESULTS

IFNs-I Dysregulate Zn Homeostasis Genes in the Spleen during Systemic *Cg* Infections

We have previously reported that IFNs-I are detrimental for the host during systemic *Cg* infections (Bourgeois et al., 2011). *Ifnar1*$^{-/-}$ mice (which lack the Interferon alpha and beta receptor subunit 1) are unable to respond to IFN-I signals (Müller et al., 1994), and exhibit reduced fungal loads in liver, kidney, and spleen (Bourgeois et al., 2011). Because the spleen is a key target for microbial pathogens disseminating through the blood (Borges da Silva et al., 2015a, 2015b), we investigated the effects of IFN-I signaling on the splenic response during fungal infections. Therefore, wild-type (WT) and *Ifnar1*$^{-/-}$ mice were intravenously infected with 5 x 10^7 *Cg* colony-forming units (CFUs) per 25 g mouse weight. After 1, 3, 7, and 14 days post-infection, spleens were harvested and transcriptional profiling of splenic responses was performed by microarrays (Table S1). We showed that IFNs-I dramatically dysregulate iron homeostasis in macrophage populations and the spleen. Thereby, *Cg* inadvertently obtains IFN-I-mediated access to phagolysosomal iron pools, which facilitates fungal replication and persistence (Riedelberger et al., 2020).
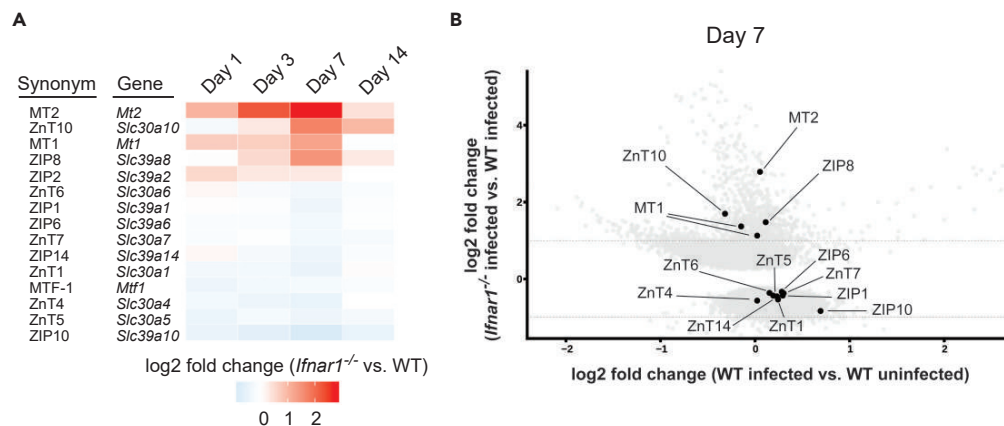
A

Synonym	Gene	Day 1	Day 3	Day 7	Day 14
MT2	*Mt2*				
ZnT10	*Slc30a10*				
MT1	*Mt1*				
ZIP8	*Slc39a8*				
ZIP2	*Slc39a2*				
ZnT6	*Slc30a6*				
ZIP1	*Slc39a1*				
ZIP6	*Slc39a6*				
ZnT7	*Slc30a7*				
ZIP14	*Slc39a14*				
ZnT1	*Slc30a1*				
MTF-1	*Mtf1*				
ZnT4	*Slc30a4*				
ZnT5	*Slc30a5*				
ZIP10	*Slc39a10*				

log2 fold change (*Ifnar1*$^{-/-}$ vs. WT)

0 1 2

B Day 7

log2 fold change (*Ifnar1*$^{-/-}$ infected vs. WT infected)

log2 fold change (WT infected vs. WT uninfected)

Figure 1. IFN-I Signaling Dysregulates the Splenic Transcriptional Response of a Zn-Homeostasis-Related Gene Set during Invasive *C. glabrata* Infection

(A) Microarray analysis of DEGs in WT and *Ifnar1*$^{-/-}$ spleens after intravenous *Cg* infection for 1, 3, 7, or 14 days (n = 3 mice per group). Total RNA extracted from spleens was hybridized to the SurePrint G3 Mouse GE 8 × 60K Microarray chip (Agilent Technologies). Heatmap shows the differentially expressed Zn-homeostasis-related genes in infected *Ifnar1*$^{-/-}$ mice relative to infected WT mice after normalization to uninfected mice (cut-off: FDR<0.05). All listed genes were up- or downregulated at least at one time point during the course of systemic infection (p < 0.05).

(B) Scatter plot of DEGs from WT and *Ifnar1*$^{-/-}$ spleens at day 7 of systemic *Cg* infection. Each dot represents one probe on the microarray, and black dots (FDR <0.05) correspond to Zn homeostasis-related genes.

DEG, differentially expressed gene; FDR, false discovery rate; see also Figure S1.

Of note, many pathogenic infections can cause subtle alterations of metal availabilities in different cellular compartments of macrophages (Wagner et al., 2005a, 2005b). Further, alterations of zinc homeostasis as well as interferon signaling impact the hepatic immune responses in different disease models (Read et al., 2017). Thus, based on the effects of IFNs-I on splenic iron homeostasis regulation (Riedelberger et al., 2020), we assumed a possible involvement of IFN-I signaling in Zn homeostasis during *Cg* infections. Based on an in-depth literature search, we used a defined set of immunity-associated Zn homeostasis genes for the bioinformatic analysis of our existing microarray dataset (Table S2) (Riedelberger et al., 2020). Interestingly, *Cg*-infected *Ifnar1*$^{-/-}$ spleens exhibited dysregulated expression of genes involved in the regulation of Zn homeostasis at least once during the time course of systemic infection (Figure 1A). For example, Zn importers (ZIPs; *Slc39a1-14*), Zn exporters (ZnTs; *Slc30a1-10*), metallothioneins (MT), as well as the transcriptional master regulator for Zn homeostasis MTF-1 showed significant expression changes upon loss of IFN-I signaling. Strikingly, the metallothioneins MT1 and MT2, which are cytoplasmic Zn chaperones orchestrating potent antimicrobial defences (Subramanian Vignesh and Deepe, 2017), were swiftly induced upon *Cg* infection (Figures S1A and S1B) and showed highest expression in *Ifnar1*$^{-/-}$ spleens at day 7 after fungal challenge (Figure 1B). Thus, these data demonstrate that IFN-I signaling in response to *Cg* infections alters the splenic response with respect to Zn homeostasis.

IFNs-I Alter Zn Transporter Expression upon *Cg* Infection

Macrophages utilize several sophisticated mechanisms to ensure proper Zn homeostasis regulation during microbial infections (Subramanian Vignesh and Deepe, 2016). To investigate in detail how IFNs-I modulate Zn homeostasis in antifungal immunity, we infected primary bone-marrow-derived macrophages (BMDMs) with *Cg*. Interestingly, overnight treatment of BMDMs with IFNβ subsequently increased fungal survival upon macrophage infection (Figure 2A). When BMDMs were pre-treated with the cell-permeable, high-affinity Zn chelator TPEN before *Cg* challenge, the IFNβ-mediated effects on fungal survival were partially rescued (Figure 2A). BMDM functions such as *Cg* phagocytosis, autophagy, as well as cellular viability remained unaltered by IFNβ. However, IFNs-I increase the intracellular replication of phagocytosed *Cg* after 4 h of BMDM infection (Riedelberger et al., 2020). Thus, IFNs-I promote fungal survival in macrophages, which partly depends on altered Zn homeostasis regulation.

Next, we performed an unbiased expression analysis of Zn importers (ZIPs; *Slc39a1-14*) and Zn exporters (ZnTs; *Slc30a1-10*). Upon BMDM infection with *Cg*, ZIP4 and ZIP14, as well as ZnT1, were highly upregulated, but were strikingly suppressed by IFNα and IFNβ treatment (Figures 2B and S2A). Although ZIPs
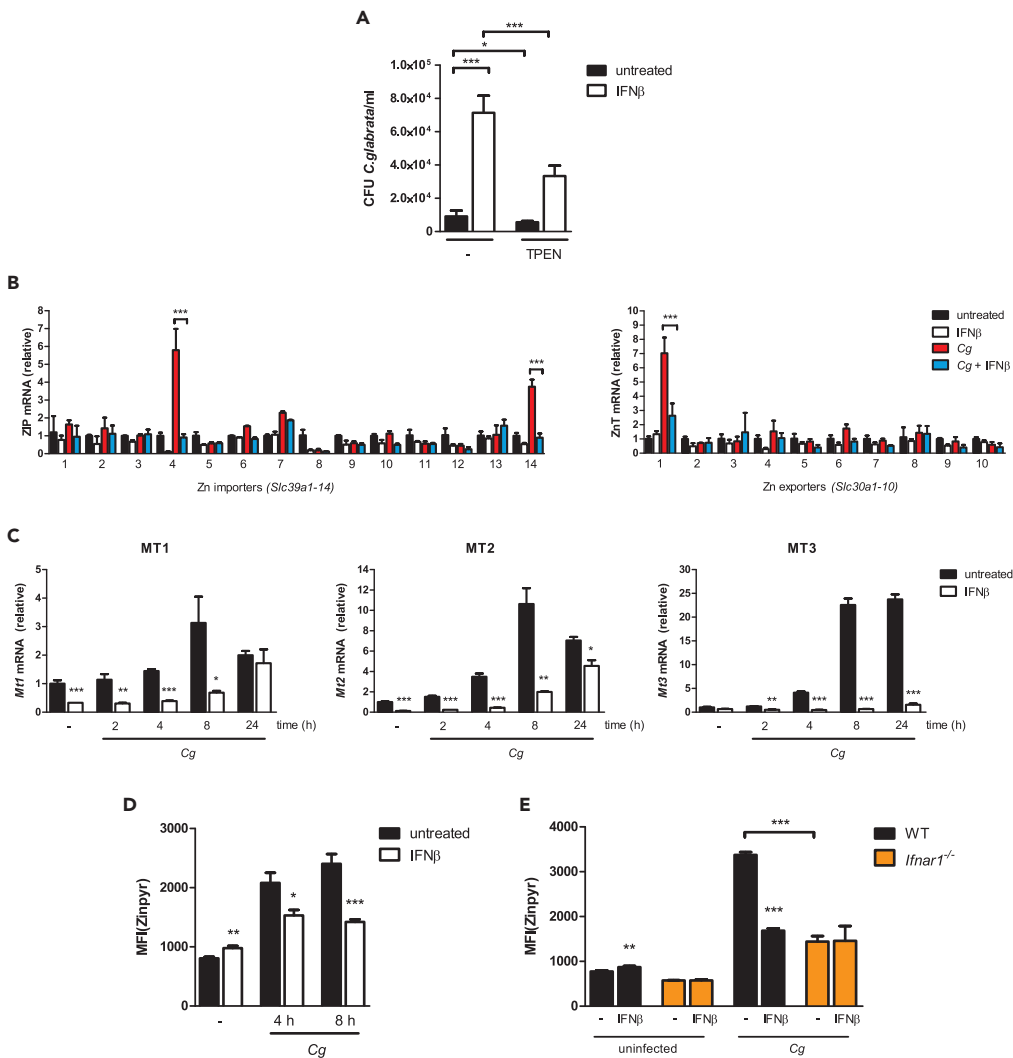
Figure 2. IFNs-I Inhibit Zn Transporter Expression and Prevent Zn Burst in *C. glabrata*-Infected BMDMs

(A) *In vitro* survival assay of *Cg* after 24-h interaction with WT BMDMs untreated or IFNβ-treated upon pre-incubation with TPEN for 1 h.

(B) RT-qPCR analysis of *Slc39a1-14* and *Slc30a1-10* mRNA levels in WT BMDMs untreated or IFNβ-treated during *Cg* infection (normalization to *Actb*). One-way ANOVA with Bonferroni's post hoc analysis.

(C) RT-qPCR analysis of *Mt1*, *Mt2*, and *Mt3* mRNA levels in WT BMDMs untreated or IFNβ-treated during *Cg* infection (normalization to *Actb*).

(D) Zinpyr assay of WT BMDMs untreated or IFNβ-treated after 4 and 8 h of *Cg* infection.

(E) Zinpyr assay of BMDMs untreated or IFNβ-treated during *Cg* infection for 8 h.

Data are representative of two (B–E) or three (A) independent experiments. Mean and SD are shown; * p value < 0.05, ** p value < 0.01, *** p value < 0.001; (A and C–E) Student's t test; (B) one-way ANOVA with Bonferroni's post hoc analysis. See also Figure S2.

are responsible for Zn mobilization into the cytoplasm (Subramanian Vignesh and Deepe, 2016), ZnT1 may mediate Zn transport into mycobacteria-containing phagolysosomes for Zn intoxication (Botella et al., 2011). In addition, IFNα and IFNβ inhibited the *Cg*-induced expression of the metallothioneins *Mt1*, *Mt2*, and *Mt3* (Figures 2C and S2A). These data suggest that *Cg* infections induce Zn mobilization and, perhaps Zn transport to intracellular organelles in macrophages, which is suppressed by IFN-I responses.

The IFN-I-mediated dysregulation of Zn homeostasis genes prompted our hypothesis that IFNs-I might alter Zn metal ion concentrations in BMDMs upon *Cg* infections. Thus, we performed inductively coupled plasma mass spectrometry (ICP-MS) to quantify Zn concentrations in whole-cell lysates of *Cg*-infected BMDMs after excluding

fungal debris. Although Zn levels remained unaltered upon IFNβ treatment (Figure S2B), the quantification of total steady-state Zn concentrations might miss dynamic exchanges between Zn storage organelles (e.g. mitochondria, ER, Golgi) with the labile, bioactive Zn pool in the cytoplasm (Kambe et al., 2015). To quantify cytoplasmic Zn alterations, we stained BMDMs with the Zn-specific fluorescent dye Zinpyr (Walkup et al., 2000), which binds intracellular, labile Zn^{2+} ions, leading to increased Zinpyr fluorescence (Figueroa et al., 2015). Thus, intracellular Zn levels positively correlate with the fluorescence intensity of Zinpyr. As observed by flow cytometry analysis, overnight treatment with IFNβ resulted in slightly increased Zinpyr fluorescence and, therefore, elevated intracellular Zn levels in uninfected BMDMs (Figure 2D). Strikingly, after 4 h of Cg infection, a burst of free Zn was observed in BMDMs, which was diminished by IFNβ treatment (Figures 2D and S2C). However, the IFNα/β-mediated inhibition of the Zn burst was absent in $Ifnar1^{-/-}$ BMDMs (Figures 2E and S2D). Of note, the basal, constitutive IFN-I signaling (Gough et al., 2012) in BMDMs was still required for the subsequent Zn burst following Cg infections, because $Ifnar1^{-/-}$ BMDMs failed to upregulate intracellular Zn levels (Figures 2E and S2D). Taken together, these results show that IFNs-I suppress ZIP/ZnT gene expression in infected macrophages, thus preventing the burst of free intracellular Zn in BMDMs. By contrast, basal IFNAR1 signaling is still required for Zn mobilization during fungal challenge, which reflects a paradoxical dichotomy IFNs-I can exhibit in certain infection settings.

Zn Shuttling to Cg-Containing Phagolysosomes Is Attenuated by IFNs-I

Next, we wanted to visualize the spatiotemporal regulation of Zn distribution in Cg-infected BMDMs using confocal microscopy and Zinpyr staining. Uninfected BMDMs showed minor Zinpyr fluorescence within the cytoplasm (Figures 3A and 3B). Strikingly, upon infection with a mCherry-expressing Cg strain, we identified two discrete BMDM populations. First, Zn-resting BMDMs showed only minor cytoplasmic Zn signals and second, a Zn-activating BMDM population, which triggered a cytoplasmic Zn burst and Zn accumulation in phagocytosed Cg yeast cells, as judged from the observed Zinpyr-mCherry colocalization (Figures 3C, S3A, and S3B). Indeed, $Zn^{high}Cg$ cells colocalized with acidic phagocytic compartments, as evident from the staining by LysoBlue (Figure 4A), showing that Zn is transported into Cg-engulfing mature phagolysosomes. However, in IFNβ-treated BMDMs, $Zn^{high}Cg$ are barely detected, suggesting that IFNβ indeed inhibits phagolysosomal Zn accumulation (Figure 3D).

Interestingly, two discrete populations of Cg were visualized within macrophages, which were the aforementioned $Zn^{high}Cg$ population and a Zn^{low} population (Figure 4B). Although Zn^{high} yeast cells were entirely stained by Zinpyr, only an intracellular organelle was Zinpyr-positive in Zn^{low} fungal cells. Of note, the vacuole in the non-pathogenic yeast Saccharomyces cerevisiae acts as crucial detoxification system upon Zn stress, because large amounts of Zn can be transported and stored in this organelle (Gerwien et al., 2018; Simm et al., 2007). Indeed, by using the vacuolar membrane-specific dye FM4-64, we identified the vacuole as the Zn-rich organelle within $Zn^{low}Cg$ (Figures 4C and S3C). In addition, $Zn^{low}Cg$ remained negative for lysosomal staining, showing that $Zn^{low}Cg$ were able to actively inhibit phagolysosomal maturation (Figure 4D). In contrast, $Zn^{high}Cg$ failed to suppress lysosomal fusion and, therefore, localized only to acidic phagolysosomes. Notably, Zn detoxification via vacuolar sequestration and inhibition of phagolysosomal maturation by Cg are active processes that require a functional fungal metabolism (Kumar et al., 2019). Thus, we speculated that the $Zn^{low}Cg$ population contains viable yeast cells within macrophages, whereas $Zn^{high}Cg$ cells were killed by macrophages. Indeed, $Zn^{high}Cg$ corresponded to dead fungal cells owing to their positive PI staining, whereas $Zn^{low}Cg$ remained viable because they were PI-negative (Figure 4E). Of note, the regulation of Zn homeostasis in Cg in general is little understood. However, in S. cerevisiae, Zn sequestration into the vacuole is regulated by Zrc1 and Cot1 (MacDiarmid et al., 2000; Wilson and Deepe, 2019). Indeed, a genetic deletion of ZRC1 in Cg resulted in a substantial survival defect upon BMDM infection (Figure 4F), showing that ZRC1 is crucial for fungal immune evasion by Cg.

Taken together, these results show that upon Cg infection, BMDMs induce a Zn burst for subsequent Zn transport and accumulation into Cg-containing phagolysosomes. Thereby, Cg cells fail to suppress lysosomal fusion, leading to Zn accumulation and fungal killing, whereas viable, metabolically active $Zn^{low}Cg$ manage to inhibit phagolysosomal maturation and detoxify Zn by sequestration into the fungal vacuole. However, IFNs-I suppress the spatiotemporal Zn distribution in BMDMs, implying a survival and fitness advantage for Cg.

IFNs-I Suppress Zn Intoxication of Cg

Next, we wanted to investigate in detail the relationship between Zn concentrations and fungal survival during host-pathogen interactions. When we performed flow cytometry analysis, we again observed
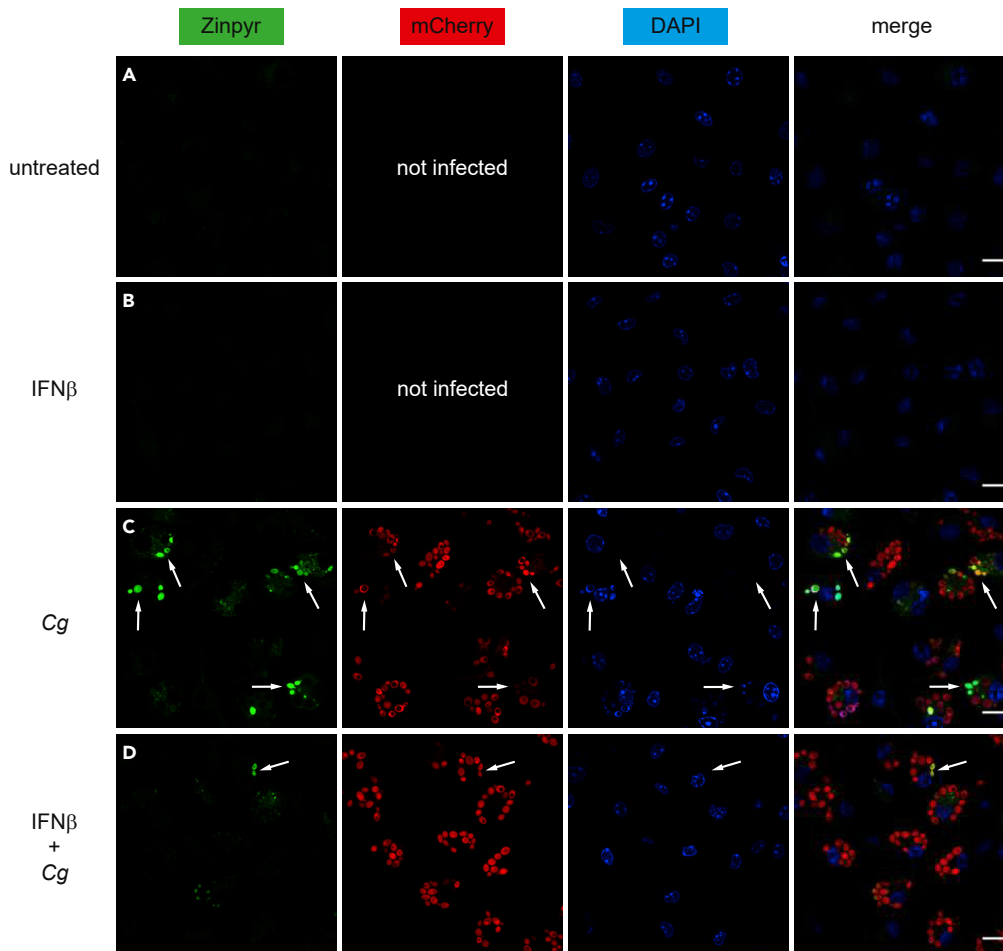
Figure 3. IFNs-I Prevent Zn Transport into *C. glabrata*-Containing Phagolysosomes

(A–D) Confocal microscopy analysis of Zn (Zinpyr; green), mCherry-expressing *Cg* (red), and nucleus (DAPI; blue) in untreated or IFNβ-treated WT BMDMs after 4 h of *Cg* infection. Merge, overlay of all three channels. Arrows point at Zn^{high} yeast cells within infected BMDMs. The scale bar represents 10 μm.

Data are representative of two (A–D) independent experiments. See also Figure S3.

Zn-resting and Zn-activating macrophage populations after *Cg* infections, which can be discriminated by their different Zinpyr fluorescence intensity (Figure S4A). Upon *Cg* infection, Zn levels remained similar in Zn-resting BMDMs when compared with uninfected BMDMs. By contrast, Zn levels where increased in *Cg*-infected, Zn-activating BMDMs. Interestingly, IFNβ treatment reduced the generation of Zn-activating BMDMs during *Cg* infection (Figure S4A). Thus, we reasoned that the appearance of Zn-activating BMDMs might represent an antifungal defense mechanism, which macrophages use for Zn intoxication and killing of *Cg*. Indeed, high Zn concentrations were toxic for *Cg* and prevented fungal growth (Figure S4B), which is fully consistent with previous reports (Crawford et al., 2018; Gerwien et al., 2018).

In order to test our hypothesis, we conducted two approaches. First, after mCherry$^+$ *Cg* infection, we separated Zn-resting and Zn-activating BMDMs via cell sorting. Then, following BMDM lysis, we plated the cell lysates on YPD plates to quantify surviving fungal CFUs (Figure 5A). Thereby, we determined the *Cg* survival ratio in BMDMs (Figure 5B), which is calculated as the surviving *Cg* CFUs per sorted BMDMs divided by the total amount of *Cg* per sorted BMDM (represented by total mCherry fluorescence). Strikingly, *Cg* viability was strongly reduced in Zn-activating BMDMs when compared with Zn-resting BMDMs (Figure 5A), showing that Zn-activating BMDMs can execute efficient fungal killing. A graphic illustration depicts this notion (Figure S4C). Second, we aimed to quantify the inviable Zn^{high} *Cg* population upon host-pathogen interactions. Therefore, we infected BMDMs with WT *Cg* and incubated BMDMs with Zinpyr at the end of
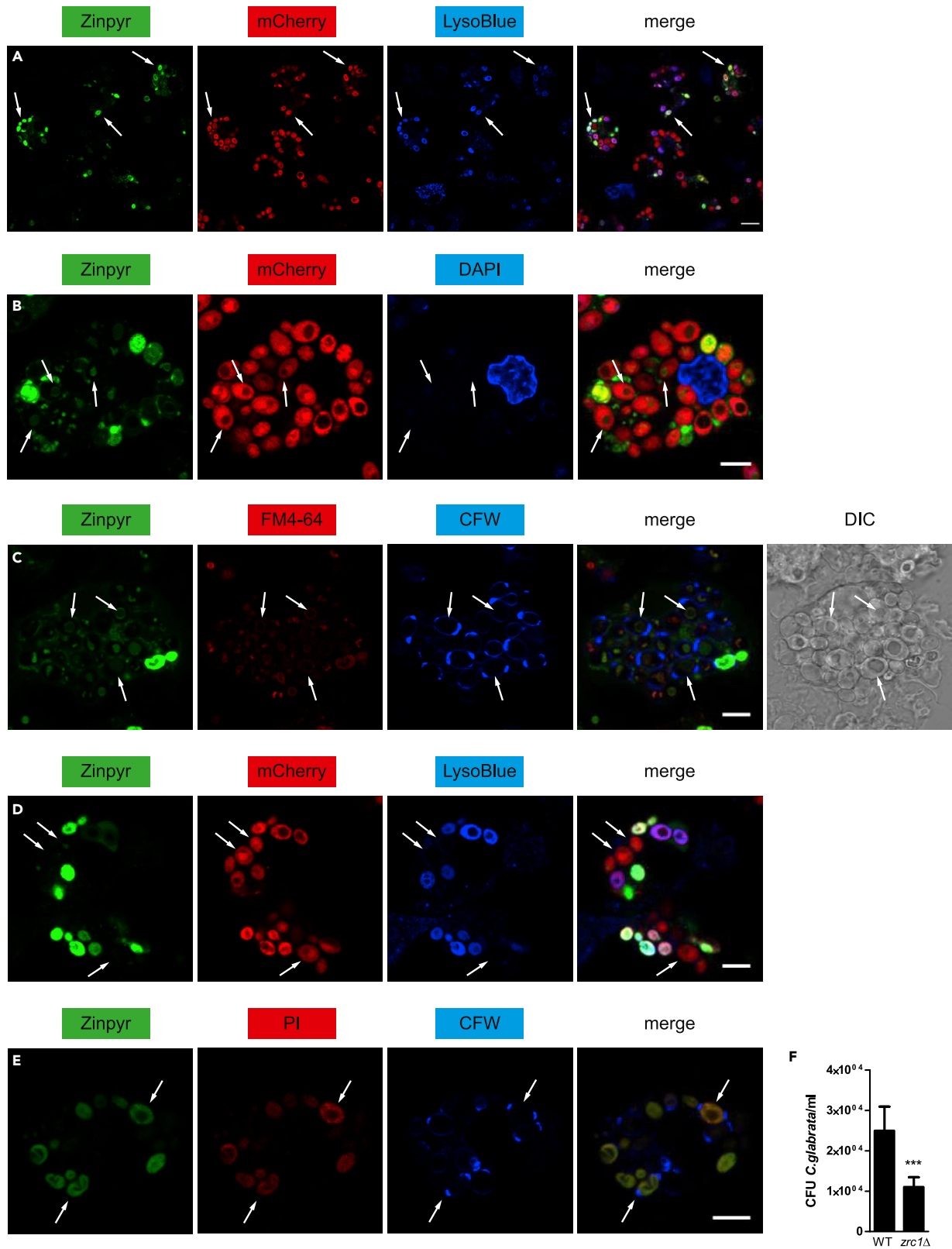
Figure 4. *C. glabrata* Counteracts Phagolysosomal Zn Stress by Vacuolar Zn Sequestration

(A–E) Confocal microscopy analysis in WT BMDMs after 4 h of *Cg* infection. Analysis of Zn (Zinpyr; green), mCherry-expressing *Cg* (red), vacuolar membranes of *Cg* (FM4-64; red), dead fungal cells (PI; red), acidic/lysosomal staining (LysoBlue; blue), nucleus (DAPI; blue), and Calcofluor-White-stained *Cg* (CFW; blue). Arrows point at (A) yeasts within phagolysosomes, (B) Zn^{low}*Cg*(C) vacuolar localization of Zn in *Cg*(D) Zn^{low}*Cg* prevents phagolysosomal maturation, and (E) Zinpyr$^+$ PI$^+$ fungal cells. Merge, overlay of all three channels. DIC, differential interference contrast. The scale bar represents (A) 10 μm or (B–E) 5 μm.

(F) *In vitro* survival assay of WT and zrc1Δ *Cg* after 24-h interaction with WT BMDMs.

Data are representative of two (A–E) or four (F) independent experiments. Mean and SD are shown; *** p value < 0.001 (Student's t test). See also Figure S3.

infection (to stain Zn^{high} yeast cells). We then lysed BMDMs to release intracellular *Cg* and finally stained these fungal cells with PI. Flow cytometry allows for easy separation of fungal cells from smaller particles using forward scatter/side scatter (FSC/SSC) discrimination (Figures 5C and S5A). Interestingly, after 2 h of infection, almost all *Cg* cells isolated from BMDMs were Zinpyr-positive, with about 30% of these Zinpyr$^+$ *Cg* being inviable since also PI-positive (Figure 5C). As expected, the Zinpyr$^+$ PI$^+$ *Cg* population further increased, when alive but heat-stressed fungal cells (1 min at 65°C) were used as a positive control for BMDM infection. Next, we performed a time course experiment to follow the Zinpyr$^+$ PI$^+$ *Cg* population over time. We observed that *Cg* was rapidly loaded with Zn, and after 4 h, approximately 40% of all fungal cells were within the Zn^{high} PI$^+$ dead *Cg* population (Figure 5D). When we discriminated between live (PI-negative) and dead (PI-positive) *Cg*, we observed that Zn levels for dead *Cg* remained high throughout the infection course (Figure 5E). However, the Zn levels of live *Cg* continually decreased over time, presumably due to inhibition of phagolysosomal maturation and/or vacuolar Zn sequestration by *Cg*. In support of our hypothesis, the *Cg zrc1Δ* mutant strain showed an increased Zn^{high} PI$^+$ dead population (Figure S5B), which might be caused by the defective ability to cope with toxic Zn concentrations (Figure S5C). Strikingly, upon treatment of BMDMs with IFNα or IFNβ, we observed that IFNs-I strongly inhibited the appearance of the Zn^{high} PI$^+$ dead *Cg* population (Figures 5D and S5D), which is fully consistent with our confocal microscopy data. Accordingly, mCherry$^+$*Cg* cells isolated from IFNβ-treated BMDMs showed reduced Zn acquisition when compared with fungal cells from untreated BMDMs (Figure 5F).

Further, we assumed that the IFNβ-mediated reduction in fungal Zn stress also translates into altered expression of Zn homeostasis genes in *Cg*. Therefore, we performed gene expression analysis from sorted *Cg*-infected BMDMs to exclude a possible interference from extracellular adherent *Cg* cells. Indeed, *Cg* isolated from IFNβ-treated BMDMs exhibited minor metallothionein expression of *MT-I*, showing that *Cg* encounters reduced intracellular Zn stress when phagocytosed by IFNβ-treated BMDMs (Figure 5G). Next, we infected BMDMs with live and heat-killed *Cg* upon pre-treatment with Bafilomycin A$_1$ or DPI. Bafilomycin A$_1$ is a selective inhibitor of vacuolar H$^+$ ATPase, which prevents phagolysosomal maturation (Yamamoto et al., 1998), and DPI represents an NADPH oxidase inhibitor (Hancock and Jones, 1987). Strikingly, Bafilomycin A$_1$ and DPI robustly reduced the generation of Zn^{high} PI$^+$ *Cg* population (Figure 5H), showing that both phagolysosomal maturation and ROS production are required for potent Zn intoxication of *Cg*, presumably due to ROS-mediated Zn dissociation from Zn-MT complexes (Krężel and Maret, 2017). Taken together, these results show that BMDMs rapidly mobilize Zn to phagocytosed fungal cells to elicit Zn intoxication, which depends on phagolysosomal maturation and ROS generation. However, IFN-I signaling inhibits this antifungal immune defense mechanism, thus diminishing Zn stress *Cg* encounters in macrophages.

MT1 and MT2 Are Required for Zn Intoxication of Pathogens

Zinc-scavenging metallothioneins are key players for cytoplasmic Zn shuttling during intracellular Zn mobilization (Subramanian Vignesh and Deepe, 2017). Of note, our data revealed that IFNs-I robustly suppress metallothionein gene expression upon *Cg* infection both *in vitro* and *in vivo*. To investigate whether metallothioneins are involved in antifungal Zn intoxication, we undertook two different approaches. First, we used CRISPR/Cas9-generated *Mt1$^{-/-}$ Mt2$^{-/-}$* double knock-out RAW 264.7 cells (Wu et al., 2017) for *Cg* infection. Strikingly, lack of MT1 and MT2 abrogated the generation of the Zn^{high} PI$^+$ dead *Cg* population (Figure 6A), which was also accompanied with reduced Zn loading of *Cg* (Figure 6B). Second, we used primary bone marrow-derived macrophages from *Mt1$^{-/-}$ Mt2$^{-/-}$* mice to verify the role of MT1 and MT2 (Rice et al., 2016). Interestingly, MT1 and MT2 were indeed required for Zn transport into *Cg*-containing vacuoles, because *Mt1$^{-/-}$ Mt2$^{-/-}$* BMDMs revealed reduced amounts of Zn^{high}*Cg*, whereby remaining fungal cells in *Mt1$^{-/-}$ Mt2$^{-/-}$* BMDMs comprised the Zn^{low}*Cg* population that displayed a remarkable vacuolar Zn staining (Figure 6C). These results were further supported by flow cytometry analysis, because lack of MT1 and MT2 in BMDMs reduced the generation of the Zn^{high} PI$^+$ dead *Cg* population (Figure 6D), which was even more diminished upon IFNβ treatment. Moreover, the inhibition of Zn intoxication upon loss of MT1 and MT2 resulted in a decreased fungicidal activity of *Mt1$^{-/-}$ Mt2$^{-/-}$* BMDMs (Figure 6E). However, as

A Cg-infected macrophages:

B

Cg survival ratio:

$$= \frac{\text{live } Cg \text{ per BMDM}}{\text{total } Cg \text{ amount per BMDM}}$$

OR

$$= \frac{Cg \text{ CFUs per sorted BMDM}}{\text{MFI(mCherry) of BMDMs}}$$
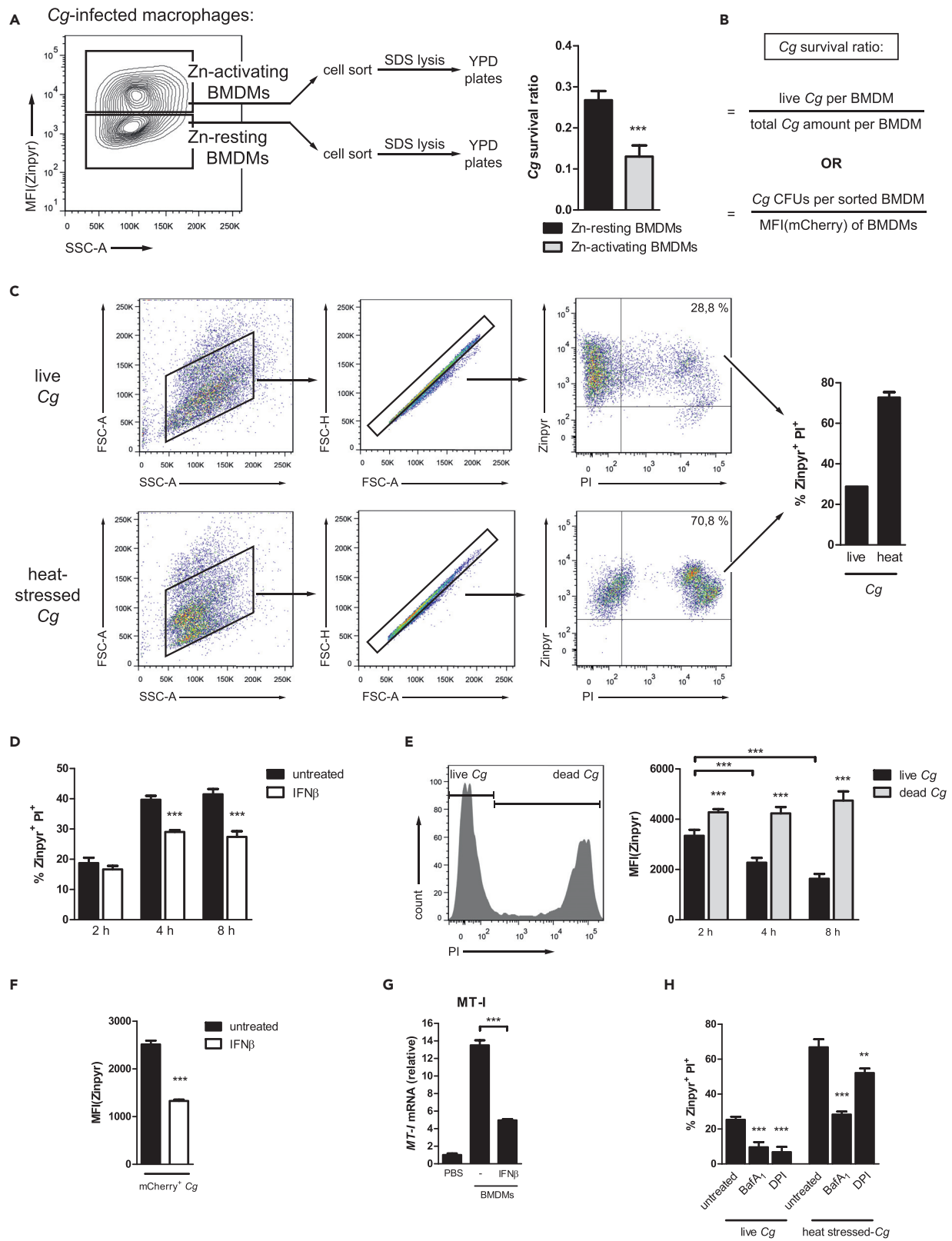
C

D

E

F

G

H

Figure 5. IFNs-I Inhibit Fungal Zn Intoxication during BMDM Infection

(A) Schematic representation and survival ratio quantification of *Cg* isolated from FACS-sorted Zn-resting and Zn-activating WT BMDMs after 4 h of infection.

(B) Calculation of the *Cg* survival ratio. The amount of CFUs per BMDM was normalized to the MFI(mCherry) of the respective BMDM population.

(C) Fungal Zn intoxication assay. Gating strategy and quantification of Zinpyr$^+$ PI$^+$*Cg* after WT BMDM infection with live or heat-stressed fungal cells for 2 h.

(D) Fungal Zn intoxication assay of *Cg* isolated from untreated or IFNβ-treated WT BMDMs.

(E) Histogram and quantified Zinpyr fluorescence intensity of live and dead Zinpyr$^+$ *Cg* isolated from WT BMDMs after several hours of infection.

(F) Zinpyr-based fungal Zn acquisition of mCherry$^+$ *Cg* isolated from WT BMDMs after 8 h of infection.

(G) RT-qPCR analysis of *MT-I* mRNA levels in *Cg* upon infection of untreated or IFNβ-treated BMDMs for 4 h (normalization to *ACT1*).

(H) Fungal Zn intoxication assay of live or heat-stressed *Cg* isolated from BMDMs untreated or treated with Bafilomycin A$_1$ or DPI after 2 h of fungal challenge.

Data are representative of two (A, C, G, and H) or three (D–F) independent experiments. Mean and SD are shown; *** p value < 0.001 (Student's t test). See also Figures S4 and S5.

expected, the Zn burst upon *Cg* infection was unaffected in *Mt1*$^{-/-}$ *Mt2*$^{-/-}$ BMDMs (Figure 6F), because Zn mobilization within the cytoplasm is primarily controlled by ZIP and ZnT zinc transporters. Because MTs do not co-localize with mCherry$^+$-*Cg*, we believe that MTs are not directly shuttled into *Cg*-containing phagosomes (Figure S6). Taken together, these results uncover an exciting role for MT1 and MT2 in antifungal immunity in addition to Zn sequestration (Subramanian Vignesh et al., 2013b). Once Zn is shuttled into the cytoplasm from intracellular compartments or the extracellular space, MT1 and MT2 act as Zn chaperones to facilitate subsequent Zn transport into *Cg*-containing phagosomes that drives fungal Zn intoxication and pathogen killing.

JAK1 and IRF3 Are Engaged by IFNs-I for Zn Homeostasis Inhibition

Next, we wanted to identify signal transduction components IFNs-I engage for subsequent inhibition of Zn homeostasis regulation. Upon binding of IFNs-I to IFNAR1, the receptor-associated kinases, Janus kinase 1 (JAK1) and TYK2, are phosphorylated and activated, triggering signaling pathways via STATs (via IRFs), PI3K, as well as MAPK signaling (Hervas-Stubbs et al., 2011). Strikingly, when we pre-treated BMDMs with the specific JAK1 inhibitor Filgotinib (GLPG0634) (Van Rompaey et al., 2013) prior to IFNβ stimulation, the inhibitory effect of IFNβ on Zn mobilization upon *Cg* infection was fully restored (Figure 7A). TYK2 was not required, because the inhibitory effect of IFNβ was observed upon loss of TYK2 (Figure 7B). Thus, JAK1 was exclusively engaged upon IFNβ stimulation. Further, JAK1 inhibition abolished the IFNβ-mediated transcriptional suppression of MT1, MT2, MT3, ZnT1, and increased transcription of MTF-1, the master regulator of key Zn homeostasis genes such as MTs (Figure 7C) (Günther et al., 2012). Notably, the inhibitory effects of IFNs-I bypassed STAT signaling (STAT1, STAT2, STAT3, STAT4, STAT5a/b, STAT6), p85α signaling, MAPK signaling (via MEK1), or the signal transducers IRF1 and IRF9 (Figures S7A–S7I). Strikingly, *Irf3*$^{-/-}$ BMDMs were completely rescued from IFNβ-mediated Zn homeostasis inhibition, because their Zn burst was completely unaffected by IFNβ treatment (Figure 7D).

However, signaling via PTEN (Chen and Guo, 2017; Worby and Dixon, 2014) was necessary for an efficient Zn mobilization upon BMDM challenge with *Cg*, because *Pten*$^{-/-}$ BMDMs failed to mount a robust Zn burst during *Cg* infection (Figure 7E). These results are in line with a previous report showing that PTEN also controls MTF-1 activation by associating with MTF-1 in the cytoplasm. Further, the PTEN protein phosphatase activity dephosphorylates MTF-1, which is required for regulation of target genes such as ZnT1 (Lin et al., 2012). Taken together, these data highlight that IFN-I stimulation engages JAK1 in a central role as "signaling relay" acting downstream of IFNAR1 to control signaling via IRF3 to regulate Zn homeostasis inhibition upon *Cg* infection. Moreover, BMDMs engage PTEN signaling for robust Zn mobilization, presumably via the regulation of MTF-1 activity.

Dysregulation of Zn Homeostasis Suppresses the Generation of Fungicidal ROS

To ensure potent oxidative responses upon microbial challenge, macrophages must tightly control cytoplasmic Zn concentrations (Subramanian Vignesh et al., 2013b). Of note, cytoplasmic Zn ions suppress the NADPH oxidase-dependent ROS generation by inhibiting the hydrogen voltage-gated channel HV1 (*Hvcn1*) (DeCoursey et al., 2003). Consequently, upon infection with *Histoplasma capsulatum*, BMDMs upregulate MTs for subsequent Zn sequestration to sustain HV1 function and ROS generation (Subramanian Vignesh et al., 2013a). Because IFNs-I prevented *Mt* gene expression during *Cg* infection, we investigated whether IFN-I-mediated dysregulation of Zn homeostasis can also affect the antifungal ROS response. Indeed, BMDM stimulation with IFNβ suppressed the basal and *Cg*-induced amounts of intracellular ROS by about 30% (Figure 8A). However, phosphorylation of p40, a key regulatory subunit and activation marker of NADPH oxidase (Belambri et al., 2018), remained unaffected by IFNβ stimulation (Figure 8B). As a consequence of altered ROS generation, *Cg* sorted from IFNβ-treated BMDMs revealed a diminished oxidative stress response, due to the reduced expression of the ROS-detoxifying fungal catalase *CTA1* (Figure 8C) (Cuéllar-Cruz et al., 2008). Strikingly, TPEN treatment strongly increased ROS
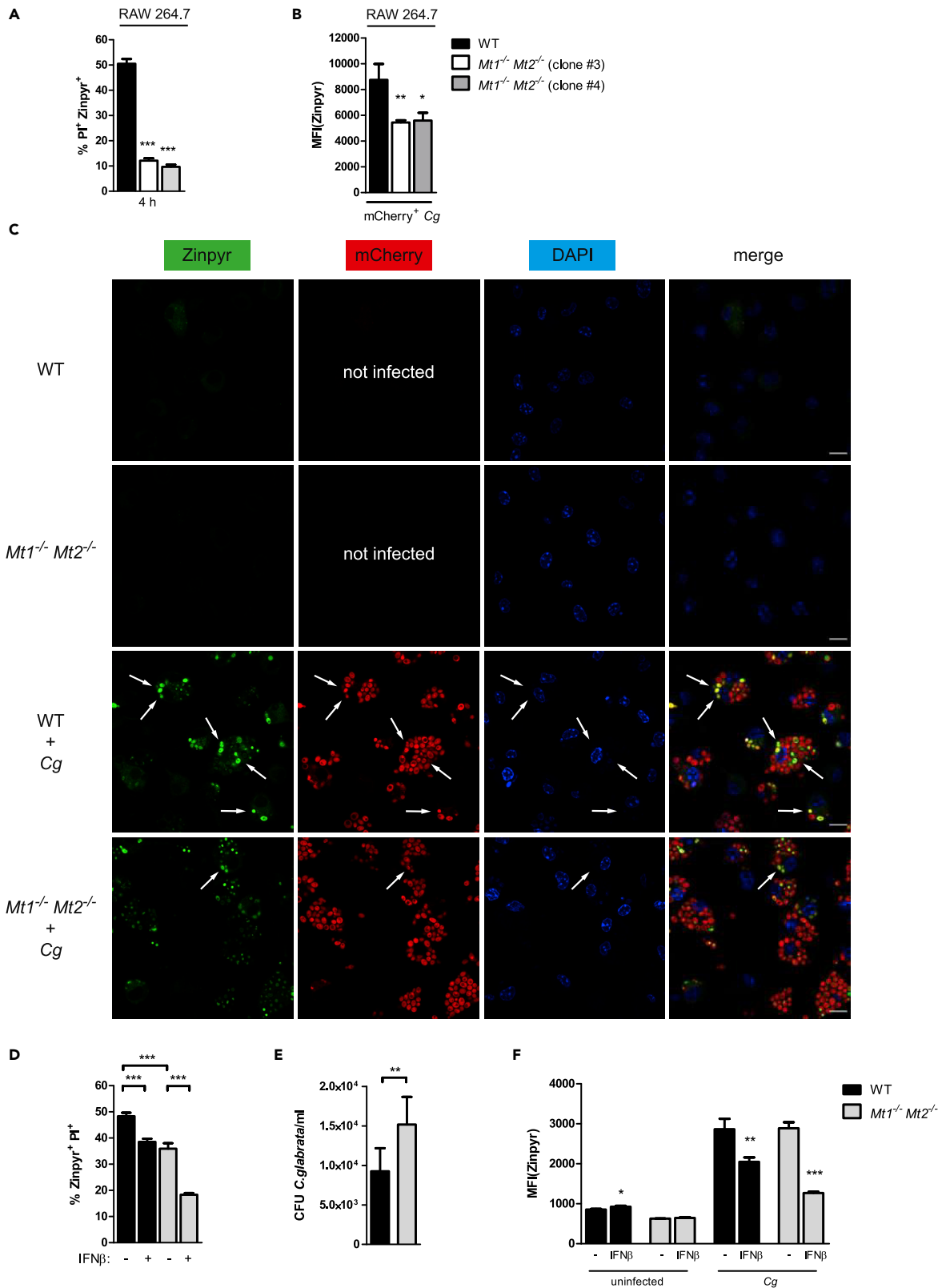
Figure 6. MT1 and MT2 Promote Fungal Zn Intoxication

(A) Fungal Zn intoxication assay of *Cg* isolated from RAW264.7 cells after 4 h of infection.

(B) Zinpyr-based fungal Zn acquisition of *Cg* isolated from RAW 264.7 cells after 6 h of infection.

(C) Confocal microscopy analysis of Zn (Zinpyr; green), mCherry-expressing *Cg* (mCherry; red), and nucleus (DAPI; blue) in BMDMs after 4 h of *Cg* infection.

(D) Fungal Zn intoxication assay of *Cg* isolated from untreated or IFNβ-treated BMDMs after 4 h of infection.

(E) *In vitro* survival assay of *Cg* after 24 h interaction with BMDMs.

(F) Zinpyr-assay of BMDMs untreated or IFNβ-treated during *Cg* infection for 8 h.

Merge, overlay of all three channels. Arrows point at Zn^{high} yeast cells within infected BMDMs. The scale bar represents 10 μm. Data are representative of two (A–E) or three (F) independent experiments. Mean and SD are shown, * p value < 0.05, ** p value < 0.01, *** p value < 0.001 (Student's t test). See also Figure S6.

generation in untreated and IFNβ-treated BMDMs, showing that IFNβ-mediated ROS inhibition can be rescued by Zn chelation (Figure 8A). Consistently, the presence of exogenous Zn completely abrogated the *Cg*-induced ROS response (Figure S8A). In addition, Zn chelation by MTs was crucial for a robust ROS generation upon *Cg* infection, because both primary *Mt1*$^{−/−}$ *Mt2*$^{−/−}$ BMDMs (Figure 8D) and *Mt1*$^{−/−}$ *Mt2*$^{−/−}$ RAW 264.7 cells (Figure S8B) showed a diminished ROS response. Further, we detected substantially reduced *Hvcn1* mRNA levels in IFNα- as well as IFNβ-treated BMDMs, showing that IFNs-I, in addition to the previously observed reduction of *Mt* gene expression, also suppressed *Hvcn1* gene expression (Figures 8E and S8C). These data show that MT-mediated cytoplasmic Zn sequestration is crucial for the antifungal ROS response, which is suppressed by IFNs-I via a dual mechanism. First, IFN-I-mediated suppression of *Mt* gene expression results in BMDM failure to efficiently chelate Zn ions, and second, expression of ROS-promoting *Hvcn1* is dysregulated by IFNs-I.

IFNs-I Modulate Splenic Macrophage Zn Pools upon Invasive *Cg* Infections

Tissue-resident macrophages in the spleen represent a heterogeneous phagocyte population, which exert crucial defense mechanisms during systemic infections by microbial pathogens (Borges da Silva et al., 2015a, 2015b). Our data clearly show that IFN-I signaling modulates the splenic transcriptional regulation of Zn homeostasis genes and that Zn intoxication of pathogens by macrophages represents an antifungal defense strategy. Therefore, we wanted to monitor cellular Zn homeostasis alterations in splenic macrophage populations upon systemic *Cg* infection. After harvesting spleens from WT and *Ifnar1*$^{−/−}$ mice, two populations of CD11b$^+$ SSC^{int} splenic macrophages (SpMs) were identified: an F4/80^{int} SpM population and an F4/80^{hi} SpM population (Figure 9A). Of note, F4/80^{int} and F4/80^{hi} SpMs show intermediate to high CD11c expression (Riedelberger et al., 2020). Indeed, previous studies reported that red pulp macrophages and splenic DCs, as well as a skin DC subset, share a common phenotype of CD11c and F4/80 co-expression (Borges da Silva et al., 2015a, 2015b; McLachlan et al., 2009).

In uninfected mice, the lack of *Ifnar1*$^{−/−}$ did not affect intracellular Zn levels in F4/80^{int} and F4/80^{hi} SpMs, although F4/80^{hi} SpMs revealed higher basal Zn acquisition (Figure 9B). Strikingly, at day 1 after *Cg* challenge, F4/80^{int} SpMs from *Ifnar1*$^{−/−}$ mice showed reduced Zn levels when compared with WT SpMs, an effect that was not observed in F4/80^{hi} SpMs. These results are consistent with our *in vitro* data showing the double-edged effects of IFN-I signaling on Zn homeostasis. Thereby, BMDM treatment with IFNα/IFNβ suppressed the Zn burst upon *Cg* infection. However, basal IFNAR1 signaling was still required for cytoplasmic Zn mobilization, because *Ifnar1*$^{−/−}$ BMDMs failed to trigger a Zn burst (Figures 2E and S2D). Therefore, we propose that F4/80^{int} SpMs from *Ifnar1*$^{−/−}$ mice fail to upregulate intracellular Zn levels upon systemic *Cg* infection due to the lack of basal IFNAR1 signaling. Of note, at day 7 of *Cg* challenge, F4/80^{int} SpMs in WT and *Ifnar1*$^{−/−}$ mice exhibited similar Zn levels (Figure 9B). Taken together, Zn mobilization in splenic macrophages upon systemic *Cg* infection represents a swift but transient response process, for which F4/80^{int} SpMs require basal IFNAR1 signaling.

To investigate the antifungal effector functions of SpMs in more detail, we cultivated primary splenic macrophages *ex vivo*. Strikingly, in line with our *in vitro* BMDM data, IFNβ-treated SpMs showed reduced fungal Zn intoxication after 8 h of *Cg* infection, which was fully rescued in *Ifnar1*$^{−/−}$ SpMs (Figure 9C). However, *Cg*-infected SpMs failed to mount a robust Zn burst (Figure 9D), suggesting that SpMs do not rely on extensive intracellular Zn mobilization as observed before in BMDMs. Again, and seen in the microarray data, IFNβ suppresses *Mt3* expression, whereby *Ifnar1*$^{−/−}$ SpMs show increased *Mt3* transcript levels (Figure 9E). Importantly, IFNβ promoted fungal survival and fitness in splenic macrophages, because IFNβ-treated SpMs revealed elevated intracellular replication of *Cg* (Riedelberger et al., 2020). In conclusion, as for other microbial infections, IFN-I signaling is detrimental for the host during *Cg* infections, because it also dysregulates the spatiotemporal Zn distribution in macrophages, thereby inadvertently suppressing other antifungal defense mechanisms that enable increased fungal fitness and immune evasion.
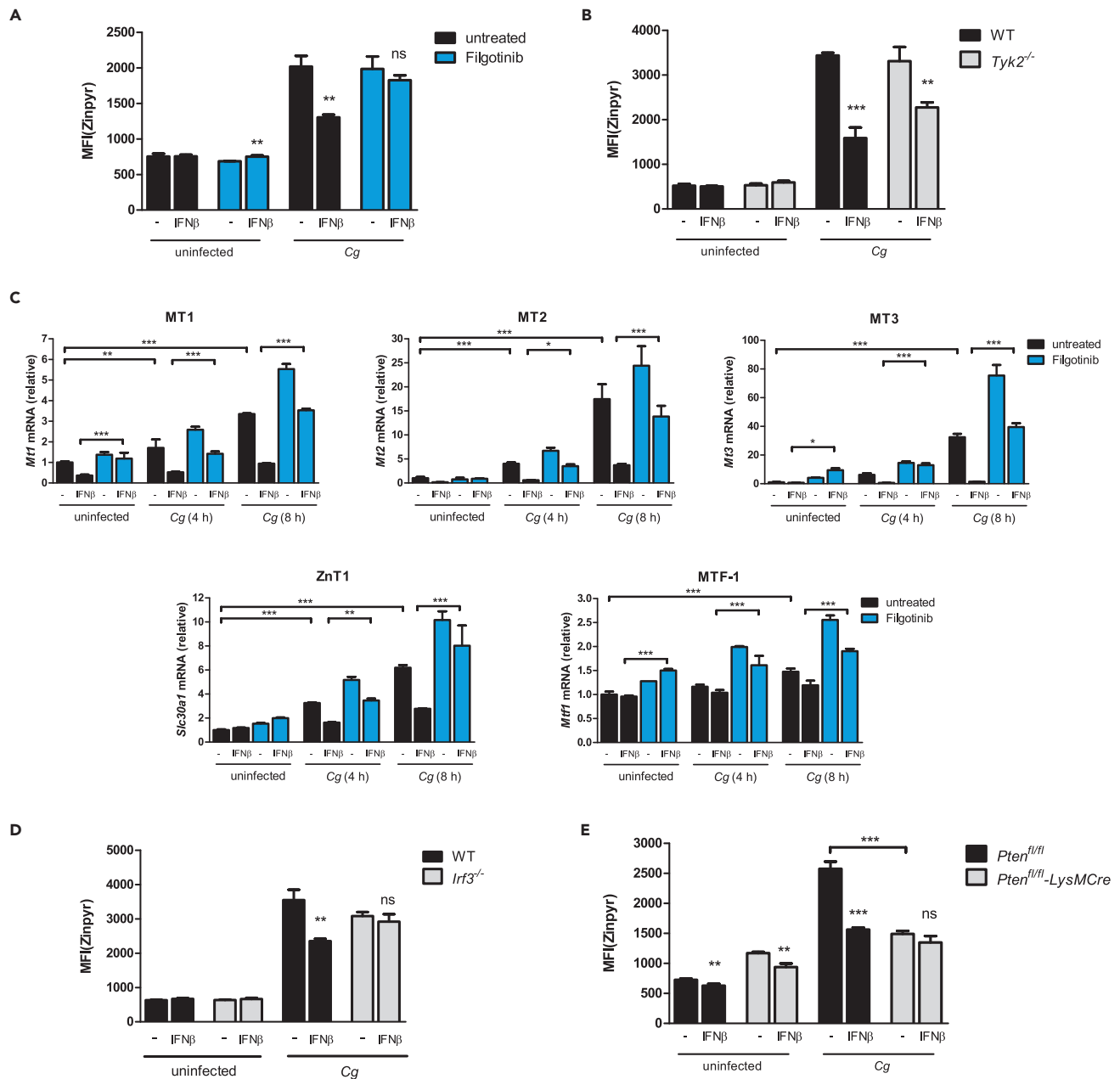
Figure 7. IFNs-I Engage JAK1 and IRF3 for Zn Homeostasis Dysregulation

(A) Zinpyr-assay of untreated or IFNβ-treated BMDMs upon pre-treatment with Filgotinib and 8 h of *Cg* infection.

(B) Zinpyr-assay of untreated or IFNβ-treated WT BMDMs upon *Cg* infection for 8 h.

(C) RT-qPCR analysis of *Slc30a1*, *Mt3*, and *Mtf1* mRNA levels in untreated or IFNβ-treated WT BMDMs upon pre-treatment with Filgotinib and *Cg* infection (normalization to *Actb*). One-way ANOVA with Bonferroni's post hoc analysis.

(D and E) Zinpyr assay of untreated or IFNβ-treated BMDMs upon *Cg* infection for 8 h.

Data are representative of two (A–E) independent experiments. Mean and SD are shown; * p value < 0.05, ** p value < 0.01, *** p value < 0.001; ns, not statistically significant; (A, B, D, and E) Student's t test; (C) one-way ANOVA with Bonferroni's post hoc analysis. See also Figure S7.

DISCUSSION

We have reported that IFN-I signaling is detrimental for the host during *Cg* infection by promoting fungal persistence in various organs (Bourgeois et al., 2011), thereby IFNs-I dysregulating host iron homeostasis, leading to unrestricted exploitation of intramacrophage iron pools by *Cg* (Riedelberger et al., 2020). Although confirming reports have been scarce, iron and Zn homeostasis in mammalian cells might be
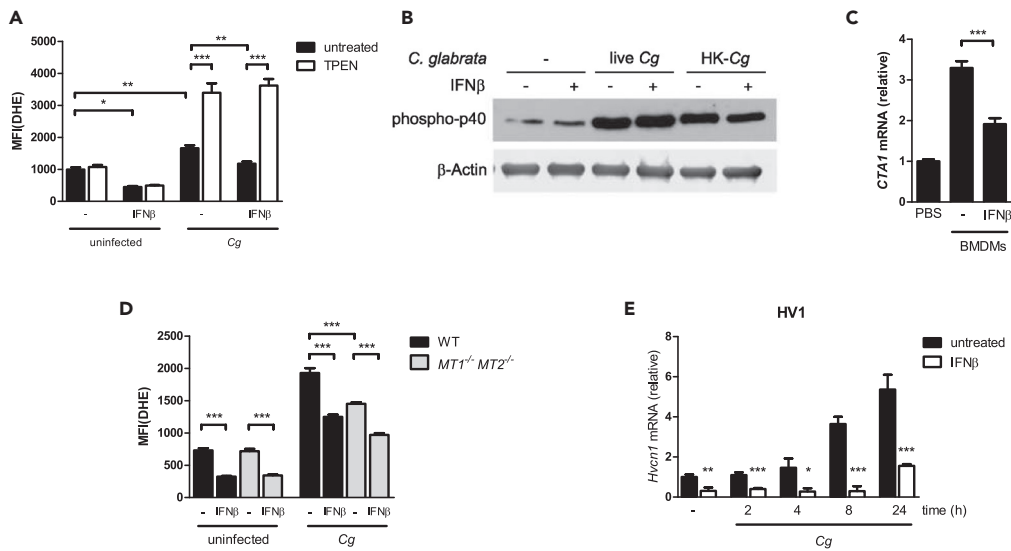
Figure 8. Fungicidal ROS Response in BMDMs Is Inhibited by IFNs-I

(A) Detection of intracellular ROS by DHE in untreated or IFNβ-treated WT BMDMs challenged with Cg for 2 h and simultaneous TPEN (20 μM) treatment.

(B) Immunoblot analysis of phospho-p40 activation in untreated or IFNβ-treated WT BMDMs challenged with live or heat-killed Cg for 60 min.

(C) RT-qPCR analysis of CTA1 mRNA levels in Cg upon infection of untreated or IFNβ-treated BMDMs for 2 h (normalization to ACT1).

(D) Detection of intracellular ROS by DHE in untreated or IFNβ-treated BMDMs after 2 h of Cg infection.

(E) RT-qPCR analysis of Hvcn1 in WT BMDMs untreated or IFNβ-treated during Cg infection (normalization to Actb).

Data are representative of two (A–E) independent experiments. Mean and SD are shown; * p value < 0.05, ** p value < 0.01, *** p value < 0.001; (B, C, and E) Student's t test (A and D); one-way ANOVA with Bonferroni's post hoc analysis. See also Figure S8.

tightly intertwined and co-regulated, as reported before by our group for *Saccharomyces cerevisiae* (Landstetter et al., 2010). Further, reports showing an involvement of IFNs-I in Zn homeostasis regulation are limited, especially under infectious conditions (Guevara-Ortiz et al., 2005; Van Miert et al., 1990; Morris and Huang, 1987; Read et al., 2017; Sato et al., 1996). Here, we provide an in-depth mechanistic view of how IFN-I-mediated immune responses trigger a dysregulation of Zn homeostasis and spatiotemporal metal ion distribution in macrophages during *Cg* infection. IFN-I signaling diminishes several antifungal defense mechanisms at the cellular as well as organ level. First, we uncover that primary macrophages utilize MT1/MT2-mediated Zn intoxication to eradicate an intracellular fungal pathogen. However, host IFNs-I impair this antimicrobial defense by preventing Zn shuttling to *Cg*-containing phagolysosomes. Second, Zn homeostasis dysregulation by IFNs-I debilitates a potent fungicidal ROS response. Third, upon invasive *Cg* infection, IFNs-I suppress the transcriptional regulation of Zn homeostasis genes in the spleen and affect the cellular Zn regulation in splenic macrophages.

Zn intoxication has not been recognized as fungicidal mechanism to clear the intracellular pathogen *Cg*. However, our data demonstrate that MT1 and MT2 adopt a crucial role in antifungal immunity. Zn mobilization by Zn transporters, and MT1 and MT2, acting as Zn chaperones for Zn shuttling into *Cg*-containing phagolysosomes, drives Zn intoxication of phagosomally entrapped fungal cells. Interestingly, this process requires phagolysosomal maturation and ROS generation, presumably due to ROS-mediated dissociation of Zn from Zn-MT complexes (Kręźel and Maret, 2017). The involvement of MTs in Zn intoxication during mycobacterial infections has been proposed but experimental evidence has been lacking (Botella et al., 2011). However, beautiful work shows that MT1 and MT2 are required for intracellular Zn sequestration by shuttling Zn away from phagolysosomes that contain *H. capsulatum* (Subramanian Vignesh et al., 2013a). In contrast, MT3 facilitates the access of *H. capsulatum* to labile Zn pools in macrophages, inadvertently leading to fungal Zn acquisition and persistence (Chowdhury et al., 2019; Subramanian Vignesh et al., 2016) Therefore, our data further highlight the function of MT1 and MT2 as central hubs that control the bidirectional Zn shuttling into or out of phagolysosomes during fungal infections. How MTs modulate
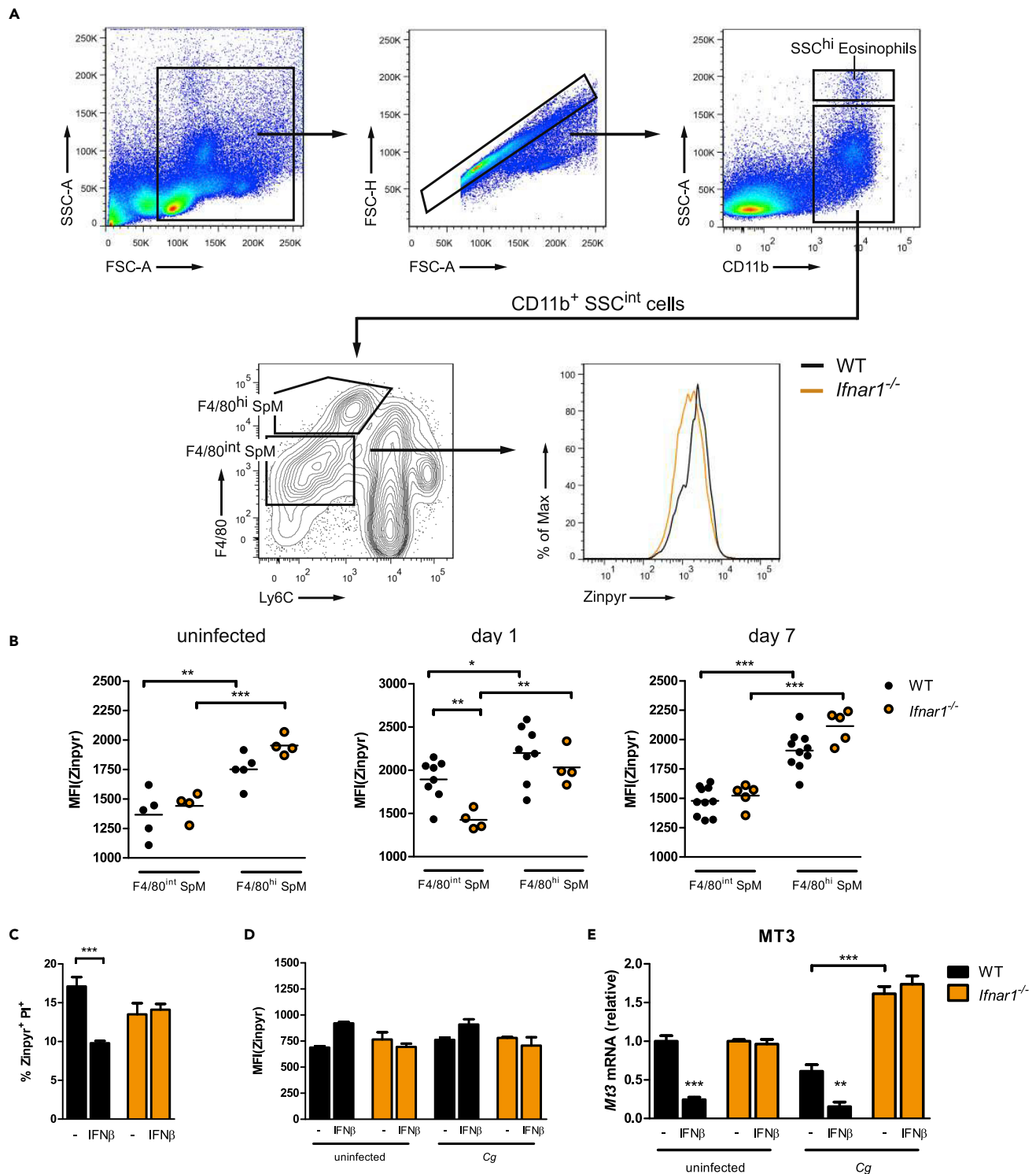
Figure 9. IFNs-I Suppress Zn Homeostasis Regulation in Splenic Macrophages during Invasive *C. glabrata* Infection *In Vivo*

(A) Gating strategy for quantification of intracellular Zn levels in splenic macrophage subsets during *Cg* infection. Histogram of Zinpyr fluorescence by F4/80^{int}SpMs from WT and *Ifnar1*$^{-/-}$ mice.

(B) Zinpyr-assay of splenic CD11b$^+$ SSC^{int} F4/80$^+$ macrophages isolated from WT and *Ifnar1*$^{-/-}$ mice uninfected or IV infected with 5 × 10^7 CFUs *Cg* for up to 7 days (n = 4–10 mice per group). Each symbol represents one mouse; horizontal bars indicate the calculated mean.

(C) Fungal Zn intoxication assay of *Cg* isolated from untreated or IFNβ-treated *ex vivo* SpMs after 8 h of fungal challenge.

Figure 9. *Continued*

(D) Zinpyr assay of untreated or IFNβ-treated *ex vivo* SpMs upon *Cg* infection for 8 h.

(E) RT-qPCR analysis of *Mt3* mRNA levels in untreated or IFNβ-treated *ex vivo* SpMs upon and *Cg* infection for 8 h (normalization to *Actb*).

Data are representative of two (B, C, and E) or three (D) independent experiments. Mean and SD are shown, * p value < 0.05, ** p value < 0.01, *** p value < 0.001 (Student's t test).

the bivalent zinc transport into/out of pathogen-containing phagosomes for antimicrobial zinc intoxication or pathogen zinc starvation remains elusive. Potential mechanisms have been proposed, including direct MT shuttling into the phagosome for zinc release, MT binding to phagolysosomal membranes and ZIP/ZnT-mediated Zn transport, as well as simultaneous engulfment of extracellular zinc-bound MTs with the pathogen upon phagocytosis (Subramanian Vignesh and Deepe, 2017). It is also tantalizing to speculate that autophagosomal fusion with lysosomes could play a role in this phagosomal Zn delivery.

However, IFN-I responses suppress Zn intoxication of pathogens by transcriptional downregulation of Zn transporters and MTs, thereby promoting fungal fitness and survival. Further, we show that the receptor-associated JAK1, which is exclusively engaged by IFNs-I to transduce inhibitory signals via IRF3, enhances the dysregulation of Zn homeostasis. Interestingly, IFN-I signaling operates as double-edged sword for Zn intoxication, because IFNs-I suppress this antifungal defense mechanism, but basal, constitutive IFNAR1 signaling is required to mount a robust Zn burst. Resting immune cells rely upon basal IFNAR1 signaling by constitutively producing or responding to IFNs-I for the proper regulation of numerous cell functions (Gough et al., 2012). However, such functions can be suppressed by massive IFN-I production and over-shooting IFN-I responses, which could even induce opposing signaling effects downstream of IFNAR1 receptor signaling (Gough et al., 2012; Hertzog and Williams, 2013; Schreiber and Piehler, 2015). In addition, although not affected by IFNs-I, we show that PTEN signaling is critical for Zn intoxication. PTEN is crucial for a potent Zn burst during *Cg* infection, presumably due to its involvement in MTF-1 activation as previously described (Lin et al., 2012). Thus, these data provide an in-depth mechanistic view how immune cells exploit Zn intoxication for clearing pathogens. Moreover, the dysregulation of Zn homeostasis by IFN-I signaling appears as an additional role of pro-inflammatory IFNs-I and likely plays a role in most, if not all, known functions of IFN-I responses.

IFNs-I are involved in multiple infectious diseases by exerting a plethora of pleiotropic functions in immune surveillance. Whether these effects drive pathogen clearance or inadvertently promote pathogen persistence is highly context and model dependent (Kernbauer et al., 2013; McNab et al., 2015; Stifter and Feng, 2015). In viral infections, IFNs-I activate cytotoxic effector cells (NK cells, CD8+ T cells) to orchestrate lysis of virus-infected cells, boost the production of virus-neutralizing antibodies, and induce antibody class switching (Teijaro, 2016). However, in certain settings, IFNs-I can also increase viral persistence and immunopathology (Snell et al., 2017) by inducing chronic immunosuppression of T cells and by promoting apoptosis of epithelial cells (Davidson et al., 2014; Teijaro et al., 2013; Wilson et al., 2013). During bacterial infections, IFNs-I augment leukocyte recruitment by controlling cytokine/chemokine production and by inducing expression of antibacterial effector molecules such as IDO, iNOS, or guanylate-binding proteins (Boxx and Cheng, 2016; Huang et al., 2019; MacMicking, 2012). However, IFN-I responses are also immunosuppressive during infections with several intracellular pathogens, including *Listeria monocytogenes* and *M. tuberculosis*. Thereby, IFNs-I sensitize several immune cell types to bacterial virulence factors and elicit apoptosis, suppress macrophage activation by inducing the downregulation of IFNγR expression, inhibit the production of pro-inflammatory cytokines, or downregulate iNOS expression (Calame et al., 2016; Dhariwala and Anderson, 2014; Donovan et al., 2017; Snyder et al., 2017; Toledo Pinto et al., 2018). In *C. albicans* infections, IFNs-I promote antifungal immunity by controlling chemokine production, leukocyte migration, NK cell activation, and epithelial barrier functions (Biondo et al., 2011; delFresno et al., 2013; Domínguez-Andrés et al., 2017; Li et al., 2017, 2019). In contrast, exaggerated IFN-I responses reveal detrimental effects such as inhibition of inflammasome activation and inadvertently drive hyperinflammation and immunopathology during Candida spp infections (Bourgeois et al., 2011; Gabrielli et al., 2015; Guarda et al., 2011; Jensen et al., 1992; Majer et al., 2012; Stawowczyk et al., 2018; Riedelberger et al., 2020). Further, patients suffering from chronic mucocutaneous candidiasis exhibit defective IFN-I responses and suppressed antifungal IL-17 immunity (Casanova et al., 2012; Liu et al., 2011; Smeekens et al., 2013; van de Veerdonk et al., 2011). Finally, IFNs-I reveal double-edged functions in fungal infections with *Aspergillus fumigatus* (Espinosa et al., 2017; Gafa et al., 2010; Loures et al., 2015; Ramirez-Ortiz et al., 2011; Romani et al., 2006; Seyedmousavi et al., 2018), *Cryptococcus neoformans* (Biondo et al., 2008; Sato et al., 2015; Sionov et al., 2015), and *H. capsulatum*

(Inglis et al., 2010; Van Prooyen et al., 2016). Owing to our presented data, we propose that dysregulation of metal ion homeostasis by IFN-I signaling represents an unrecognized concept of IFN-I biology in infectious diseases.

In addition to altering Zn homeostasis, IFNs-I strongly control the potency of the ROS response by macrophages, which is a key innate antifungal defense utilized by most phagocytes (Belambri et al., 2018; Cachat et al., 2015; Hogan and Wheeler, 2014). IFNs-I modulate the expression of ZnT/ZIP transporters and MTs in uninfected BMDMs, leading to increased intracellular Zn levels. However, cytoplasmic, unbound Zn ions are well known to inhibit the function of the proton channel HV1, which is required to mount a robust ROS response (DeCoursey, 2016; DeCoursey et al., 2003; Subramanian Vignesh et al., 2013a). During ROS production upon pathogen recognition, phagocytes simultaneously induce the expression of antioxidative MTs to minimize deleterious side effects on host tissues (Ruttkay-Nedecky et al., 2013). In addition, MTs are simultaneously required to bind cytoplasmic Zn, thereby augmenting antimicrobial ROS responses (Subramanian Vignesh and Deepe, 2017). Thus, our work reveals a dichotomous function of Zn sequestration by MT1 and MT2 in antifungal immunity. First, phagolysosomal Zn transport for Zn intoxication and second, promotion of HV1 function for maximal ROS production.

The dual functions of Zn ions may seem paradoxical at first hand. However, Zn is an essential metal required by numerous fundamental cellular process (Ferreira and Gah, 2017), but owing to the potent toxicity, Zn levels and subcellular Zn pools must be subject to tight and dynamic control (Lonergan and Skaar, 2019). Indeed, intraphagolysosomal/cytoplasmic Zn ions have to be kept low due to the mentioned inhibitory effects on the ROS response. However, Zn ions within the phagolysosome are required for fungal Zn intoxication. Thus, we propose a model in which cellular Zn homeostasis represents a delicate balance, for which macrophages are obliged to dynamically regulate the spatiotemporal distribution of Zn to ensure maximal efficiency for fungal clearance. First, the generation of ROS represents a swift but only temporary antifungal mechanism at the phagocytosis step (Blanco-Menéndez et al., 2015; Frohner et al., 2009; Salvatori et al., 2018; Warnatsch et al., 2017; Wellington et al., 2009). MTs are then engaged for Zn sequestration to boost HV1 function. Although the vast majority of fungal cells are killed in this initial phase by the oxidative burst, a considerable amount of Cg cells employ immune evasion mechanisms to establish intracellular niches for fungal replication and survival (Kumar et al., 2019). Thus, as a second line of defense, macrophages utilize Zn intoxication to tackle Cg survivors. Once Zn transporters are expressed and localize to the phagolysosome, MTs operate as Zn shuttling system to drive Zn intoxication, reaching maximal efficiency approximately 4 h after macrophage infection. We propose that ZnT1 is crucial for phagolysosomal Zn accumulation, and our data fully support earlier results concerning the role of ZnT1 (Botella et al., 2011).

We also show that IFNs-I suppress Zn homeostasis genes *in vivo* during the splenic response to systemic Cg infections. Remarkably, *ZnT10, ZIP2, ZIP8*, as well as *Mt1* and *Mt2* expressions are strongly diminished by IFNAR1 signaling. Interestingly, our microarray results are consistent with *in vitro* primary macrophage experiments, where the downregulation of MTs by IFNs-I is seen. Thus, our data additionally demonstrate a pivotal role for MTs in the spleen during fungal infections. Of note, and as proposed, the observed IFN-I-mediated transcriptional alterations also translate into a temporary dysregulation of cellular Zn levels in splenic macrophages upon invasive Cg infection *in vivo*.

However, the IFN-I-mediated suppression of MTs is contrasting previous studies showing that IFNα induces hepatic MT expression in several animal models (Guevara-Ortiz et al., 2005; Morris and Huang, 1987; Sato et al., 1996) and humans (Friedman and Stark, 1985; Nagamine et al., 2005). Of note, the reported transcriptional induction of MTs was only transient and timely restricted. Because we have primed our macrophages overnight with IFNs-I, a possible explanation could be that long-term stimulation with IFNs-I facilitates MT suppression. Further, cell-type-specific effects and differences in cellular environments in varying anatomical locations might also contribute to the reported observations. Moreover, we have not looked into the liver response, which displays an entirely different immunological competence. Although tissue-resident macrophage populations such as Kupffer cells are highly abundant in liver tissues (Macpherson et al., 2016), their role in antifungal defense at large has not been explored (Xu and Shinohara, 2017). Of note, Kupffer cells do phagocytose circulating *C. albicans* and *C. neoformans* cells to prevent fungal dissemination and launch pro-inflammatory cytokine responses (Øverland et al., 2005; Sun et al., 2019).

Virulence of fungal pathogens requires a tightly balanced Zn homeostasis (Wilson and Deepe, 2019). For example, Zn transporters are transcriptionally regulated in the yeast *S. cerevisiae* by the Zap1 regulator (Ballou and Wilson, 2016). In *C. albicans*, Zrt1 and Zrt2 are required for Zn uptake in a pH-dependent manner, thereby contributing to fungal virulence (Crawford et al., 2018; Kim et al., 2008). This regulatory mechanism closely resembles fungal Zn uptake in *A. fumigatus* (Amich et al., 2009), suggesting that the pH-dependency of Zn transport has been evolutionary conserved in fungal pathogens (Wilson, 2015). When encountering Zn limitation during phagocytosis, *C. albicans* secretes the protein Pra1 to sequester host-cell-derived Zn ions. Subsequently, Pra1 re-associates with fungal cells via cell-surface-localized Zrt1 to mediate Zn delivery, thereby also contributing to endothelial tissue invasion (Citiulo et al., 2012). Pra1 also contributes to fungal cell enlargement during Zn limitation (Malavia et al., 2017). Interestingly, metal acquisition via uptake of secreted cation-binding proteins/metabolites is predominantly conserved for bacterial pathogens (Kramer et al., 2019; Neumann et al., 2017; Palmer and Skaar, 2016), highlighting a distinguished role for the Pra1-Zrt1 system in *C. albicans*. Although a conserved locus structure *aspf2-zrfC* appears to exist in *A. fumigatus* (Amich et al., 2010), the Pra1-Zrt1 interaction represents a confirmed but unique zincophore system in fungi (Gerwien et al., 2018; Lehtovirta-Morley et al., 2017). In contrast, *C. albicans* counteracts environmental Zn excess and toxicity by Zrc1-mediated Zn compartmentalization in intracellular zincosomes, which is also implicated in fungal virulence (Crawford et al., 2018).

Likewise, bacterial pathogens have evolved sophisticated defense mechanisms to specifically prevent Zn intoxication. For instance, *M. tuberculosis* and *E. coli* employ P_1-type ATPases to facilitate cellular Zn efflux, whereas *S. typhimurium* relies on Salmonella pathogenicity island 1 (SPI-I) (Botella et al., 2011; Kapetanovic et al., 2016; Stocks et al., 2019). In contrast, our data show that *Cg* detoxifies Zn by sequestration into the vacuoles, although the fungal transporters remain elusive. Of note, the regulation of Zn homeostasis in *Cg* in general is little understood. Most data come from the non-pathogenic yeast *Saccharomyces cerevisiae* (Gerwien et al., 2018; Wilson and Deepe, 2019). The vacuole represents the major Zn storage site, because it is the default Zn sink in yeast. The Zn importers Zrc1 and Cot1 localize to vacuolar membranes and control Zn transport, engaging V-ATPase activity (MacDiarmid et al., 2000, 2002). Strikingly, vacuolar Zn concentrations can reach up to 100 mM, and Zn can be rapidly mobilized to provide Zn supply for multiple progeny cells from one Zn-loaded mother (Simm et al., 2007). Thus, we propose that Zn sequestration into vacuoles represents a nutritional immunity mechanism of phagolysosomally trapped *Cg* to buffer otherwise toxic Zn levels, thereby facilitating fungal fitness and immune evasion. Strikingly, we show that genetic ablation of the putative Zn transporter orthologue Zrc1 renders *Cg* cells unable to sequester Zn ions into the vacuole, thereby strongly reducing fungal survival in macrophages. This notion is strongly supported by a recent study, showing that failure to assemble the vacuolar ATPase in *Cg* triggers a vacuolar pH imbalance, increased susceptibility to Zn stress, and attenuated fungal fitness *in vivo* (Minematsu et al., 2019).

Owing to the pleiotropic functions of IFNs-I in pathogenic infections (McNab et al., 2015), additional mechanisms might account for the reduced fungal organ loads in *Ifnar1*$^{-/-}$ mice (Bourgeois et al., 2011; Riedelberger et al., 2020). However, the IFN-I-mediated dysregulation of Zn homeostasis highlights a possible and as yet unrecognized therapeutic concept for disseminated fungal infections. Because the inhibitory effects of IFNs-I were entirely controlled by JAK1, Filgotinib (GLPG0634) or related compounds might represent a promising option in order to lower otherwise detrimental IFN-I responses. Further *in vivo* experiments will be required to test this notion for fungal pathogens. Strikingly, Filgotinib has been used for the successful treatment of IFN-I-driven chronic inflammatory conditions, including inflammatory bowel disease, ankylosing spondylitis, psoriatic arthritis, and rheumatoid arthritis (Genovese et al., 2018; van der Heijde et al., 2018; Mease et al., 2018; Pérez-Jeldres et al., 2019). Further, specific inhibitors targeting fungal Zn homeostasis could constitute an exciting therapeutic option (Li et al., 2018), especially for hard-to-treat invasive infections with *Cg* or *C. auris*, owing to their intrinsic antifungal drug resistance (Perlin et al., 2017; Pristov and Ghannoum, 2019). Indeed, EDTA, TPEN, and zinc-attenuating compounds that indirectly also target Zn-dependent fungal processes have been effectively used for fungal infections with *C. albicans* and *A. fumigatus* (Cohrt et al., 2018; Hachem et al., 2006; Hein et al., 2015; Laskaris et al., 2016).

Limitations of the Study

Pro-inflammatory IFN-I signaling acts as a double-edge sword at multiple intersections of host-pathogen interactions (McNab et al., 2015). IFNs-I can provide both detrimental and beneficial immune surveillance in a pathogen-specific manner, because they engage in multiple signal transduction pathways. IFNs-I control

a plethora of immune cell functions during infectious diseases and thus also affect nutritional immunity (Boxx and Cheng, 2016; Stifter and Feng, 2015; Teijaro, 2016). Therefore, IFN-I response mechanisms are of ultrahigh complexity and dynamics as they engage or activate often unrelated immune pathways. Thus, we suggest that IFNs-I likely exert additional effects during systemic *Cg* infections, which might contribute to fungal organ persistence, perhaps in an organ-dependent fashion. Moreover, *in vivo* data addressing Zn fluctuations in various organs or immune cells in an organ- and or pathogen-specific manner are technically extremely challenging, owing to the ultrafast kinetics underlying adaptive metal ion changes in either host or pathogens. However, our data provide compelling evidence that dysregulation of Zn homeostasis and suppression of Zn intoxication in macrophages via metallothioneins contributes to the deleterious effects of IFN-I immune surveillance during infections with a major intracellular fungal pathogen.

Resource Availability

Lead Contact

Further information and requests for resources and reagents should be directed to and will be fulfilled by the Lead Contact, Karl Kuchler (karl.kuchler@meduniwien.ac.at).

Materials Availability

Plasmids and fungal strains generated in this study will be made available upon request.

Data and Code Availability

The microarray data are deposited at the National Center for Biotechnology Information Gene Expression Omnibus (GEO: GSE134016) and are freely available.

METHODS

All methods can be found in the accompanying Transparent Methods supplemental file.

SUPPLEMENTAL INFORMATION

Supplemental Information can be found online at https://doi.org/10.1016/j.isci.2020.101121.

AUTHOR CONTRIBUTIONS

M.R. and K.K designed experiments; M.R. and P.P. performed experiments; C.Bourgeois performed systemic *Cg* infections for microarray analysis and RNA isolation; A.P. carried out microarray hybridization; W.G. conducted raw data analysis; M.T. performed microarray analysis; S.J. constructed fungal strains; C. Brunnhofer and A.L. performed ICP-MS analysis and wrote the corresponding method description; B.H. and A.S. contributed to RT-qPCR; M.A.L., G.S., and G.W. provided materials and critical input; M.R. and K.K. coordinated the study and wrote the manuscript.

DECLARATION OF INTERESTS

M.A.L. has competing interests in the form of licensed intellectual property related to the therapeutic application of an anti-metallothionein antibody. The authors declare no competing interests.

REFERENCES

Amich, J., Leal, F., and Calera, J.A. (2009). Repression of the acid ZrfA/ZrfB zinc-uptake system of *Aspergillus fumigatus* mediated by PacC under neutral, zinc-limiting conditions. Int. Microbiol. *12*, 39–47.

Amich, J., Vicentefranqueira, R., Leal, F., and Calera, J.A. (2010). *Aspergillus fumigatus* survival in alkaline and extreme zinc-limiting environments relies on the induction of a zinc homeostasis system encoded by the *zrfc* and *aspf2* genes. Eukaryot. Cell *9*, 424–437.

Ballou, E.R., and Wilson, D. (2016). The roles of zinc and copper sensing in fungal pathogenesis. Curr. Opin. Microbiol. *32*, 128–134.

Belambri, S.A., Rolas, L., Raad, H., Hurtado-Nedelec, M., Dang, P.M.C., and El-Benna, J. (2018). NADPH oxidase activation in neutrophils: role of the phosphorylation of its subunits. Eur. J. Clin. Invest. *48*, e12951.

Biondo, C., Midiri, A., Gambuzza, M., Gerace, E., Falduto, M., Galbo, R., Bellantoni, A., Beninati, C., Teti, G., Leanderson, T., et al. (2008). IFN-alpha/beta signaling is required for polarization of cytokine responses toward a protective type 1 pattern during experimental cryptococcosis. J. Immunol. *181*, 566–573.

Biondo, C., Signorino, G., Costa, A., Midiri, A., Gerace, E., Galbo, R., Bellantoni, A., Malara, A., Beninati, C., Teti, G., et al. (2011). Recognition of yeast nucleic acids triggers a host-protective type I interferon response. Eur. J. Immunol. *41*, 1969–1979.

Blanco-Menéndez, N., del Fresno, C., Fernandes, S., Calvo, E., Conde-Garrosa, R., Kerr, W.G., and Sancho, D. (2015). SHIP-1 couples to the dectin-1 hemITAM and selectively modulates reactive oxygen species production in dendritic cells in response to *Candida albicans*. J. Immunol. *195*, 4466–4478.

Borges da Silva, H., Fonseca, R., Dos Anjos Cassado, A., Machado de Salles, É., de Menezes, M.N., Langhorne, J., Perez, K.R., Cuccovia, I.M., Ryffel, B., Barreto, V.M., et al. (2015a). *In vivo* approaches reveal a key role for DCs in CD4+ T cell activation and parasite clearance during the acute phase of experimental blood-stage malaria. PLoS Pathog. *11*, e1004598.

Borges da Silva, H., Fonseca, R., Pereira, R.M., Cassado, A.A., Álvarez, J.M., and D'Império Lima, M.R. (2015b). Splenic macrophage subsets and their function during blood-borne infections. Front. Immunol. *6*, 480.

Botella, H., Peyron, P., Levillain, F., Poincloux, R., Poquet, Y., Brandli, I., Wang, C., Tailleux, L., Tilleul, S., Charrire, G.M., et al. (2011). Mycobacterial P 1-Type ATPases mediate resistance to Zinc poisoning in human macrophages. Cell Host Microbe *10*, 248–259.

Bourgeois, C., Majer, O., Frohner, I.E., Lesiak-Markowicz, I., Hildering, K.-S., Glaser, W., Stockinger, S., Decker, T., Akira, S., Müller, M., et al. (2011). Conventional dendritic cells mount a type I IFN response against *Candida* spp. requiring novel phagosomal TLR7-mediated IFN-β signaling. J. Immunol. *186*, 3104–3112.

Boxx, G.M., and Cheng, G. (2016). The roles of type I interferon in bacterial infection. Cell Host Microbe *19*, 760–769.

Brieger, A., Rink, L., and Haase, H. (2013). Differential regulation of TLR-dependent MyD88 and TRIF signaling pathways by free zinc ions. J. Immunol. *191*, 1808–1817.

Cachat, J., Deffert, C., Hugues, S., and Krause, K.H. (2015). Phagocyte NADPH oxidase and specific immunity. Clin. Sci. *128*, 635–648.

Calame, D.G., Mueller-Ortiz, S.L., and Wetsel, R.A. (2016). Innate and adaptive immunologic functions of complement in the host response to *Listeria monocytogenes* infection. Immunobiology *221*, 1407–1417.

Casanova, J.L., Holland, S.M., and Notarangelo, L.D. (2012). Inborn errors of human JAKs and STATs. Immunity *36*, 515–528.

Chen, L., and Guo, D. (2017). The functions of tumor suppressor PTEN in innate and adaptive immunity. Cell. Mol. Immunol. *14*, 581–589.

Chowdhury, D., Alrefai, H., Landero Figueroa, J.A., Candor, K., Porollo, A., Fecher, R., Divanovic, S., Deepe, G.S., and Subramanian Vignesh, K. (2019). Metallothionein 3 controls the phenotype and metabolic programming of alternatively activated macrophages. Cell Rep. *27*, 3873–3886.

Citiulo, F., Jacobsen, I.D., Miramón, P., Schild, L., Brunke, S., Zipfel, P., Brock, M., Hube, B., and Wilson, D. (2012). *Candida albicans* scavenges host zinc via Pra1 during endothelial invasion. PLoS Pathog. *8*, e1002777.

Cohrt, K., Marín, L., Kjellerup, L., Clausen, J., Dalby-Brown, W., Calera, J., and Winther, A. (2018). Novel zinc-attenuating compounds as potent broad-spectrum antifungal agents with *in vitro* and *in vivo* efficacy. Antimicrob. Agents Chemother. *62*, e02024-17.

Crawford, A.C., Lehtovirta-Morley, L.E., Alamir, O., Niemiec, M.J., Alawfi, B., Alsarraf, M., Skrahina, V., Costa, A.C.B.P., Anderson, A., Yellagunda, S., et al. (2018). Biphasic zinc compartmentalisation in a human fungal pathogen. PLoS Pathog. *14*, e1007013.

Cuéllar-Cruz, M., Briones-Martin-del-Campo, M., Cañas-Villamar, I., Montalvo-Arredondo, J., Riego-Ruiz, L., Castaño, I., and De Las Peñas, A. (2008). High resistance to oxidative stress in the fungal pathogen *Candida glabrata* is mediated by a single catalase, Cta1p, and is controlled by

the transcription factors Yap1p, Skn7p, Msn2p, and Msn4p. Eukaryot. Cell *7*, 814–825.

Davidson, S., Crotta, S., McCabe, T.M., and Wack, A. (2014). Pathogenic potential of interferon αβ in acute influenza infection. Nat. Commun. *5*, 3864.

DeCoursey, T.E. (2016). The intimate and controversial relationship between voltage-gated proton channels and the phagocyte NADPH oxidase. Immunol. Rev. *273*, 194–218.

DeCoursey, T.E., Morgan, D., and Cherny, V.V. (2003). The voltage dependence of NADPH oxidase reveals why phagocytes need proton channels. Nature *422*, 531–534.

delFresno, C., Soulat, D., Roth, S., Blazek, K., Udalova, I., Sancho, D., Ruland, J., and Ardavín, C. (2013). Interferon-βproduction via dectin-1-Syk-IRF5 signaling in dendritic cells is crucial for immunity to *C.albicans*. Immunity *38*, 1176–1186.

Dhariwala, M.O., and Anderson, D.M. (2014). Bacterial programming of host responses: Coordination between type I interferon and cell death. Front. Microbiol. *5*, 1–13.

Domínguez-Andrés, J., Feo-Lucas, L., Minguito de la Escalera, M., González, L., López-Bravo, M., and Ardavín, C. (2017). Inflammatory Ly6Chigh monocytes protect against candidiasis through IL-15-driven NK cell/neutrophil activation. Immunity *46*, 1059–1072.e4.

Donovan, M.L., Schultz, T.E., Duke, T.J., and Blumenthal, A. (2017). Type I interferons in the pathogenesis of tuberculosis: molecular drivers and immunological consequences. Front. Immunol. *8*, 1633.

Egefjord, L., Jensen, J.L., Bang-Berthelsen, C.H., Petersen, A.B., Smidt, K., Schmitz, O., Karlsen, A.E., Pociot, F., Chimienti, F., Rungby, J., et al. (2009). Zinc transporter gene expression is regulated by pro-inflammatory cytokines: a potential role for zinc transporters in beta-cell apoptosis? BMC Endocr. Disord. *9*, 7.

Espinosa, V., Dutta, O., McElrath, C., Du, P., Chang, Y.-J., Cicciarelli, B., Pitler, A., Whitehead, I., Obar, J.J., Durbin, J.E., et al. (2017). Type III interferon is a critical regulator of innate antifungal immunity. Sci. Immunol. *2*, eaan5357.

Ferreira, C.R., and Gah, W.A. (2017). Disorders of metal metabolism. Transl Sci. Rare Dis. *2*, 465–498.

Figueroa, J., Vignesh, K., Deepe, G., and Caruso, J. (2015). Selectivity and specificity of small molecule fluorescent dyes/probes used for the detection of Zn2+ and Ca2+ in cells. Metallomics *6*, 301–315.

Fisher, M.C., Hawkins, N.J., Sangland, D., and Gurr, S.J. (2018). Worldwide emergence of resistance to antifungal drugs challenges human health and food security. Science *742*, 739–742.

Friedman, R.L., and Stark, G.R. (1985). alpha-Interferon-induced transcription of HLA and metallothionein genes containing homologous upstream sequences. Nature 314, 637–639.

Frohner, I.E., Bourgeois, C., Yatsyk, K., Majer, O., and Kuchler, K. (2009). *Candida albicans* cell surface superoxide dismutases degrade host-derived reactive oxygen species to escape innate immune surveillance. Mol. Microbiol. 71, 240–252.

Gabrielli, E., Pericolini, E., Luciano, E., Sabbatini, S., Roselletti, E., Perito, S., Kasper, L., Hube, B., and Vecchiarelli, A. (2015). Induction of caspase-11 by aspartyl proteinases of *Candida albicans* and implication in promoting inflammatory response. Infect. Immun. 83, 1940–1948.

Gafa, V., Remoli, M.E., Giacomini, E., Severa, M., Grillot, R., and Coccia, E.M. (2010). Enhancement of anti-*Aspergillus* T helper type 1 response by interferon-β-conditioned dendritic cells. Immunology 131, 282–288.

Genovese, M., Westhovens, R., Meuleners, L., Van der Aa, A., Harrison, P., Tasset, C., and Kavanaugh, A. (2018). Effect of filgotinib, a selective JAK 1 inhibitor, with and without methotrexate in patients with rheumatoid arthritis: Patient-reported outcomes. Arthritis Res. Ther. 20, 57.

Gerwien, F., Skrahina, V., Kasper, L., Hube, B., and Brunke, S. (2018). Metals in fungal virulence. FEMS Microbiol. Rev. 42, 1–21.

Gough, D.J., Messina, N.L., Clarke, C.J.P., Johnstone, R.W., and Levy, D.E. (2012). Constitutive type I interferon modulates homeostatic balance through tonic signaling. Immunity 36, 166–174.

Guarda, G., Braun, M., Staehli, F., Tardivel, A., Mattmann, C., Förster, I., Farlik, M., Decker, T., Du Pasquier, R.a., Romero, P., et al. (2011). Type I interferon inhibits interleukin-1 production and inflammasome activation. Immunity 34, 213–223.

Guevara-Ortiz, J.M., Omar-Castellanos, V., León-Chávez, B.A., Achanzar, W.E., and Brambila, E. (2005). Interferon alpha induction of metallothionein in rat liver is not linked to interleukin-1, interleukin-6, or tumor necrosis factor alpha. Exp. Mol. Pathol. 79, 33–38.

Günther, V., Lindert, U., and Schaffner, W. (2012). The taste of heavy metals: gene regulation by MTF-1. Biochim.Biophys. Acta 1823, 1416–1425.

Hachem, R., Bahna, P., Hanna, H., Stephens, L.C., and Raad, I. (2006). EDTA as an adjunct antifungal agent for invasive pulmonary aspergillosis in a rodent model. Antimicrob. Agents Chemother. 50, 1823–1827.

Hancock, J.T., and Jones, O.T. (1987). The inhibition by diphenyleneiodonium and its analogues of superoxide generation by macrophages. Biochem. J. 242, 103–107.

van der Heijde, D., Baraliakos, X., Gensler, L.S., Maksymowych, W.P., Tseluyko, V., Nadashkevich, O., Abi-Saab, W., Tasset, C., Meuleners, L., Besuyen, R., et al. (2018). Efficacy and safety of filgotinib, a selective Janus kinase 1 inhibitor, in patients with active ankylosing spondylitis (TORTUGA): results from a randomised, placebo-controlled, phase 2 trial. Lancet 392, 2378–2387.

Hein, K.Z., Takahashi, H., Tsumori, T., Yasui, Y., Nanjoh, Y., Toga, T., Wu, Z., Grötzinger, J., Jung, S., Wehkamp, J., et al. (2015). Disulphide-reduced psoriasin is a human apoptosis-inducing broad-spectrum fungicide. Proc. Natl. Acad. Sci. U S A 112, 13039–13044.

Hertzog, P.J., and Williams, B.R.G. (2013). Fine tuning type I interferon responses. Cytokine Growth Factor Rev. 24, 217–225.

Hervas-Stubbs, S., Perez-Gracia, J.L., Rouzaut, A., Sanmamed, M.F., Le Bon, A., and Melero, I. (2011). Direct effects of type I interferons on cells of the immune system. Clin. Cancer Res. 17, 2619–2627.

Hogan, D., and Wheeler, R.T. (2014). The complex roles of NADPH oxidases in fungal infection. Cell. Microbiol. 16, 1156–1167.

Huang, S., Meng, Q., Maminska, A., and MacMicking, J.D. (2019). Cell-autonomous immunity by IFN-induced GBPs in animals and plants. Curr. Opin. Immunol. 60, 71–80.

Inglis, D.O., Berkes, C.a., Hocking Murray, D.R., and Sil, A. (2010). Conidia but not yeast cells of the fungal pathogen *Histoplasma capsulatum* trigger a type I interferon innate immune response in murine macrophages. Infect. Immun. 78, 3871–3882.

Jensen, J., Vazquez-Torre, A., and Balish, E. (1992). Poly(I.C)-induced interferons enhance susceptibility of SCID mice to systemic candidiasis. Infect. Immun. 60, 4549–4557.

Kambe, T., Tsuji, T., Hashimoto, A., and Itsumura, N. (2015). The physiological, biochemical, and molecular roles of zinc transporters in zinc homeostasis and metabolism. Physiol. Rev. 95, 749–784.

Kapetanovic, R., Bokil, N.J., Achard, M.E.S., Ong, C.L.Y., Peters, K.M., Stocks, C.J., Phan, M.D., Monteleone, M., Schroder, K., Irvine, K.M., et al. (2016). *Salmonella* employs multiple mechanisms to subvert the TLR-inducible zinc-mediated antimicrobial response of human macrophages. FASEB J. 30, 1901–1912.

Kasper, L., Seider, K., and Hube, B. (2015). Intracellular survival of *Candida glabrata* in macrophages: immune evasion and persistence. FEMS Yeast Res. 15, fov042.

Kernbauer, E., Maier, V., Rauch, I., Müller, M., and Decker, T. (2013). Route of infection determines the impact of type i interferons on innate immunity to *Listeria monocytogenes*. PLoS One 8, e65007.

Kim, M.J., Kil, M., Jung, J.H., and Kim, J. (2008). Roles of zinc-responsive transcription factor Csr1 in filamentous growth of the pathogenic yeast *Candida albicans*. J. Microbiol. Biotechnol. 18, 242–247.

Kramer, J., Özkaya, Ö., and Kümmerli, R. (2019). Bacterial siderophores in community and host interactions. Nat. Rev. Microbiol. 18, 152–163.

Krężel, A., and Maret, W. (2017). The functions of metamorphic metallothioneins in zinc and copper metabolism. Int. J. Mol. Sci. 18, E1237.

Kumar, K., Askari, F., Sahu, M., and Kaur, R. (2019). *Candida glabrata*: a lot more than meets the eye. Microorganisms 7, 39.

Landstetter, N., Glaser, W., Gregori, C., Seipelt, J., and Kuchler, K. (2010). Functional genomics of drug-induced ion homeostasis identifies a novel regulatory crosstalk of iron and zinc regulons in yeast. OMICS 14, 651–663.

Laskaris, P., Atrouni, A., Calera, J.A., D'Enfert, C., Munier-Lehmann, H., Cavaillon, J.-M., Latgé, J.-P., and Ibrahim-Granet, O. (2016). Administration of zinc chelators improves survival of mice infected with *Aspergillus fumigatus*both in monotherapy and in combination with caspofungin. Antimicrob. Agents Chemother. 60, 5631–5639.

Lehtovirta-Morley, L.E., Alsarraf, M., and Wilson, D. (2017). Pan-domain analysis of ZIP zinc transporters. Int. J. Mol. Sci. 18, E2631.

Li, T., Niu, X., Zhang, X., Wang, S., and Liu, Z. (2017). Recombinant human IFNα-2b response promotes vaginal epithelial cells defense against *Candida albicans*. Front. Microbiol. 8, 697.

Li, T., Liu, Z., Zhang, X., Chen, X., and Wang, S. (2019). Therapeutic effectiveness of type I interferon in vulvovaginal candidiasis. Microb. Pathog. 134, 103562.

Li, Y., Sun, L., Lu, C., Gong, Y., Li, M., and Sun, S. (2018). Promising antifungal targets against *Candida albicans*based on ion homeostasis. Front. Cell. Infect. Microbiol. 8, 286.

Lin, M., Liu, Y., Tam, M., Lu, Y., Hsieh, Y., and Lin, L. (2012). PTEN interacts with metal-responsive transcription factor 1 and stimulates its transcriptional activity. Biochem. J. 441, 367–377.

Liu, L., Okada, S., Kong, X.-F., Kreins, A.Y., Cypowyj, S., Abhyankar, A., Toubiana, J., Itan, Y., Audry, M., Nitschke, P., et al. (2011). Gain-of-function human STAT1 mutations impair IL-17 immunity and underlie chronic mucocutaneous candidiasis. J. Exp. Med. 208, 1635–1648.

Lonergan, Z.R., and Skaar, E.P. (2019). Nutrient zinc at the host–pathogen interface. Trends Biochem. Sci. 44, 1041–1056.

Lopez, C.A., and Skaar, E.P. (2018). The impact of dietary transition metals on host-bacterial interactions. Cell Host Microbe 23, 737–748.

Loures, F.V., Röhm, M., Lee, C.K., Santos, E., Wang, J.P., Specht, C.A., Calich, V.L.G., Urban, C.F., and Levitz, S.M. (2015). Recognition of *Aspergillus fumigatus*hyphae by human plasmacytoid dendritic cells is mediated by dectin-2 and results in formation of extracellular traps. PLoS Pathog. 11, e1004643.

Maares, M., and Haase, H. (2016). Zinc and immunity: an essential interrelation. Arch. Biochem. Biophys. 611, 58–65.

MacDiarmid, C., Gaither, L., and Eide, D. (2000). Zinc transporters that regulate vacuolar zinc storage in *Saccharomyces cerevisiae*. EMBO J. 19, 2845–2855.

MacDiarmid, C.W., Milanick, M.A., and Eide, D.J. (2002). Biochemical properties of vacuolar zinc transport systems of *Saccharomyces cerevisiae*. J. Biol. Chem. 277, 39187–39194.

MacMicking, J.D. (2012). Interferon-inducible effector mechanisms in cell-autonomous immunity. Nat. Rev. Immunol. 12, 367–382.

Macpherson, A.J., Heikenwalder, M., and Ganal-Vonarburg, S.C. (2016). The liver at the nexus of host-microbial interactions. Cell Host Microbe 20, 561–571.

Majer, O., Bourgeois, C., Zwolanek, F., Lassnig, C., Kerjaschki, D., Mack, M., Müller, M., and Kuchler, K. (2012). Type I interferons promote fatal immunopathology by regulating inflammatory monocytes and neutrophils during Candida infections. PLoS Pathog. 8, e1002811.

Malavia, D., Lehtovirta-Morley, L.E., Alamir, O., Weiß, E., Gow, N.A.R., Hube, B., and Wilson, D. (2017). Zinc limitation induces a hyper-adherent Goliath phenotype in Candida albicans. Front. Microbiol. 8, 1–16.

McLachlan, J.B., Catron, D.M., Moon, J.J., and Jenkins, M.K. (2009). Dendritic cell antigen presentation drives simultaneous cytokine production by effector and regulatory T cells in inflamed skin. Immunity 30, 277–288.

McNab, F., Mayer-Barber, K., Sher, A., Wack, A., and O'Garra, A. (2015). Type I interferons in infectious disease. Nat. Rev. Immunol. 15, 87–103.

Mease, P., Coates, L.C., Helliwell, P.S., Stanislavchuk, M., Rychlewska-Hanczewska, A., Dudek, A., Abi-Saab, W., Tasset, C., Meuleners, L., Harrison, P., et al. (2018). Efficacy and safety of filgotinib, a selective Janus kinase 1 inhibitor, in patients with active psoriatic arthritis (EQUATOR): results from a randomised, placebo-controlled, phase 2 trial. Lancet 392, 2367–2377.

Melia, J.M.P., Lin, R., Xavier, R.J., Thompson, R.B., Fu, D., Wan, F., Sears, C.L., and Donowitz, M. (2019). Induction of the metal transporter ZIP8 by interferon gamma in intestinal epithelial cells: potential role of metal dyshomeostasis in Crohn's disease. Biochem. Biophys. Res. Commun. 515, 325–331.

Van Miert, A., Van Duin, C., and Wensing, T. (1990). Fever and changes in plasma zinc and iron concentrations in the goat.The effects of interferon inducers and recombinant IFN-alpha 2a. J. Comp. Path. 103, 289–300.

Minematsu, A., Miyazaki, T., Shimamura, S., Nishikawa, H., Nakayama, H., Takazono, T., Saijo, T., Yamamoto, K., Imamura, Y., Yanagihara, K., et al. (2019). Vacuolar proton-translocating ATPase is required for antifungal resistance and virulence of Candida glabrata. PLoS One 14, e0210883.

Morimoto, A., Murakami, N., Takada, M., Teshirogi, S., and Watanabe, T. (1987). Fever and acute phase response induced in rabbits by human recombinant interferon-gamma. J. Physiol. 391, 209–218.

Morris, S., and Huang, P.C. (1987). Transient response of amplified metallothionein genes in CHO cells to induction by alpha interferon. Mol. Cell. Biol. 7, 600–605.

Müller, U., Steinhoff, U., Reis, L.F.L., Hemmi, S., Paviovic, J., Zinkernagel, R.M., and Aguet, M. (1994). Functional role of type I and type II interferons in antiviral defense. Science 264, 1918–1921.

Nagamine, T., Suzuki, K., Kondo, T., Nakazato, K., Kakizaki, S., Takagi, H., and Nakajima, K. (2005). Interferon-alpha-induced changes in metallothionein expression in liver biopsies from patients with chronic hepatitis C. Can. J. Gastroenterol. 19, 481–486.

Nairz, M., Fritsche, G., Brunner, P., Talasz, H., Hantke, K., and Weiss, G. (2008). Interferon-g limits the availability of iron for intramacrophage Salmonella typhimurium. Eur. J. Immunol. 38, 1923–1936.

Nairz, M., Dichtl, S., Schroll, A., Haschka, D., Tymoszuk, P., Theurl, I., and Weiss, G. (2018). Iron and innate antimicrobial immunity—Depriving the pathogen, defending the host. J. Trace Elem. Med. Biol. 48, 118–133.

Netea, M.G., Joosten, L.a.B., van der Meer, J.W.M., Kullberg, B.-J., and van de Veerdonk, F.L. (2015). Immune defence against Candida fungal infections. Nat. Rev. Immunol. 15, 630–642.

Neumann, W., Gulati, A., and Nolan, E.M. (2017). Metal homeostasis in infectious disease: recent advances in bacterial metallophores and the human metal-withholding response. Curr. Opin. Chem. Biol. 37, 10–18.

Øverland, G., Stuestøl, J.F., Dahle, M.K., Myhre, A.E., Netea, M.G., Verweij, P., Yndestad, A., Aukrust, P., Kullberg, B.J., Warris, A., et al. (2005). Cytokine responses to fungal pathogens in Kupffer cells are toll-like receptor 4 independent and mediated by tyrosine kinases. Scand. J. Immunol. 62, 148–154.

Palmer, L.D., and Skaar, E.P. (2016). Transition metals and virulence in bacteria. Annu. Rev. Genet. 50, 67–91.

Pappas, P.G., Lionakis, M.S., Arendrup, M.C., Ostrosky-Zeichner, L., and Kullberg, B.J. (2018). Invasive candidiasis. Nat. Rev. Dis. Prim. 4, 18026.

Pérez-Jeldres, T., Tyler, C.J., Boyer, J.D., Karuppuchamy, T., Yarur, A., Giles, D.A., Yeasmin, S., Lundborg, L., Sandborn, W.J., Patel, D.R., et al. (2019). Targeting cytokine signaling and lymphocyte traffic via small molecules in inflammatory bowel disease: JAK inhibitors and S1PR agonists. Front. Pharmacol. 10, 212.

Perlin, D.S., Rautemaa-Richardson, R., and Alastruey-Izquierdo, A. (2017). The global problem of antifungal resistance: prevalence, mechanisms, and management. Lancet Infect. Dis. 17, e383–e392.

Pristov, K.E., and Ghannoum, M.A. (2019). Resistance of Candida to azoles and echinocandins worldwide. Clin.Microbiol. Infect. 25, 792–798.

Van Prooyen, N., Henderson, C.A., Hocking Murray, D., and Sil, A. (2016). CD103+ conventional dendritic cells are critical for TLR7/9-dependent host defense against Histoplasma capsulatum, an endemic fungal pathogen of humans. PLoS Pathog. 12, e1005749.

Ramirez-Ortiz, Z.G., Lee, C.K., Wang, J.P., Boon, L., Specht, C.A., and Levitz, S.M. (2011). A nonredundant role for plasmacytoid dendritic cells in host defense against the human fungal pathogen Aspergillus fumigatus. Cell Host Microbe 9, 415–424.

Read, S.A., O'Connor, K.S., Suppiah, V., Ahlenstiel, C.L.E., Obeid, S., Cook, K.M., Cunningham, A., Douglas, M.W., Hogg, P.J., Booth, D., et al. (2017). Zinc is a potent and specific inhibitor of IFN-λ3 signalling. Nat. Commun. 8, 15245.

Reiber, C., Brieger, A., Engelhardt, G., Hebel, S., Rink, L., and Haase, H. (2017). Zinc chelation decreases IFN-beta-induced STAT1 upregulation and iNOS expression in RAW 264.7 macrophages. J. Trace Elem. Med. Biol. 44, 76–82.

Rice, J.M., Zweifach, A., and Lynes, M.A. (2016). Metallothionein regulates intracellular zinc signaling during CD4+T cell activation. BMC Immunol. 17, 13.

Riedelberger, M., Penninger, P., Tscherner, M., Strobl, B., Weiss, G., Kuchler, K., Riedelberger, M., Penninger, P., Tscherner, M., Seifert, M., et al. (2020). Type I interferon response dysregulates host iron homeostasis and enhances Candida glabrata infection. Cell Host Microbe 27, 454–466.e8.

Romani, L., Bistoni, F., Perruccio, K., Montagnoli, C., Gaziano, R., Bozza, S., Bonifazi, P., Bistoni, G., Rasi, G., Velardi, A., et al. (2006). Thymosin α1 activates dendritic cell tryptophan catabolism and establishes a regulatory environment for balance of inflammation and tolerance. Blood 108, 2265–2274.

Van Rompaey, L., Galien, R., van der Aar, E.M., Clement-Lacroix, P., Nelles, L., Smets, B., Lepescheux, L., Christophe, T., Conrath, K., Vandeghinste, N., et al. (2013). Preclinical characterization of GLPG0634, a selective inhibitor of JAK1, for the treatment of inflammatory diseases. J. Immunol. 191, 3568–3577.

Ruttkay-Nedecky, B., Nejdl, L., Gumulec, J., Zitka, O., Masarik, M., Eckschlager, T., Stiborova, M., Adam, V., and Kizek, R. (2013). The role of metallothionein in oxidative stress. Int. J. Mol. Sci. 14, 6044–6066.

Salvatori, O., Pathirana, R., Kay, J., and Edgerton, M. (2018). Candida albicans Ras1 inactivation increases resistance to phagosomal killing by human neutrophils. Infect. Immun. 86, e00685–18.

Sato, K., Yamamoto, H., Nomura, T., Matsumoto, I., Miyasaka, T., Zong, T., Kanno, E., Uno, K., Ishii, K., and Kawakami, K. (2015). Cryptococcus neoformans infection in mice lacking type I interferon signaling leads to increased fungal clearance and IL-4-dependent mucin production in the lungs. PLoS One 10, e0138291.

Sato, M., Yamaki, J., Oguro, T., Yoshida, T., Nomura, N., and Nakajima, K. (1996). Metallothionein synthesis induced by interferon alpha/beta in mice of various zinc status. Tohoku J. Exp. Med. 178, 241–250.

Schreiber, G., and Piehler, J. (2015). The molecular basis for functional plasticity in type I interferon signaling. Trends Immunol. 36, 139–149.

Seider, K., Brunke, S., Schild, L., Jablonowski, N., Wilson, D., Majer, O., Barz, D., Haas, A., Kuchler, K., Schaller, M., et al. (2011). The facultative intracellular pathogen Candida glabrata subverts macrophage cytokine production and

phagolysosome maturation. J. Immunol. *187*, 3072–3086.

Seyedmousavi, S., Davis, M., Sugui, J., Pinkhasov, T., Moyer, S., Salazar, A., Chang, Y., and Kwon-Chung, K. (2018). Exogenous stimulation of type I interferon protects mice with chronic granulomatous disease from aspergillosis through early recruitment of host-protective neutrophils into the lung. MBio *9*, e00422-18.

Simm, C., Lahner, B., Salt, D., LeFurgey, A., Ingram, P., Yandell, B., and Eide, D.J. (2007). *Saccharomyces cerevisiae* vacuole in zinc storage and intracellular zinc distribution. Eukaryot. Cell *6*, 1166–1177.

Sionov, E., Mayer-Barber, K.D., Chang, Y.C., Kauffman, K.D., Eckhaus, M.A., Salazar, A.M., Barber, D.L., and Kwon-Chung, K.J. (2015). Type I IFN induction via poly-ICLC protects mice against cryptococcosis. PLoS Pathog. *11*, e1005040.

Smeekens, S.P., Ng, A., Kumar, V., Johnson, M.D., Plantinga, T.S., van Diemen, C., Arts, P., Verwiel, E.T.P., Gresnigt, M.S., Fransen, K., et al. (2013). Functional genomics identifies type I interferon pathway as central for host defense against *Candida albicans*. Nat. Commun. *4*, 1342.

Snell, L.M., McGaha, T.L., and Brooks, D.G. (2017). Type I interferon in chronic virus infection and cancer. Trends Immunol. *38*, 542–557.

Snyder, D.T., Hedges, J.F., and Jutila, M.A. (2017). Getting "inside" type I IFNs: type I IFNs in intracellular bacterial infections. J. Immunol. Res. *2017*, 9361802.

Stawowczyk, M., Naseem, S., Montoya, V., Baker, D., Konopka, J., and Reich, N. (2018). Pathogenic effects of IFIT2 and interferon-β during fatal systemic *Candida albicans* Infection. MBio *9*, e00365-18.

Stifter, S.a., and Feng, C.G. (2015). Interfering with immunity: detrimental role of type I IFNs during infection. J. Immunol. *194*, 2455–2465.

Stocks, C.J., Phan, M.-D., Achard, M.E.S., Nhu, N.T.K., Condon, N.D., Gawthorne, J.A., Lo, A.W., Peters, K.M., McEwan, A.G., Kapetanovic, R., et al. (2019). Uropathogenic *Escherichia coli* employs both evasion and resistance to subvert innate immune-mediated zinc toxicity for dissemination. Proc. Natl. Acad. Sci. U S A *116*, 6341–6350.

Subramanian Vignesh, K., and Deepe, G.J. (2017). Metallothioneins: Emerging modulators in immunity and infection. Int. J. Mol. Sci. *18*, E2197.

Subramanian Vignesh, K., and Deepe, G.S. (2016). Immunological orchestration of zinc homeostasis: the battle between host mechanisms and pathogen defenses. Arch. Biochem. Biophys. *611*, 66–78.

Subramanian Vignesh, K., LanderoFigueroa, J.A., Porollo, A., Caruso, J.A., and Deepe, G.S. (2013a). Granulocyte macrophage-colony stimulating factor induced Zn sequestration enhances macrophage superoxide and limits intracellular pathogen survival. Immunity *39*, 697–710.

Subramanian Vignesh, K., Landero Figueroa, J., Porollo, A., Caruso, J., and Deepe, G. (2013b). Zinc sequestration: arming phagocyte defense against fungal attack. PLoS Pathog. *9*, 1–5.

Subramanian Vignesh, K., Landero Figueroa, J.A., Porollo, A., Divanovic, S., Caruso, J.A., and Deepe, G.S. (2016). IL-4 induces metallothionein 3- and SLC30A4-dependent increase in intracellular Zn2+ that promotes pathogen persistence in macrophages. Cell Rep. *16*, 3232–3246.

Sun, D., Sun, P., Li, H., Zhang, M., Liu, G., Strickland, A.B., Chen, Y., Fu, Y., Xu, J., Yosri, M., et al. (2019). Fungal dissemination is limited by liver macrophage filtration of the blood. Nat. Commun. *10*, 4566.

Taff, H.T., Mitchell, K.F., Edward, J.A., and Andes, D.R. (2013). Mechanisms of *Candida* biofilm drug resistance. Future Microbiol. *8*, 1325–1337.

Teijaro, J.R. (2016). Pleiotropic roles of type 1 interferons in antiviral immune responses. Adv. Immunol. *132*, 135–158.

Teijaro, J.R., Ng, C., Lee, A.M., Sullivan, B.M., Sheehan, K.C.F., Welch, M., Schreiber, R.D., De La Torre, J.C., and Oldstone, M.B.A. (2013). Persistent LCMV infection is controlled by blockade of type I interferon signaling. Science *340*, 207–211.

Toledo Pinto, T., Batista-Silva, L., Medeiros, R., Lara, F., and Moraes, M. (2018). Type I interferons, autophagy and host metabolism in leprosy. Front. Immunol. *9*, 806.

Vaeth, M., and Feske, S. (2018). Ion channelopathies of the immune system. Curr. Opin. Immunol. *52*, 39–50.

Vale-Silva, L.A., and Sanglard, D. (2015). Tipping the balance both ways: drug resistance and virulence in *Candida glabrata*. FEMS Yeast Res. *15*, fov025.

van de Veerdonk, F., Plantinga, T., Hoischen, A., Smeekens, S., Joosten, L., Gilissen, C., Arts, P., Rosentul, D., Carmichael, A., Smits-van der Graaf, C., et al. (2011). STAT1 mutations in autosomal dominant chronic mucocutaneous candidiasis. N. Engl. J. Med. *365*, 54–61.

Wagner, D., Maser, J., Lai, B., Cai, Z.H., Barry, C.E., Bentrup, K.H.Z., Russell, D.G., and Bermudez, L.E. (2005a). Elemental analysis of *Mycobacterium avium*-, *Mycobacterium tuberculosis*-, and *Mycobacterium smegmatis*-containing phagosomes indicates pathogen-induced microenvironments within the host cell's endosomal system. J. Immunol. *174*, 1491–1500.

Wagner, D., Maser, J., Moric, I., Boechat, N., Vogt, S., Gicquel, B., Lai, B., Reyrat, J.M., and Bermudez, L. (2005b). Changes of the phagosomal elemental concentrations by Mycobacterium Tuberculosis Mramp. Microbiology *151*, 323–332.

Walkup, G.K., Burdette, S.C., Lippard, S.J., and Tsien, R.Y. (2000). A new cell-permeable fluorescent probe for Zn2+. J. Am. Chem. Soc. *122*, 5644–5645.

Warnatsch, A., Tsourouktsoglou, T.D., Branzk, N., Wang, Q., Reincke, S., Herbst, S., Gutierrez, M., and Papayannopoulos, V. (2017). Reactive oxygen species localization programs inflammation to clear microbes of different size. Immunity *46*, 421–432.

Weiss, G., and Carver, P.L. (2018). Role of divalent metals in infectious disease susceptibility and outcome. Clin. Microbiol. Infect. *24*, 16–23.

Wellington, M., Dolan, K., and Krysan, D.J. (2009). Live *Candida albicans* suppresses production of reactive oxygen species in phagocytes. Infect. Immun. *77*, 405–413.

Wessels, I., Maywald, M., and Rink, L. (2017). Zinc as a gatekeeper of immune function. Nutrients *9*, 9–12.

Wilson, D. (2015). An evolutionary perspective on zinc uptake by human fungal pathogens. Metallomics *7*, 979–985.

Wilson, D., and Deepe, G.S. (2019). The intersection of host and fungus through the zinc lens. Curr. Opin. Microbiol. *52*, 35–40.

Wilson, E., Yamada, D., Elsaesser, H., Herskovitz, J., Deng, J., Cheng, G., Aronow, B., Karp, C., and Brooks, D. (2013). Blockade of chronic type I interferon signaling to control persistent LCMV infection. Science *340*, 202–207.

Worby, C., and Dixon, J. (2014). Pten. Annu. Rev. Biochem. *83*, 641–669.

Wu, A., Tymoszuk, P., Haschka, D., Heeke, S., Dichtl, S., Petzer, V., Seifert, M., Hilbe, R., Sopper, S., Talasz, H., et al. (2017). *Salmonella* utilizes zinc to subvert antimicrobial host defense of macrophages via modulation of NF-κB signaling. Infect. Immun. *85*, e00418–17.

Xu, S., and Shinohara, M.L. (2017). Tissue-resident macrophages in fungal infections. Front. Immunol. *8*, 1798.

Yamamoto, A., Tagawa, Y., Yoshimori, T., Moriyama, Y., Masaki, R., and Tashiro, Y. (1998). Bafilomycin A1 prevents maturation of autophagic vacuoles by inhibiting fusion between autophagosomes and lysosomes in rat hepatoma cell line, H-4-II-E cells. Cell Struct. Funct. *23*, 33–42.

Zackular, J.P., Chazin, W.J., and Skaar, E.P. (2015). Nutritional immunity: S100 proteins at the host-pathogen interface. J. Biol. Chem. *290*, 18991–18998.

Supplemental Information

Type I Interferons Ameliorate Zinc

Intoxication of *Candida glabrata* by Macrophages

and Promote Fungal Immune Evasion

Michael Riedelberger, Philipp Penninger, Michael Tscherner, Bernhard Hadriga, Carina Brunnhofer, Sabrina Jenull, Anton Stoiber, Christelle Bourgeois, Andriy Petryshyn, Walter Glaser, Andreas Limbeck, Michael A. Lynes, Gernot Schabbauer, Guenter Weiss, and Karl Kuchler
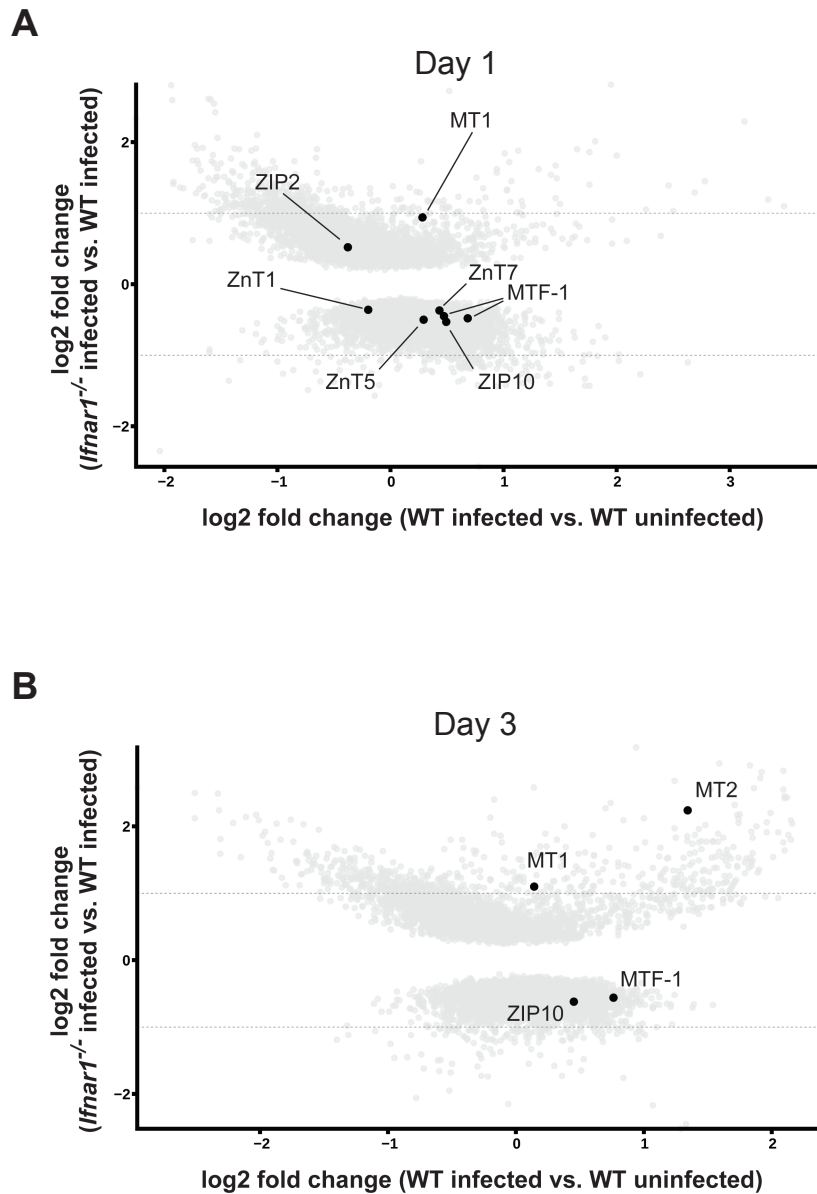
A

Day 1

B

Day 3

Figure S1. Microarray analysis of Zn homeostasis genes in *C. glabrata*-infected WT and *Ifnar1*^{-/-} spleens. *Related to Figure 1.*
A-B) Scatter blots of DEGs from WT and *Ifnar1*^{-/-} spleens at day 1 and day 3 of systemic *Cg* infection. Each dot represents one probe on the microarray and black dots (FDR < 0.05) correspond to Zn homeostasis-related genes.
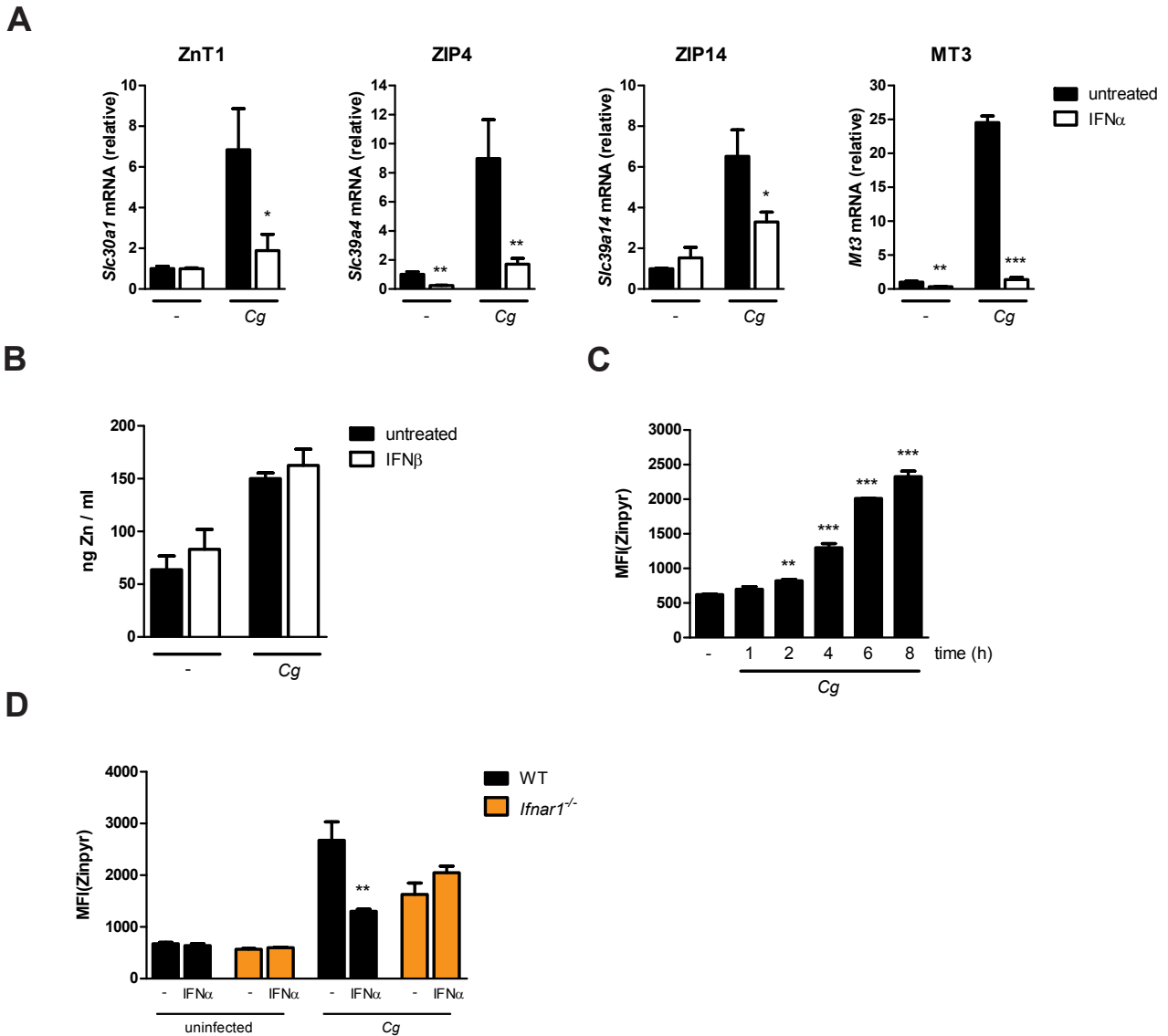DEG = Differentially Expressed Gene; FDR = False Discovery Rate

Figure S2. Regulation of Zn homeostasis by IFNα. *Related to Figure 2.*
A) RT-qPCR analysis of *ZnT1*, *ZIP4*, *ZIP14* and *Mt3* mRNA levels in untreated or IFNα-treated WT BMDMs challenged with *Cg* for 8 h (normalization to *Actb*).
B) Quantification of total Zn metal concentrations by ICP-MS in whole cell lysates from untreated or IFNβ-treated WT BMDMs infected with *Cg* for 8 h.
C) Zinpyr-assay of WT BMDMs infected with *Cg* for up to 8 h.
D) Zinpyr-assay of untreated or IFNα-treated BMDMs after 8 h *Cg* infection.
Data are representative of two (**A-D**) independent experiments. Mean and SD are shown, * p-value < 0.05, ** p-value < 0.01, *** p-value < 0.001 (**A-B,D**) Student's t-test (**C**) one-way ANOVA with Bonferroni's post hoc analysis.
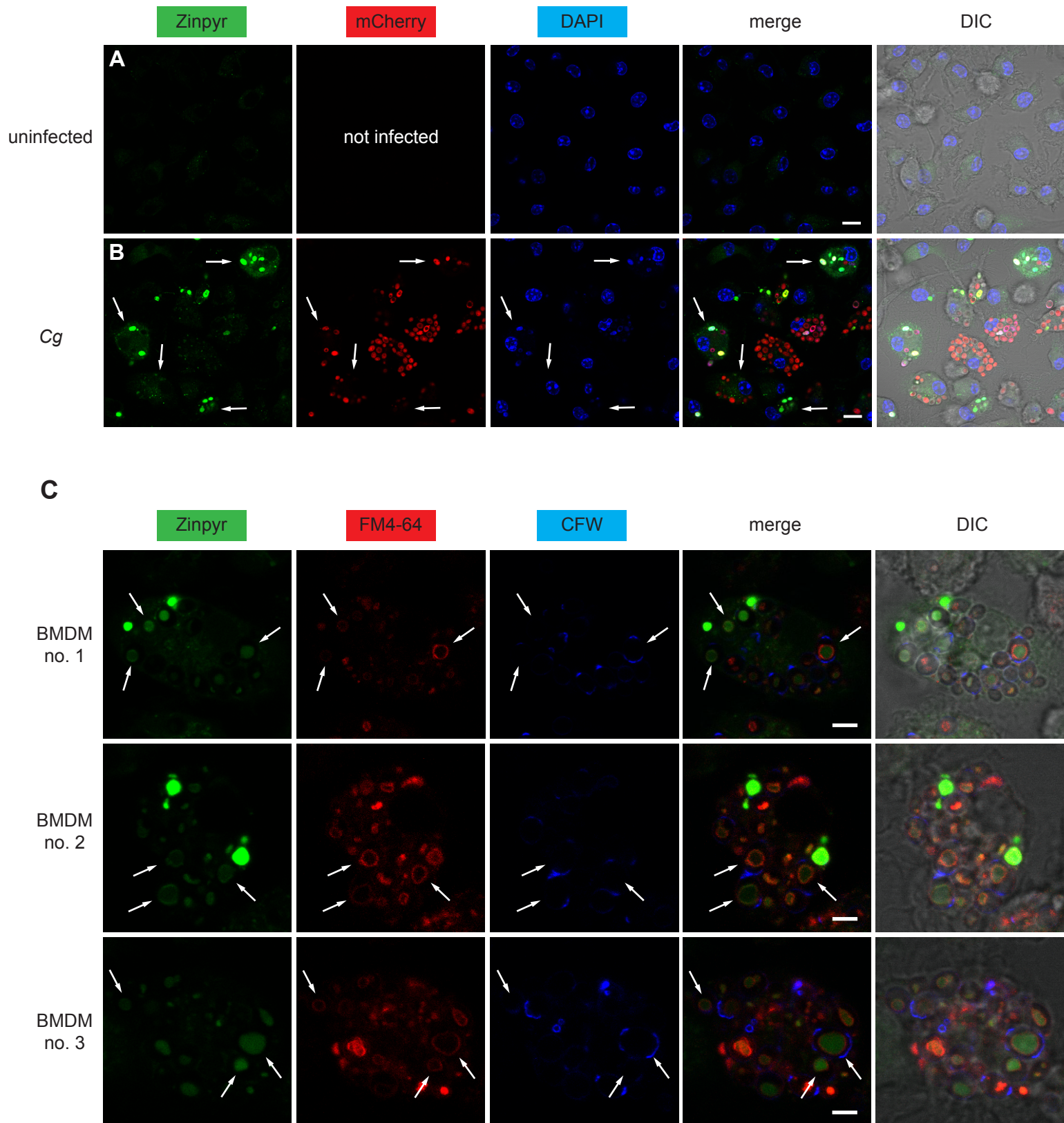
Figure S3. Zn localization in BMDMs during *Cg* infection. *Related to Figure 3 and 4.*
A-B) Confocal microscopy analysis of Zn (Zinpyr; green), mCherry-expressing *Cg* (red) and nucleus (DAPI; blue) in uninfected or *Cg*-infected WT BMDMs for 4 h.
C) Confocal microscopy analysis of three different WT BMDMs after 4 h *Cg* infection. Analysis of Zn (Zinpyr; green), vacuolar membranes of *Cg* (FM4-64; red) and Calcofluor-White-stained *Cg* (CFW; blue).
Merge, overlay of all three channels. DIC, Differential Interference Contrast. Arrows point at (**A-B**) BMDMs with increased cytoplasmic Zinpyr signal or at (**C**) vacuolar localization of Zn in *Cg*. The scale bar represents (**A-B**) 10 µm or (**C**) 5 µm. Data are representative of two (**A-C**) independent experiments.
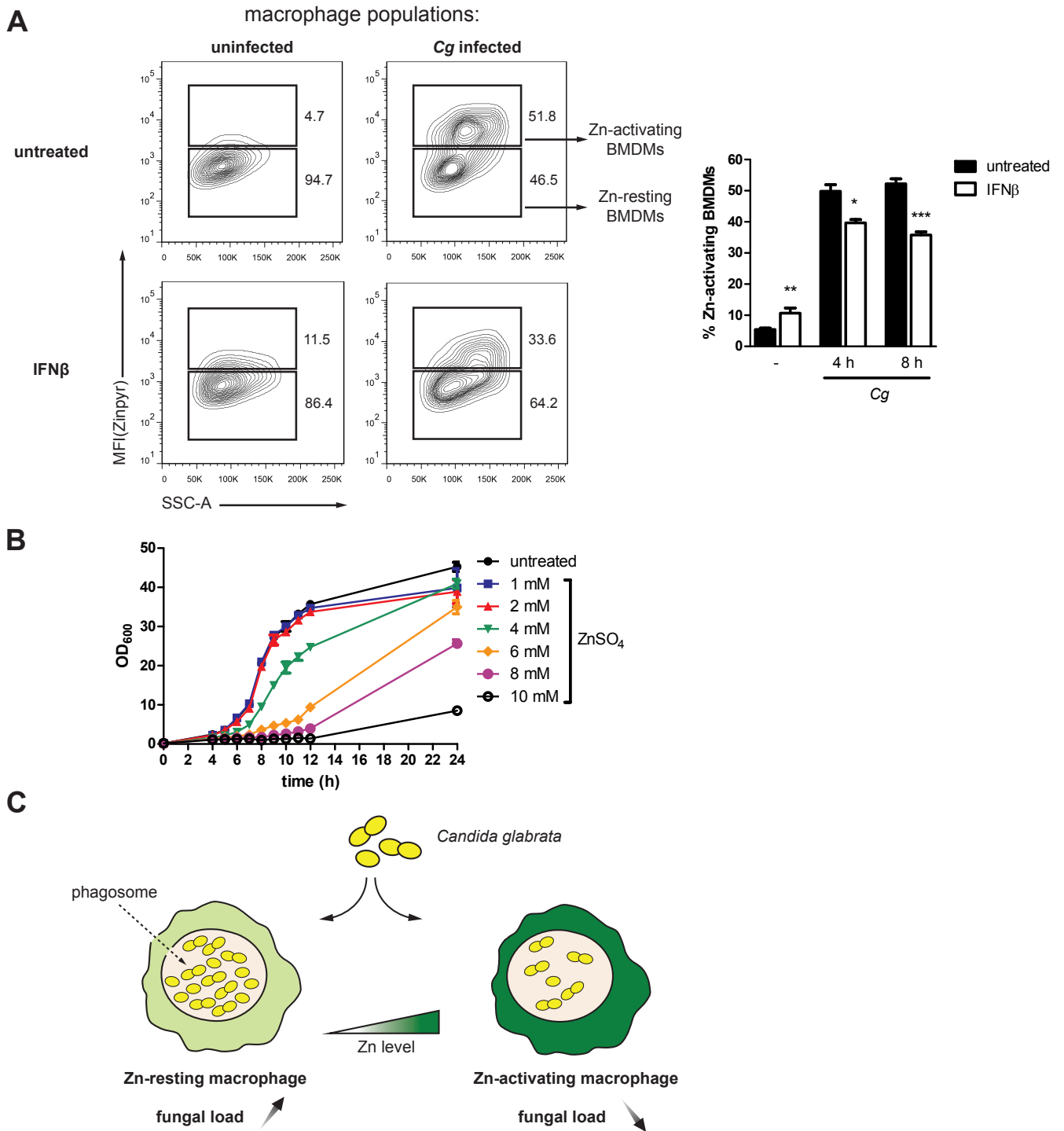
Figure S4. BMDMs and Zinc stress upon *Cg* infection. *Related to Figure 5.*
A) Flow cytometric quantification of Zn-activating WT BMDMs untreated or IFNβ-treated during *Cg* infection.
B) Quantification of fungal growth in liquid cultures upon incubation with varying Zn concentrations.
C) Graphical illustration. Macrophages separate into a Zn-resting and a Zn-activating population during *Cg* infection.

OD, Optical Density. Data are representative of two (**A-B**) independent experiments. Mean and SD are shown, * p-value < 0.05, ** p-value < 0.01, *** p-value < 0.001 (Student's t-test).
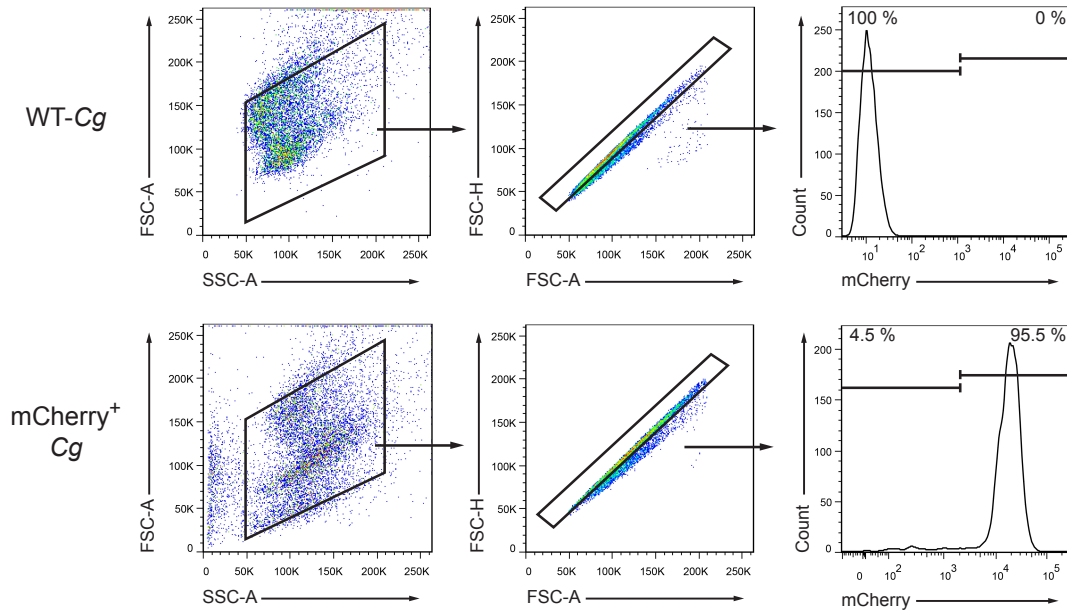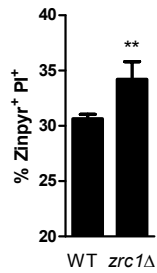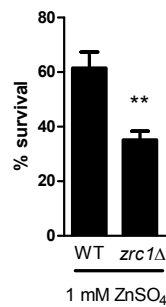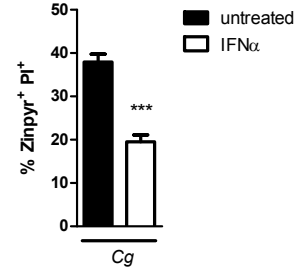
Figure S5. *Cg* **and Zinc intoxication.** *Related to Figure 5.*

A) Gating strategy for *Cg* identification. Via FSC/SSC discrimination, fungal cells can be accurately separated from smaller particles, since the entire *Cg* gate revealed mCherry$^+$ cells.

B) Fungal Zn intoxication assay of WT and *zrc1Δ Cg* isolated from WT BMDMs after 8 h infection.

C) Fungal survival of WT and *zrc1Δ Cg* after 3 h incubation in 1 mM ZnSO$_4$/ddH$_2$O. Aliquots were serially diluted in PBS and plated on YPD plates for CFU enumeration.

D) Fungal Zn intoxication assay of *Cg* isolated from untreated or IFNα-treated WT BMDMs after 8 h infection.

Data are representative of two (**A-C**) or three (**D**) independent experiments. Mean and SD are shown, ** p-value < 0.01, *** p-value < 0.001 (Student's t-test).
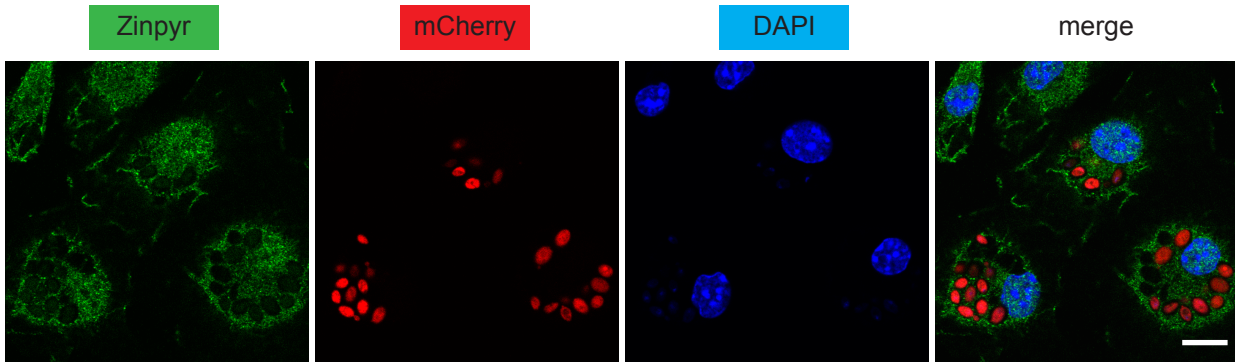
Figure S6. Nuclear and cytoplasmic localization of MTs in BMDMs during *Cg* infection. *Related to Figure 6.*

Confocal microscopy analysis of Zn (Zinpyr; green), mCherry-expressing *Cg* (red) and nucleus (DAPI; blue) in WT BMDMs after 4 h infection. Merge, overlay of all three channels. The scale bar represents 5 μm. Data are representative of two independent experiments.
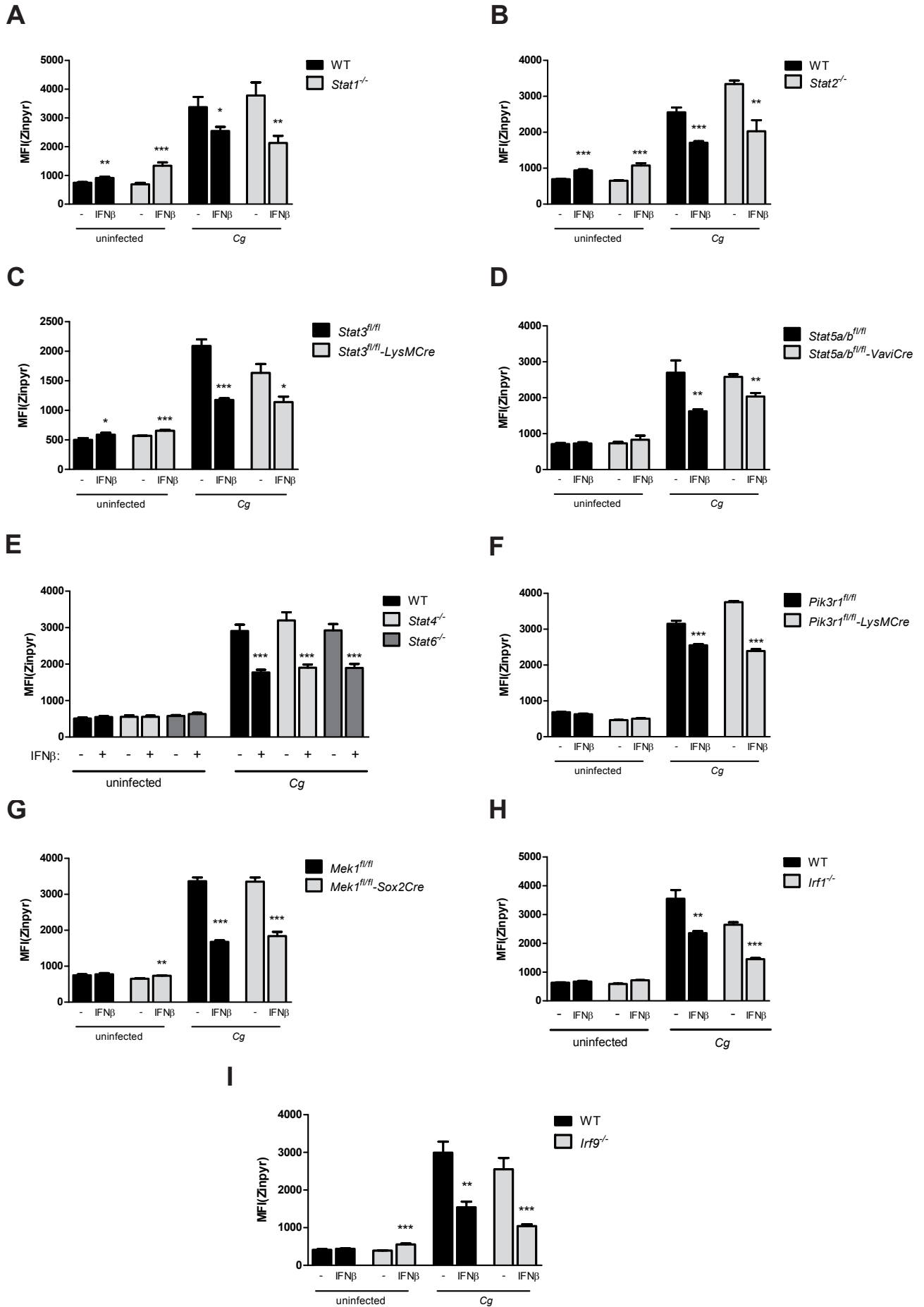
Figure S7. IFN-I-mediated dysregulation of Zn homeostasis is independent of various signaling pathways. *Related to Figure 7.*

A-I) Zinpyr-assay of untreated or IFNβ-treated BMDMs upon *Cg* infection for 8 h.

Data are representative of two (**A-I**) independent experiments. Mean and SD are shown, * p-value < 0.05, ** p-value < 0.01, *** p-value < 0.001 (Student's t-test).
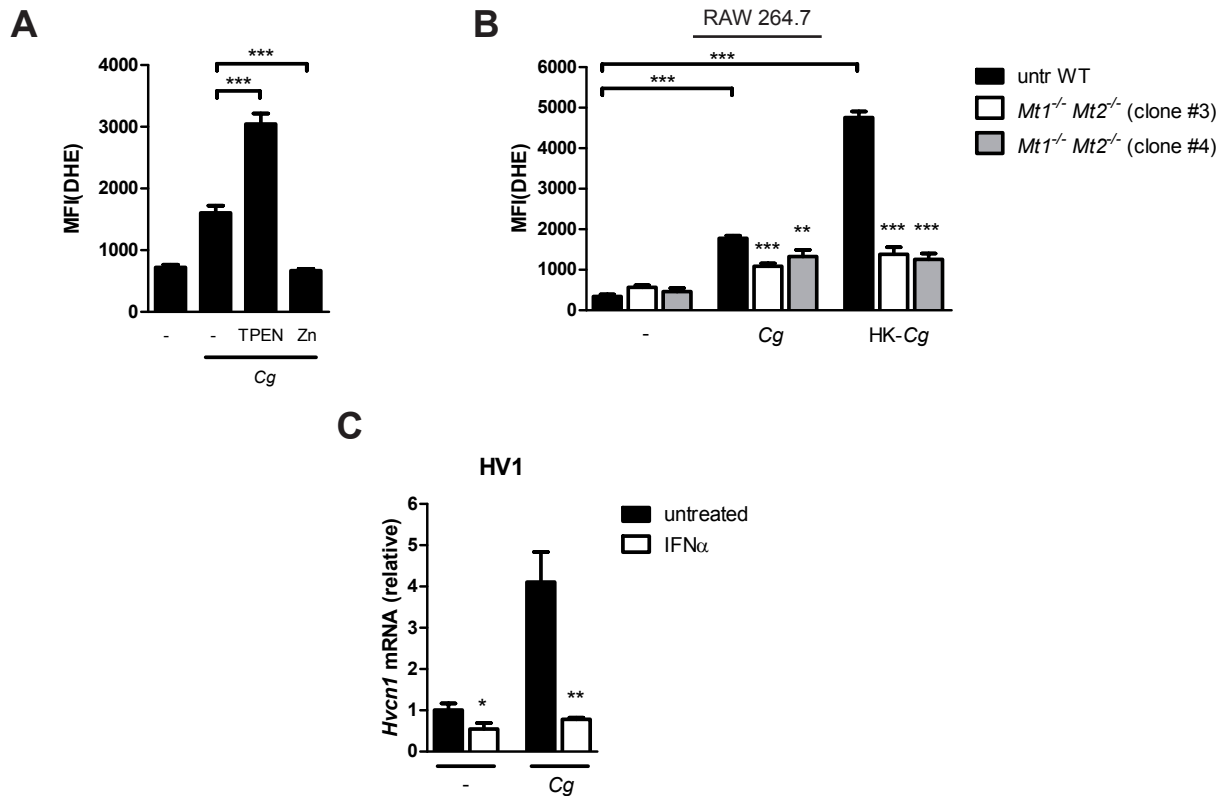
Figure S8. ROS response is modulated by Zn homeostasis. *Related to Figure 8.*

A) Detection of intracellular ROS by DHE. BMDMs were infected with *Cg* for 2 h and simultaneously treated with TPEN (20 µM) or ZnSO$_4$ (100 µM).

B) Detection of intracellular ROS by DHE in RAW 264.7 cells infected with live or heat-killed *Cg* for 2 h.

C) RT-qPCR analysis of *Hvcn1* in WT BMDMs untreated or IFNα-treated during *Cg* infection for 8 h (normalization to *Actb*).

Data are representative of two (**A-C**) independent experiments. Mean and SD are shown, * p-value < 0.05, ** p-value < 0.01, *** p-value < 0.001 (**A,C**) Student's t-test (**B**) one-way ANOVA with Bonferroni's post hoc analysis.

Table S2. List of Zn homeostasis-related genes involved in nutritional immunity. *Related to Figure 1.*

We recommend reviews focusing on nutritional immunity (Lopez and Skaar, 2018), Copper/Zinc intoxication (Sheldon and Skaar, 2019), Zinc homeostasis in infection and inflammation (Alker and Haase, 2018; Bonaventura et al., 2015; Gammoh and Rink, 2017; Gao et al., 2018; Sapkota and Knoell, 2018; Subramanian Vignesh and Deepe, 2016), gene regulation by MTF-1 (Günther et al., 2012) and metallothioneins in immunity (Rahman and Karim, 2018; Subramanian Vignesh and Deepe, 2017). Based on this literature, the microarray data were specifically analysed for Zn homeostasis pathways and the following Zn homeostasis-related genes have been overlayed with the microarray analysis results:

Gene	Synonym	UniGeneID
Mtf1	MTF-1	Mm.272397
Slc30a1	ZnT1	Mm.9024
Slc30a2	ZnT2	Mm.358876
Slc30a3	ZnT3	Mm.1396
Slc30a4	ZnT4	Mm.27801
Slc30a5	ZnT5	Mm.402215
Slc30a6	ZnT6	Mm.243943
Slc30a7	ZnT7	Mm.34550
Slc30a8	ZnT8	Mm.208831
Slc30a9	ZnT9	Mm.234455
Slc30a10	ZnT10	Mm.227117
Slc39a1	ZIP1	Mm.294709
Slc39a2	ZIP2	Mm.281343
Slc39a3	ZIP3	Mm.5353
Slc39a4	ZIP4	Mm.276829
Slc39a5	ZIP5	Mm.22983
Slc39a6	ZIP6	Mm.21688
Slc39a7	ZIP7	Mm.18556
Slc39a8	ZIP8	Mm.30239
Slc39a9	ZIP9	Mm.238279
Slc39a10	ZIP10	Mm.233889
Slc39a11	ZIP11	Mm.341021
Slc39a12	ZIP12	Mm.44662
Slc39a13	ZIP13	Mm.192375
Slc39a14	ZIP14	Mm.270647
Mt1	MT1	Mm.192991
Mt2	MT2	Mm.147226
Mt3	MT3	Mm.2064

Table S3. Oligonucleotides used in this study. *Related to Figure 2 and Figure 5-9.*

Primer name	Sequence (5'→3')	
Construction of *TDH3*-mCherry fusion		
55_CgTDH3_SacI	actgctgagctcGTTTGATGACCACTGTCCAC	
53_CgTDH3_BamHI	actgctggatcctGTTCTTGGCAACGTGTTCAA	
35_CgTDH3_XhoI	actgctctcgagGGAAAAGTATCAACAGAGCATAG	
33_CgTDH3_KpnI	actgctggtaccCAATCTGCGTAGTAATGAGGAGTAA	
Primers to verify genomic integration		
5C_CgTDH3_mCherry	CAAGTACACTTCTGACTTGAAGATT	
mCherry_int_rev	TGAAGCGCATGAACTCCTTG	
***ZRC1* gene deletion**		
55IC_ZRC1	ttctttcctgcgttatcccctgattctgtggataaccgtaccatggACATAAGGTCGCATTTGTAGTATAC	Amplification of the *ZRC1* upstream region; lowercase letters represent the sequence overlap to the YEp352 backbone used for Gibson assembly; underlined sequence indicates a NcoI restriciton site
53IC_ZRC1	gagggggggcccggtacccaattcgccctatagtgagtcgGTGCTAAATATTTGAGTCTGGTTC	Amplification of the *ZRC1* upstream region; lowercase letters represent the sequence overlap to the FRT-FLP-*NAT1*-FRT fragment used for Gibson assembly
35IC_ZRC1	tagtgagggttaattgcgcgcttggcgtaatcatggtcatCCGTTTTAAAATTTGAACGACC	Amplification of the *ZRC1* the downstream region; lowercase letters represent the sequence overlap to the FRT-FLP-NAT1-FRT fragment used for Gibson assembly
33IC_ZRC1	aacgcagaaaatgaaccgggggatgcgacgtgcaagattaccatATGAATATCATCACTAAAACTGGC	Amplification of the *ZRC1* downstream region; lowercase letters represent the sequence overlap to the YEp352 backbone used for Gibson assembly
5C_ZRC1	GTGTGAGTGTGAGTGTGAGAG	Upstream integration check of the *ZRC1* deletion cassette
3C_ZRC1	GATGGTAGAAAATCTCATCGGTG	Downstream integration check of the *ZRC1* deletion cassette
LOG_ZRC1_fo	GATCACGGACATAGCCACGG	Validation of *ZRC1* gene deletion
LOG_ZRC1_rev	GCAGAAATTGTGGATGGAGTGG	Validation of *ZRC1* gene deletion
YEp_ic fwd	gtaatcttgcacgtcgcatcc	Amplification of the YEp352 backbone
YEp_ic rev	tacggttatccacagaatcaggg	Amplification of the YEp352 backbone
SATflipp_fwd	CGACTCACTATAGGGCGAATTGG	Amplification of the FRT-FLP-*NAT1*-FRT cassette from pSFS3b
SATflipp_rev	ATGACCATGATTACGCCAAGC	Amplification of the FRT-FLP-*NAT1*-FRT cassette from pSFS3b
hk3	CATCATCTGCCCAGATGCGAAG	Downstream integration check of the *ZRC1* deletion cassette
SATflipp_5C	TTTGGAACTAACGATGCATACGAC	Upstream integration check of the *ZRC1* deletion cassette
Primers for RT-qPCR (mammalian cells)		
ZIP1_Fw	ATGGAGTGAGACCCTCGGGA	
ZIP1_Rev	ACTGCATCTCCCCAATTCAG	
ZIP2_Fw	GAATGGGGAGGGACTCATGC	
ZIP2_Rev	CACAAGCCCCTTATGAGCCA	
ZIP3_Fw	AGAAGGATTGGCAGCAGCAT	
ZIP3_Rev	GTGCCACTCGACAGAACTCA	

ZIP4_Fw	CTTGGCTCTAGGCAAACCTG
ZIP4_Rev	AGTGTGGCCAGGTAATCGTC
ZIP5_Fw	CTGGCAGTCCTGTTCCTCAG
ZIP5_Rev	GACCCAGGTCCTCCTCTGAT
ZIP6_Fw	TGACCTTTGCCCTTTGGGTT
ZIP6_Rev	ATGGTGTCGCTGCATGGTAA
ZIP7_Fw	GAGAGGAGGAAACACTGGGC
ZIP7_Rev	GTTGTGTGCCAAGTCAGCAG
ZIP8_Fw	GAGACAATGCAAGGGGCTCT
ZIP8_Rev	CTTCGGGGCATTGAAGAGGT
ZIP9_Fw	TGTGTGACGCTCCTCACTTC
ZIP9_Rev	GCTGTTCCACTTCTCCACGA
ZIP10_Fw	GTTAAAAGCCGCCCCAACTC
ZIP10_Rev	CTGTAGCTCCGCGCTAGTTT
ZIP11_Fw	CAAGGTTACAGCTCCGTGGT
ZIP11_Rev	GTCTAAGATCCGCCTCTGCC
ZIP12_Fw	AACACAACCCAAGCCCAAGA
ZIP12_Rev	GGATGGTTGAGGGACCAGTG
ZIP13_Fw	CCCATGGTATGAGGCGGAAG
ZIP13_Rev	CAGTGGCAGAGGTGGCAG
ZIP14_Fw	CGTGGGAGCCAACTGATAAT
ZIP14_Rev	AACGGCCACATTTTCAACTC
ZnT1_Fw	GCTCTCGAGTTGGTCCTGTC
ZnT1_Rev	GCCTCATGGTGAGGTAGGAA
ZnT2_Fw	AGCCCGGTCCTTCTTAGGAT
ZnT2_Rev	GGATCCGGCTAGCTTCACTC
ZnT3_Fw	AGGCGTGGGAGATAGAGACT
ZnT3_Rev	TCCAAGGACCACTCGGACTC
ZnT4_Fw	TGAGTGGCACAACCTCTCAG
ZnT4_Rev	ACTGCATCTCCCCAATTCAG
ZnT5_Fw	TGTCCAAATGTGCCCGCTAT
ZnT5_Rev	CTCTGTGCTCTCCTGGTGTG
ZnT6_Fw	TTAATCGCGGACACACACCA
ZnT6_Rev	GCCCCATCCTGTTGATTCCA
ZnT7_Fw	GTGCCTGAACCTCTCTTTCG
ZnT7_Rev	TCAAAAACAGCCCATTGACA
ZnT8_Fw	TGTCCAAATGTGCCCGCTAT
ZnT8_Rev	TACTTCACACACACAACACCA
ZnT9_Fw	CTATCGTGCCTCACACCTGG
ZnT9_Rev	AGCCTCTTCAAGCCTTTCGT
ZnT10_Fw	GTCCTCCACATTTCCCCTGG
ZnT10_Rev	TTGGGGTTGGGGATTGTAGC
MT1_Fw	CACCAGATCTCGGAATGGAC
MT1_Rev	GTTCGTCACATCAGGCACAG
MT2_Fw	CCGATCTCTCGTCGATCTTC
MT2_Rev	ACTTGTCGGAAGCCTCTTTG
MT3_Fw	AGACCTGCCCCTGTCCTACT
MT3_Rev	CAGGGACACCCAGCACTATT
HV1_Fw	TCGAGCAGCTCTGGAAACTC
HV1_Rev	TGTCCTCGAAGGTCCGTTTG
MTF-1_Fw	TTCTCACAATTGGGCTGAGCA
MTF-1_Rev	ACCAGTCCGTTGTCATCCAC
b-Actin_Fw	CCTTCCTTCTTGGGTATGGA
b-Actin_Rev	ACGGATGTCAACGTCACACT
Primers for RT-qPCR (fungal cells)	
MT-I_Fw	AACGGTTGCTCCTGTCCAAA
MT-I_Rev	ACCGCACTTGCATTGTTCAC
CTA1_Fw	GGTCCAGCTCAACCATTCCA
CTA1_Rev	ACAAGTCTCTGGCTTGGACG

| Act1_Fw | AATTGAGAGTCGCCCCAGAA |
| Act1_Rev | GGCTGGAACGTTGAAGGTTT |

Table S4. Plasmids used in this study. *Related to Figure 4.*

Name	Description	Reference
pSFS3b	Donor plasmid for *NAT1*-Flipper used for Gibson assembly	(Tscherner et al., 2015)
YEp352-*SAT1*	Donor plasmid for *E. coli* replication origin and ampicillin resistance fragment for Gibson assembly	(Krauke and Sychrova, 2011)
YEp352-*NAT1*-Cg*ZRC1*urdr	*ZRC1* gene deletion plasmid generated via Gibson assembly	This study

<u>**Transparent Methods**</u>

Ethics statement

All animal experiments were evaluated by the Ethics Committee of the Medical University of Vienna and approved by the Federal Ministry for Science & Research, Austria (BMBWF-66.009/0436-V/3b/2019).

Mouse experiments

Ifnar1^{-/-} (Müller et al., 1994), *Tyk2*^{-/-} (Shimoda et al., 2000)*, Stat1*^{-/-} (Durbin et al., 1996), *Stat2*^{-/-} (Park et al., 2000), *Stat3*^{fl/fl} (Alonzi et al., 2002), *Stat4*[em3Adiuj] (#028526; obtained from the Jackson Laboratory), *Stat5a/b*[fl/fl] (Cui et al., 2004), *Stat6*^{-/-} (Kaplan et al., 1996), *Irf1*^{-/-} (Reis et al., 1994), *Irf3*^{-/-} (Sato et al., 2000), *Irf9*^{-/-} (Kimura et al., 1996), *Mek1*[fl/f] (Catalanotti et al., 2009), *Pik3r1*^{fl/fl} (Luo et al., 2005), *Pten*^{fl/fl} (Suzuki et al., 2002), C57BL/6J-*Mt1*[tm1Bri] *Mt2*[tm1Bri] (Masters et al., 1994; Rice et al., 2016), *LysMCre* (Clausen et al., 1999), *VaviCre* (Boer et al., 2003) and *Sox2Cre* (Hayashi et al., 2002) mice have been described. Wild-type (C57BL/6J) and *Ifnar1*^{-/-} mice were housed under specific pathogen-free conditions in the animal facility of the Medical University of Vienna/Max Perutz Labs Vienna. Mice breeding and maintenance was in accordance with ethical animal license protocols complying with the current Austrian law. Male and female WT and *Ifnar1*^{-/-} mice (8-12 weeks old) were infected intravenously with 5×10^7 colony-forming units (CFUs) of *C. glabrata* (in 100 µl) per 25 g mouse weight. Throughout the infection, mice were monitored daily and killed by cervical dislocation at the respective time points.

Fungal Strains and Culture Conditions

Fungal strains used in this study included the wild-type *C. glabrata* strain ATCC2001, a *zrc1Δ* mutant strain and a mCherry-expressing *C. glabrata* strain. For fungal cultivation, rich YP medium (Yeast extract: BD Biosciences; Tryptone: AppliChem) supplemented with 2 % (w/v) glucose (Sigma-Aldrich) was used (Kaiser et al., 1994). *C. glabrata* was incubated at 70 °C at 800 rpm for 10 min (heat-killing) or for 1 min (heat-stressed cells). Heat-killed cells were checked via YPD plating for surviving fungal cells. To determine fungal growth by optical density (OD_{600}) measurement, logarithmic growing *C. glabrata* were adjusted to $OD_{600} = 0.2$ in YPD medium substituted with varying $ZnSO_4$ concentrations (Sigma-Aldrich) and grown at 30 °C and 220 rpm. For confocal microscopy, *C. glabrata* was stained with 25 µg/ml Calcofluor-white (Sigma-Aldrich) at room temperature for 10 min at 800 rpm in the dark. For vacuolar staining, *C. glabrata* was incubated in 1:250 FM4-64 (Thermo Fisher Scientific) in YPD medium at 30 °C for 1 h at 800 rpm in the dark.

Plasmid and *C. glabrata* Strain Construction

Oligonucleotides and plasmids used in this study can be found in Table S3 and S4. *C. glabrata* mCherry tagging was done via C-terminal fusion of *TDH3* (CAGL0G09383g) with mCherry based on a previously published strategy (Yáñez-Carrillo et al., 2015) using the pYC56 plasmid (Addgene) as a mCherry donor. Briefly, the last 485 bp of the *TDH3* coding sequence (CDS; excluding the stop codon) and 118 bp downstream (DR) of the open reading frame were PCR amplified and cloned into pYC56

using SacI, BamHI and KpnI, XhoI (all Thermo Fisher Scientific), respectively, yielding the final plasmid pYC56-TDH3urdr. To excise the final Tdh3-mCherry tagging cassette, pYC56-TDH3urdr was digested with SacI and KpnI and transformed into *C. glabrata* using electroporation as described earlier (Reuss et al., 2004). The integration of the mCherry tagging cassette into the *TDH3* locus was confirmed by colony PCR.

C. glabrata ZRC1 (CAGL0K07392g) gene deletion was done in the ATCC2001 strain background using a modified *SAT1* flipper technique (Reuss et al., 2004; Tscherner et al., 2015). Briefly, a YEp352-*NAT1*-Cg*ZRC1*urdr plasmid was generated via a Gibson assembly approach (Gibson et al., 2009). Therefore, approximately 500 bp fragments of up- and downstream regions of the *ZRC1* coding sequence (CDS) were PCR amplified and fused with a FRT-FLP-*NAT1*-FRT cassette generated from pSFS3b (Tscherner et al., 2012) and the backbone from YEp352-*SAT1* containing the *E. coli* replication origin and an ampicillin resistance marker. Gibson assembly was done using a 2x Gibson assembly master mix (New England Biolabs) and 10 ng/kb of agarose gel-purified fragments. The generated YEp352-*NAT1*-Cg*ZRC1*urdr plasmid was digested with FastDigest NcoI and PvuI (both ThermoFisher Scientific) and transformed into *C. glabrata* using electroporation as described earlier (Reuss et al., 2004). The up- and downstream integration, as well as the deletion of *ZRC1* were confirmed by colony PCR.

For Colony PCR, a single colony of *C. glabrata* was resuspended in 50 µl H_2O and incubated for 10 minutes at 95 °C. Cell debris were spun down and 5 µl of the supernatant were used for PCR using the DreamTaq Green DNA Polymerase (Thermo Fisher Scientific) in accordance to the manufacture's protocol as previously described (Tscherner et al., 2015).

Microarray Sample Preparation and Analysis

WT and *Ifnar1*^{-/-} mice were intravenously infected with *C. glabrata* (see above). Spleens were collected at day 1, 3, 7 and 14 post-infection and stored in RNA*later*[TM] Stabilization Solution (Thermo Fisher Scientific). Organs were homogenized in 1.5 ml RNA lysis buffer (Promega) with occasional cooling on ice by using an Ika T10 basic Ultra-Turrax homogenizer (IKA). For RNA isolation, the SV Total RNA Isolation System (Promega) was used according to the manufacturer's instructions.

RNA quality was checked on RNA 6000 Nano chips (Agilent) using a Bioanalyzer 2100 (Agilent). The Low Input Quick Amp Labeling Kit (one-color) (Agilent) was used to generate fluorescent cRNA. The amplified cyanine 3-labeled cRNA samples were then purified using SV Total RNA Isolation System (Promega) and hybridized to the SurePrint G3 Mouse GE 8x60K microarray (Agilent). Microarray slides were washed and scanned with a DNA Microarray Scanner (Agilent), according to the standard protocol of the manufacturer. Information from probe features was extracted from microarray scan images using the Feature Extraction software v10.7.3 (Agilent).

Further analyses were performed using R Bioconductor (Gentleman et al., 2004). The raw intensities were imported into Bioconductor using spot weighting and further processed with the limma package (Smyth, 2004). Quality Controls were performed using the arrayQualityMetrics package (Kauffmann et al., 2009). To reduce the effects of outlier arrays, arrays were weighted using the arrayWeights function of limma. Normalization between arrays was performed using the quantile method and a linear model was fitted. P-values were adjusted for multiple testing using the Benjamini

& Hochberg method. Log2 intensities for $Ifnar1^{-/-}$ and WT samples were normalized to uninfected controls first and subsequently differentially expressed genes in $Ifnar1^{-/-}$ versus WT samples were determined for each day. After filtering out of low-intensity probes (average log2 intensity > 6), cutoffs for differential expression were set to a minimum 2-fold up- or down regulation and a maximum adjusted p-value of 0.05 with at least one probe matching these criteria. Normalized log2 intensity values were used to perform gene set enrichment analysis using gene set permutation and Signal2Noise ranking metric (Subramanian et al., 2005). After conducting an in-depth literature search, a defined set of Zn homeostasis genes (involved in the concept of nutritional immunity) was included into the analysis (Table S2). The microarray data are deposited at the National Center for Biotechnology Information Gene Expression Omnibus (GSE134016) and are freely available.

Macrophage Cultivation and Infection

Primary bone marrow-derived macrophages (BMDMs) were cultivated as previously described (Bourgeois et al., 2009; Riedelberger et al., 2020). Bone marrow cells from femurs and tibias of C57BL/6 mice (male and female) were cultured in 10 cm square Petri dishes (Thermo Fisher Scientific) at 37 °C, 5 % CO_2 in 9 ml BMDM medium consisting of DMEM (#11584486, Thermo Fisher Scientific), 10 % heat-inactivated fetal calf serum (hiFCS; #F7524, Sigma-Aldrich), 100 µg/ml Penicillin/Streptomycin (Sigma-Aldrich) and 15 % L929 fibroblast cell supernatant. After three days, 5 ml BMDM medium was added and at day 7 of cultivation, the old medium was aspirated and BMDMs were splitted 1:2 in 12 ml fresh BMDM medium. On day 10 of cultivation, adherent cells were harvested by gently scraping with a natural-rubber scraper (Deutsch & Neumann) and pelleted at 300 g, 20 °C for 6.5 min. After counting BMDMs with a CASY counter, BMDMs were seeded in the respective tissue culture plates in BMDM medium and incubated overnight at 37 °C, 5 % CO_2. The experiment was performed on day 11 of cultivation.

Splenic macrophages (SpMs) were cultivated as previously described (Alatery and Basta, 2008). Spleens from male and female WT and $Ifnar1^{-/-}$ mice were passed through a 70 µm cell strainer (Corning) and red blood cells (RBCs) were lysed in 2 ml RBC lysis buffer (0.01 M Tris-HCl buffer pH = 7.0 containing 8.3 g/l NH_4Cl; all Sigma-Aldrich) per every spleen. Subsequently, obtained splenocytes were cultured in 12 SpM medium consisting of RPMI-1640 medium (Thermo Fisher Scientific) with 10 % heat-inactivated FCS and 100 µg/ml Penicillin/Streptomycin (both from Sigma-Aldrich) in 10 cm square Petri dishes (Thermo Fisher Scientific). On day 3, non-adherent cells were washed away with 1x PBS and 12 ml fresh SpM medium was replenished. On day 7 of cultivation, adherent SpMs were gently scraped with a natural-rubber scraper and seeded in respective well plates in SpM medium for the following experiment on day 8 of cultivation.

The $Mt1^{-/-}$ $Mt2^{-/-}$ RAW 264.7 macrophage cell line (clone #3 and #4) (Wu et al., 2017) was cultivated in DMEM (Thermo Fisher Scientific), 10 % hiFCS (Sigma-Aldrich) and 100 µg/ml Penicillin/Streptomycin (Sigma-Aldrich) at 37 °C, 5 % CO_2.

17 h before the infection, BMDMs and SpMs were left untreated or treated with 500 U/ml IFNα or IFNβ (both BioLegend). Where indicated, BMDMs were pre-treated with 10 µM Filgotinib (GLPG0634) (Selleckchem) 60 min before IFNβ treatment. 10 µM freshly-dissolved TPEN, 3 µM Bafilomycin A_1 or 3 mM DPI (all Sigma-Aldrich) was added 60 min before *C. glabrata* infection.

Immune cells were challenged with logarithmic growing fungal strains at a MOI = 2 (multiplicity of infection; 2 yeast cells per immune cell) if not otherwise stated. Throughout *C. glabrata* infection, IFNs-I/Filgotinib/TPEN/Bafilomycin A_1/DPI were left within the cell culture medium.

In Vitro C. glabrata Survival Assays

$1x10^5$ BMDMs were seeded into 96-well plates (at least 4 technical replicates per condition) in 100 µl BMDM medium the day before use. BMDMs were infected with *C. glabrata* (MOI = 0.1; in 50 µl BMDM medium) for 24 h. After BMDM lysis with SDS and scraping, dilutions of cell lysates were plated on YPD plates and CFUs were counted after 48 h at 30 °C.

RNA Isolation and RT-qPCR

$1x10^6$ BMDMs were lysed in 1 ml TRI Reagent® (Molecular Research Center) and RNA was isolated exactly as previously described (Schmittgen and Livak, 2008). After treatment with DNase I (Thermo Fisher Scientific), cDNA was generated using the Reverse Transcription System (Promega) and RT-qPCR was performed by using the Luna® Universal qPCR Master Mix (New England Biolabs) according to manufacturer's instructions. RT-qPCR results from mammalian cells were normalized to *Actb* expression and for fungal gene expression, results were normalized to *ACT1* expression. For RT-qPCR primer sequences, see Table S3.

Immunoblotting

Western blots were performed as describe before (Bourgeois et al., 2009; Riedelberger et al., 2020), whereby $1x10^6$ BMDMs were lysed in 50 µl of 4 % SDS sample buffer (Laemmli, 1970) and incubated at 95 °C for 5 min. Protein samples were loaded onto 10 % SDS-PAGE gels and subsequently transferred to 0.45 µm PVDF membranes (Millipore). After membrane blocking, immunoblotting was conducted overnight at 4 °C with 1:1000 anti-phospho-p40 (#4311), 1:1000 anti-β-Actin (D6A8) (#8457) primary antibodies and by membrane incubation with 1:2000 goat anti-rabbit IgG (H+L) HRP-linked secondary antibody (#7074) (all Cell Signaling). The membranes were incubated in SuperSignal West Pico Chemiluminescent Substrate and were exposed to CL-XPosure films (both Thermo Fisher Scientific).

Quantification of Intracellular Zn Levels

The same setup was used for BMDMs and *ex vivo* SpMs. $2x10^5$ BMDMs were cultivated in 24-well plates and challenged with the respective stimuli. At the end of BMDM challenge after 8 h (unless otherwise stated), BMDMs were washed 3x with PBS and stained with 300 µl of 10 µM Zinpyr (sc-213182, Santa Cruz) in PBS for 30 min at 37 °C. After three PBS washing steps, cells were harvested by trypsinization and resuspended in 300 µl FACS buffer (PBS + 0.1 % BSA). The MFI(Zinpyr) (median fluorescence intensity) of BMDMs was immediately collected on a LSRFortessa (BD Biosciences) and analyzed using FlowJo software version 7.6.5 (FlowJo).

In case of splenic macrophages *in vivo*, WT and *Ifnar1*^{-/-} mice (uninfected or intravenously infected with *C. glabrata*) were sacrificed, spleens were harvested and dissociated via passage through a 70 µM cell strainer. After red blood cell lysis, aliquots of $1x10^6$ splenocytes were transferred

into a 1.5 ml reaction tubes and harvested at 400 g, 4 °C for 5 min. After removing the supernatant, splenocytes were incubated in 50 µl FACS buffer containing 10 µg/ml of anti-CD16/CD32 antibody (BioLegend) for 10 min on ice. Subsequently, 50 µl FACS buffer containing CD11b-APC-Cy7 (#101226), F4/80-PE (#123110) and Ly6C-APC (#128016) (all from BioLegend) were added and splenocytes were stained for 30 min on ice and harvested at 400 g, 4 °C for 5 min. The supernatant was removed and splenocytes were stained in 200 µl 0.1 µM Zinpyr (Santa Cruz) in PBS in a thermomixer for 30 min at 37 °C. After cell harvest, splenocytes were resuspended in 300 µl FACS buffer and immediately analyzed on a LSRFortessa (BD Biosciences) as described above.

Confocal Microscopy

$1x10^5$ BMDMs were prepared and cultured in 200 µl BMDM medium on a 8-well glass bottom µ-slide (ibidi, #80827) the day before the experiment. BMDMs were infected with mCherry$^+$ *C. glabrata* or Calcofluor White-stained wild-type *C. glabrata* (see above) at a MOI = 2. After 4 h, BMDMs were 2x washed with PBS and stained with 200 µl of 10 µM Zinpyr (Santa Cruz) in DMEM for 30 min at 37 °C and, after two PBS washing steps, with 200 µl of 1 µg/ml DAPI in DMEM for 5 min at 37 °C. After three PBS washing steps, cells were cultured in PBS and images were acquired immediately on a Zeiss LSM700 inverse confocal microscope with 40x or 63x plan-apochromat objectives (ZEISS) and visualized using ZEN 2012 software. For lysosomal staining, BMDMs were incubated in 1:500 CytoPainter LysoBlue Indicator Reagent (ab176825, Abcam) in DMEM two hours before the infection. For metallothionein localization in macrophages, *Cg*-infected BMDMs were fixed in 4 % Formaldehyde (Sigma-Aldrich)/PBS for 10 min at room temperature, 3x washed with PBS and permeablized in 0.5 % Tween-20 (Sigma-Aldrich)/PBS for 10 min at room temperature. After three PBS washing steps, cells were incubated in 1 % BSA/0.5 % Tween-20/PBS for 30 min at room temperature and stained with 1:100 anti-metallothionein (UC1MT) primary antibody (ADI-SPA-550-D; Enzo Life Sciences) overnight at 4 °C. Specimens were 3x washed with PBS and incubated with 1:100 goat anti-Mouse IgG (H+L) Alexa Fluor 488-conjugated secondary antibody (A-11001; Invitrogen) for 1 h at room temperature. After staining in 5 µg/ml DAPI for 5 min, the cover slips were washed 3x in PBS before mounting on glass slides with Fluorescence Mounting Medium (S3023, Dako). The slides were dried in the dark at 4 °C and analysis was performed with a Zeiss LSM700 confocal microscope using ZEN 2012 software.

Zinpyr-Based Fungal Zn Acquisition

$1x10^6$ BMDMs were cultivated in 6-well plates and 1000 µl BMDM medium and infected with *C. glabrata* strains (MOI = 1) for 12 h, unless otherwise stated. After 2 h of infection, non-phagocytosed yeast cells were washed away with 2x 2 ml PBS and fresh BMDM medium was added. At the end of infection, BMDMs were washed 3x with 2 ml PBS to remove extracellular fungal cells and BMDMs were lysed with 1 ml 0.005 % ultra-pure SDS (Sigma-Aldrich) in PBS for 15 min on ice. Lysates were harvested by pipetting and fungal cells were pelleted at 21 000 g, 4 °C for 10 min. After completely removing the supernatant, fungal pellet was stained in 10 µl of 500 µM Zinpyr (Santa Cruz) in PBS in a thermomixer for 2 h at 30 °C and 900 rpm. Cells were resuspended in 200 µl PBS and subjected for data collection on a LSRFortessa (BD Biosciences) and analysis by using FlowJo software version

7.6.5 (FlowJo). Fungal cells could be identified by FSC/SSC discrimination, doublet exclusion and, were possible, mCherry expression. The mean fluorescence intensity of Zinpyr was recorded.

Fungal Zn Intoxication Assays

$2x10^5$ BMDMs were infected with *C. glabrata* and at the end of infection, stained with 10 µM Zinpyr (Santa Cruz) for 30 min at 37 °C. After 3x PBS washing steps, BMDMs were lysed with 0.005 % ultra-pure SDS (Sigma-Aldrich) in PBS for 15 min on ice. Fungal cells were pelleted at 21,000 g for 10 min at 4 °C and stained with 2 µg/ml PI (Sigma-Aldrich) in PBS for 5 min at 20 °C. Fungal cells were 1x washed with PBS and resuspended in FACS buffer. Data were immediately collected on a LSRFortessa (BD Biosciences) and analyzed using FlowJo software version 7.6.5 (FlowJo).

Macrophage Cell Sorting

For quantification of the *C. glabrata* survival ratio, BMDMs were infected with mCherry[+] *C. glabrata* and after 4 h, stained with 10 µM Zinpyr (Santa Cruz) for 30 min at 37 °C. BMDMs were harvested by trypsinization and immediately purified via FSC/SSC discrimination on a BD FACSAria™ III cell sorter in order to exclude extracellular *C. glabrata*. After SDS lysis of sorted BMDMs, cell lysates were plated on YPD plates and CFUs were counted after 2 days at 30 °C. The *C. glabrata* survival ratio in BMDMs is calculated as the surviving *C. glabrata* CFUs per sorted BMDMs divided by the total amount of *C. glabrata* per sorted BMDM, represented by mCherry fluorescence (median fluorescence intensity).

For RNA isolation of intracellular *C. glabrata*, at the end of the infection, BMDMs were harvested by trypsinization and immediately purified via FSC/SSC discrimination on a BD FACSAria™ III cell sorter. Sorted BMDMs were lysed in 1 ml TRI Reagent® (Molecular Research Center) and fungal RNA was isolated as described previously (Tscherner et al., 2012).

Intracellular ROS Assays

Immediately before macrophage challenge, $2x10^5$ BMDMs were washed 3x with PBS, cultivated in 280 µl DMEM and infected with *C. glabrata* (MOI = 10; in 20 µl PBS) for 2 h. After 1.5 h, 20 µl of 170 µM DHE (f.c. 10 µM) (Santa Cruz) was added to the BMDM medium and incubated for 30 min. Subsequently, BMDMs were washed 3x with PBS, harvested by trypsinization and resuspended in 300 µl FACS buffer. The MFI(DHE) (median fluorescence intensity) of BMDMs was collected on a LSRFortessa (BD Biosciences) and analyzed using FlowJo software version 7.6.5 (FlowJo).

Sample Preparation and Total Metal Quantification by ICP-MS

$1x10^6$ BMDMs were cultivated in 6-well plates and 1000 µl BMDM medium and infected with *C. glabrata* (MOI = 2) for 8 h. At the end of infection, BMDMs were washed 2x with 2 ml PBS, and excessive liquids were removed. After adding 100 µl 0.1 % ultra-pure SDS (Sigma-Aldrich) in HPLC water to the respective wells, BMDMs were scraped and lysates were transferred into 1.5 ml reaction tubes and incubated on ice for 20 min. Samples were sonicated in a Bioruptor (Diagenode), centrifuged at 25 000 g, 4 °C for 15 min, and lysates were transferred into new 1.5 ml reaction tubes and stored at -80 °C.

50 µl BMDM lysates were digested in closed PFA vials with 200 µL nitric acid (65 %, p.a. grade, Emsure) and 100 µL of hydrogen peroxide (30 %, supra-pure quality, Merck) at 80 °C for 2-3 hours. The solutions were diluted to a final volume of 5 mL with 1 % (v/v) nitric acid. Standard solutions with defined concentrations of Mg, Ca, Mn, Fe, Ni, Cu and Zn were prepared by appropriate dilution of CertiPUR multi-element standard VII (100 mg/l, Merck). Indium was used as internal standard for the ICP-MS measurements and was, therefore, spiked to all samples and standard solutions at a final concentration of 10 µg/l.

Quantitative analysis of the target analytes was accomplished using inductively coupled plasma-mass spectrometry (ICP-MS), an analytical technique which allows multi-element investigations even at extremely low concentration levels. Measurements were performed using an iCAP Qc quadrupole ICP-MS instrument (Thermo Fisher Scientific) equipped with a standard quartz tube torch and nickel sample and skimmer cones. Sample and standard solutions were brought into the ICP by means of a pneumatic nebulizer (concentric, material: Teflon) and a cyclonic glass spray chamber. Sample uptake was performed by the peristaltic pump of the iCAP Qc via a SC2-DX autosampler (Elemental Scientific) in combination with a FAST sample introduction system (1 mL sample loop, Elemental Scientific). ICP-MS analysis was carried out in "KED" mode (kinetic energy discrimination) for the separation of spectral interferences caused from polyatomic ions produced in the argon plasma. A mixture of 7 % hydrogen in helium was used as collision gas at a flow rate of 5 ml/min. A dwell time of 10 ms and 50 sweeps per reading and 4 replicates per sample was set. For analysis, the isotopes ^{25}Mg, ^{43}Ca, ^{55}Mn, ^{57}Fe, ^{60}Ni, ^{63}Cu, ^{66}Zn and ^{115}In were monitored by scanning the appropriate m/z ratios. Prior to measurement the ICP-MS instrument settings were optimized using a tune solution containing 1 µg/l of indium, barium, uranium and cerium to achieve satisfying sensitivity and oxide ratios ($CeO^+/Ce^+ < 2$ %). Data acquisition was performed using Qtegra software provided by the manufacturer of the instrument. Internal standardization with indium was carried out to compensate for potential instrument instability and signal drift. An external calibration function, using aqueous standard solutions, was used for quantification of the derived analyte signal.

Data Analysis and Statistics

Data are represented as mean ± SD. Statistical analysis was performed with GraphPad Prism version 5.04 for Windows (GraphPad). If not otherwise stated, differences between two mean values were evaluated by using unpaired t-tests with 95 % confidence intervals. Multiple groups were compared by one-way ANOVA with Bonferroni's post hoc analysis. (* p-value < 0.05; ** p-value < 0.01; *** p-value < 0.001; ns, not statistically significant)

Supplemental References

Alatery, A., and Basta, S. (2008). An efficient culture method for generating large quantities of mature mouse splenic macrophages. J. Immunol. Methods *338*, 47–57.

Alker, W., and Haase, H. (2018). Zinc and sepsis. Nutrients *10*, 1–17.

Alonzi, T., Maritano, D., Gorgoni, B., Rizzuto, G., Libert, C., and Poli, V. (2002). Essential Role of STAT3 in the Control of the Acute-Phase Response as Revealed by Inducible Gene Activation in the Liver. Mol. Cell. Biol. *21*, 1621–1632.

Boer, J. De, Williams, A., Skavdis, G., Harker, N., Coles, M., Norton, T., Williams, K., Roderick, K., and Potocnik, A.J. (2003). Transgenic mice with hematopoietic and lymphoid specific expression of Cre. Eur. J. Immunol. *33*, 314–325.

Bonaventura, P., Benedetti, G., Albarède, F., and Miossec, P. (2015). Zinc and its role in immunity and inflammation. Autoimmun. Rev. *14*, 277–285.

Bourgeois, C., Majer, O., Frohner, I., and Kuchler, K. (2009). *In vitro* systems for studying the interaction of fungal pathogens with primary cells from the mammalian innate immune system. Methods Mol. Biol. *470*, 125–139.

Catalanotti, F., Reyes, G., Jesenberger, V., Galabova-Kovacs, G., De Matos Simoes, R., Carugo, O., and Baccarini, M. (2009). A Mek1-Mek2 heterodimer determines the strength and duration of the Erk signal. Nat. Struct. Mol. Biol. *16*, 294–303.

Clausen, B.E., Burkhardt, C., Reith, W., Renkawitz, R., and Forster, I. (1999). Conditional gene targeting in macrophages and granulocytes using LysMcre mice. Transgenic Res. *8*, 265–277.

Cui, Y., Riedlinger, G., Miyoshi, K., Tang, W., Li, C., Deng, C.-X., Robinson, G.W., and Hennighausen, L. (2004). Inactivation of *Stat5* in Mouse Mammary Epithelium during Pregnancy Reveals Distinct Functions in Cell Proliferation, Survival, and Differentiation. Mol. Cell. Biol. *24*, 8037–8047.

Durbin, J.E., Hackenmiller, R., Simon, M.C., and Levy, D.E. (1996). Targeted disruption of the mouse *Stat1* gene results in compromised innate immunity to viral disease. Cell *84*, 443–450.

Gammoh, N.Z., and Rink, L. (2017). Zinc in infection and inflammation. Nutrients *9*.

Gao, H., Dai, W., Zhao, L., Min, J., and Wang, F. (2018). The Role of Zinc and Zinc Homeostasis in Macrophage Function. J. Immunol. Res. *2018*, 1–11.

Gentleman, R.C., Carey, V.J., Bates, D.M., Bolstad, B.M., Dettling, M., Dudoit, S., Ellis, B., Gautier, L., Ge, Y., Gentry, J., et al. (2004). Bioconductor: open software development for computational biology and bioinformatics. Genome Biol *5*, R80.

Gibson, D.G., Young, L., Chuang, R.-Y., Venter, J.C., Hutchison, C.A. 3rd, and Smith, H.O. (2009). Enzymatic assembly of DNA molecules up to several hundred kilobases. Nat. Methods *6*, 343–345.

Günther, V., Lindert, U., and Schaffner, W. (2012). The taste of heavy metals: Gene regulation by MTF-1. Biochim Biophys Acta *1823*, 1416–1425.

Hayashi, S., Lewis, P., Pevny, L., and Mcmahon, A.P. (2002). Efficient gene modulation in mouse epiblast using a Sox2Cre transgenic mouse strain. Gene Expr Patterns *2*, 93–97.

Kaiser, C., Michaelis, S., and Mitchell, A. (1994). Methods in Yeast Genetics. A Laboratory Course Manual (New York: Cold Spring Harbor Laboratory Press).

Kaplan, M.H., Schindler, U., Smiley, S.T., and Grusby, M.J. (1996). Stat6 is required for mediating responses to IL-4 and for the development of Th2 cells. Immunity *4*, 313–319.

Kauffmann, A., Gentleman, R., and Huber, W. (2009). arrayQualityMetrics - A bioconductor package for quality assessment of microarray data. Bioinformatics *25*, 415–416.

Kimura, T., Kadokawa, Y., Harada, H., Matsumoto, M., Sato, M., Kashiwazaki, Y., Tarutani, M., Tan, R.S., Takasugi, T., Matsuyama, T., et al. (1996). Essential and non-redundant roles of p48 (ISGF3 gamma) and IRF-1 in both type I and type II interferon responses, as revealed by gene targeting studies. Genes Cells *1*, 115–124.

Krauke, Y., and Sychrova, H. (2011). Cnh1 Na+/H+ antiporter and Ena1 Na+-ATPase play different roles in cation homeostasis and cell physiology of *Candida glabrata*. FEMS Yeast Res. *11*, 29–41.

Laemmli, U.K. (1970). Cleavage of structural proteins during the assembly of the head of bacteriophage T4. Nature *227*, 680–685.

Lopez, C.A., and Skaar, E.P. (2018). The Impact of Dietary Transition Metals on Host-Bacterial Interactions. Cell Host Microbe *23*, 737–748.

Luo, J., Zhang, L., Dorfman, A.L., Sherwood, M.C., Logsdon, M.N., Horner, J.W., Depinho, R.A., Izumo, S., and Cantley, L.C. (2005). Class IA Phosphoinositide 3-Kinase Regulates Heart Size and Physiological Cardiac Hypertrophy. Mol. Cell. Biol. *25*, 9491–9502.

Masters, B., Kelly, E., Quaife, C., Brinster, R., and Palmiter, R. (1994). Targeted disruption of metallothionein I and II genes

increases sensitivity to cadmium. Proc. Natl. Acad. Sci. *91*, 584–588.

Müller, U., Steinhoff, U., Reis, L.F.L., Hemmi, S., Paviovic, J., Zinkernagel, R.M., and Aguet, M. (1994). Functional Role of Type I and Type II Interferons in Antiviral Defense. Science (80-.). *264*, 1918–1921.

Park, C., Li, S., Cha, E., and Schindler, C. (2000). Immune response in *Stat2* knockout mice. Immunity *13*, 795–804.

Rahman, M.T., and Karim, M.M. (2018). Metallothionein: A potential link in the regulation of zinc in nutritional immunity. Biol. Trace Elem. Res. *182*, 1–13.

Reis, L.F.L., Ruffner, H., Stark, G., Aguet, M., and Weissmann, C. (1994). Mice devoid of interferon regulatory factor 1 (IRF-1) show normal expression of type I interferon genes. EMBO J. *13*, 4798–4806.

Reuss, O., Vik, Å., Kolter, R., and Morschhäuser, J. (2004). The SAT1 flipper, an optimized tool for gene disruption in *Candida albicans*. Gene *341*, 119–127.

Rice, J.M., Zweifach, A., and Lynes, M.A. (2016). Metallothionein regulates intracellular zinc signaling during CD4+T cell activation. BMC Immunol. *17*, 13.

Riedelberger, M., Penninger, P., Tscherner, M., Strobl, B., Weiss, G., Kuchler, K., Riedelberger, M., Penninger, P., Tscherner, M., Seifert, M., et al. (2020). Type I Interferon Response Dysregulates Host Iron Homeostasis and Enhances *Candida glabrata* Infection. Cell Host Microbe *27*, 454-466.e8.

Sapkota, M., and Knoell, D. (2018). Essential Role of Zinc and Zinc Transporters in Myeloid Cell Function and Host Defense against Infection. J Immunol Res *2018*.

Sato, M., Suemori, H., Hata, N., Asagiri, M., Ogasawara, K., Nakao, K., Nakaya, T., Katsuki, M., Noguchi, S., Tanaka, N., et al. (2000). Distinct and Essential Roles of Transcription Factors IRF-3 and IRF-7 in Response to Viruses for IFN-alpha/beta Gene Induction. Immunity *13*, 539–548.

Schmittgen, T.D., and Livak, K.J. (2008). Analyzing real-time PCR data by the comparative CT method. Nat. Protoc. *3*, 1101–1108.

Sheldon, J.R., and Skaar, E.P. (2019). Metals as phagocyte antimicrobial effectors. Curr. Opin. Immunol. *60*, 1–9.

Shimoda, K., Kato, K., Aoki, K., Matsuda, T., Miyamoto, A., Shibamori, M., Yamashita, M., Numata, A., Takase, K., Kobayashi, S., et al. (2000). Tyk2 plays a restricted role in IFNα signaling, although it is required for IL-12-mediated T cell function. Immunity *13*, 561–571.

Smyth, G.K. (2004). Linear models and empirical bayes methods for assessing differential expression in microarray experiments. Stat. Appl. Genet. Mol. Biol. *3*, Article3.

Subramanian, A., Tamayo, P., Mootha, V.K., Mukherjee, S., Ebert, B.L., Gillette, M.A., Paulovich, A., Pomeroy, S.L., Golub, T.R., Lander, E.S., et al. (2005). Gene set enrichment analysis: A knowledge-based approach for interpreting genome-wide expression profiles. Proc. Natl. Acad. Sci. *102*, 15545–15550.

Subramanian Vignesh, K., and Deepe, G.J. (2017). Metallothioneins: Emerging modulators in immunity and infection. Int. J. Mol. Sci. *18*.

Subramanian Vignesh, K., and Deepe, G.S. (2016). Immunological orchestration of zinc homeostasis: The battle between host mechanisms and pathogen defenses. Arch. Biochem. Biophys. *611*, 66–78.

Suzuki, A., Yamaguchi, M., Ohteki, T., Sasaki, T., Kaisho, T., Kimura, Y., Yoshida, R., Wakeham, A., Higuchi, T., Fukumoto, M., et al. (2002). T Cell-Specific Loss of Pten Leads to Defects in Central and Peripheral Tolerance. Immunity *14*, 523–534.

Tscherner, M., Stappler, E., Hnisz, D., and Kuchler, K. (2012). The histone acetyltransferase Hat1 facilitates DNA damage repair and morphogenesis in *Candida albicans*. Mol. Microbiol. *86*, 1197–1214.

Tscherner, M., Zwolanek, F., Jenull, S., Sedlazeck, F.J., Petryshyn, A., Frohner, I.E., Mavrianos, J., Chauhan, N., von Haeseler, A., and Kuchler, K. (2015). The *Candida albicans* Histone Acetyltransferase Hat1 Regulates Stress Resistance and Virulence via Distinct Chromatin Assembly Pathways. PLoS Pathog. *11*, e1005218.

Wu, A., Tymoszuk, P., Haschka, D., Heeke, S., Dichtl, S., Petzer, V., Seifert, M., Hilbe, R., Sopper, S., Talasz, H., et al. (2017). *Salmonella* Utilizes Zinc To Subvert Antimicrobial Host Defense of Macrophages via Modulation of NF-κB Signaling. Infect Immun *85*, e00418-17.

Yáñez-Carrillo, P., Orta-Zavalza, E., Gutiérrez-Escobedo, G., Patrón-Soberano, A., De Las Peñas, A., and Castaño, I. (2015). Expression vectors for C-terminal fusions with fluorescent proteins and epitope tags in *Candida glabrata*. Fungal Genet. Biol. *80*, 43–52.